



HAL
open science

Homogeneous turbulence

Anne Cadiou, Kemal Hanjalic

► **To cite this version:**

| Anne Cadiou, Kemal Hanjalic. Homogeneous turbulence. 1998. hal-00779055

HAL Id: hal-00779055

<https://hal.science/hal-00779055>

Submitted on 21 Jan 2013

HAL is a multi-disciplinary open access archive for the deposit and dissemination of scientific research documents, whether they are published or not. The documents may come from teaching and research institutions in France or abroad, or from public or private research centers.

L'archive ouverte pluridisciplinaire **HAL**, est destinée au dépôt et à la diffusion de documents scientifiques de niveau recherche, publiés ou non, émanant des établissements d'enseignement et de recherche français ou étrangers, des laboratoires publics ou privés.

Homogeneous turbulence

Anne Cadiou, Kemal Hanjalić

Report APTF-R / 98-08

Department of Applied Physics
Delft University of Technology
The Netherlands

Contents

| | | |
|----------|---|-----------|
| 1 | Introduction | 1 |
| 2 | Homogeneous equations | 3 |
| 2.1 | General form of the homogeneous closures | 3 |
| 2.1.1 | Incompressible flow | 3 |
| 2.1.2 | Extension to a weakly compressible homogeneous flow | 8 |
| 2.2 | Models considered for the incompressible flow cases | 9 |
| 2.2.1 | Models of the rapid term | 9 |
| 2.2.2 | Models of the slow term | 14 |
| 2.3 | Models considered for the compressible cases | 16 |
| 2.3.1 | Wu, Ferziger and Chapman model | 16 |
| 3 | Homogeneous test cases | 17 |
| 3.1 | Decay of isotropic turbulence | 20 |
| 3.2 | Irrotational mean deformations | 21 |
| 3.2.1 | Axisymmetric deformation | 21 |
| 3.2.2 | Plane deformation. | 45 |
| 3.2.3 | Successive plane deformations | 60 |
| 3.3 | Flows with mean rotation effect | 67 |
| 3.3.1 | Homogeneous shear | 67 |
| 3.3.2 | Homogeneous shear in a rotating frame | 67 |
| 3.4 | Return to isotropy | 73 |
| 3.4.1 | Relaxation form irrotational strains | 73 |
| 3.5 | Homogeneous flows with dilatation effects | 74 |
| 3.5.1 | Isotropic compression | 75 |
| 3.5.2 | One-dimensional compression | 81 |
| 3.6 | Comments | 91 |
| | Bibliography | 92 |

Chapter 1

Introduction

Homogeneous turbulence is rarely encountered in flows of practical relevance. Nevertheless, homogeneous turbulent flows have been long in focus of turbulence research, because they enable to study selected turbulence interactions separated or isolated from others. In addition to bringing in more transparency in turbulence dynamics, homogeneous approximation simplifies to a great degree the mathematical description and the solution of the equations. Furthermore, homogeneity in space enables the use of periodic boundary conditions, which, in turn, allow to study the turbulence dynamics in a fraction of actual flow space, making these flows very attractive for direct numerical simulations (DNS). Finally, flow homogeneity reduces the demands on experimental set up and enables the turbulence phenomena to be studied in well control conditions.

The analysis of homogeneous turbulent flows has played a major role in the development, calibration and validation of turbulent closure models. Studies of such flows offer several advantages. First, the mean flow is externally imposed and uncoupled from the fluctuating motion, so that the state of the turbulence does not affect the mean motion. However the mean motion governs directly the evolution of the turbulence. This allows to study the performance of various closure models and the response of modelled terms and equations to the imposed mean velocity field. It also enables to determine the limiting (homogeneous) values of empirical constants associated with the models of the turbulent processes that are dominant in the flow considered. Second advantage is in the simplification of the governing equations and their solutions. A common feature of all homogeneous flows is the absence (or neglect) of diffusion. Hence, the variation of the turbulent quantities can be simply reduced to the variation in time only, or in one space coordinate (with assumed constant or prescribed mean velocity in that direction). The mathematical description is then reduced to an initial value problem defined by a system of ordinary differential equations that can be conveniently solved by e.g. fourth-order order Runge-Kutta, or similar methods.

Homogeneous approximations have particularly been used to derive the second moment closure models, because they enable to study and derive the models of the pressure - strain-rate process and of the stress dissipation, separated from other interactions: modelling these two processes is still one of the most challenging issues in single-point closure

modelling (e.g. (Lumley, 1970), Speziale *et al.* (1991)).

In this report we present a comparative analysis of the performance of various second-moment closure models published in the literature, in a range of homogeneous flows. The general form of equations set for the second-moment closures for homogeneous incompressible flows is first presented, followed by an overview of models from the literature. The focus of the analysis is the pressure-strain term: it is the modelling of this term, where the proposals by various authors differ most one from another. For all models considered, the standard equation for the energy dissipation rate ε is used to provide the characteristic turbulence scale, as well as the stress dissipation tensor ε_{ij} . For the latter, the isotropic dissipation model $\varepsilon_{ij} = 2/3\varepsilon\delta_{ij}$ has been used, except in models where a different form was originally proposed, such as in the model of Fu, Launder and Tselepidakis (1987).

Models considered are then used to compute a series of homogeneous flows and the results obtained were compared with the direct numerical simulations or experiments from literature. Considered were the flows subjected separately to axisymmetric and plane deformation, successive plane strains, homogeneous shear without and with rotation, and two cases of homogeneous flows with dilatation effects: isotropic compression and one-dimensional homogeneous compression. For the latter two cases, the two-scale scalar model of Wu, Ferziger and Chapman (1985) for compressible flow is used.

Chapter 2

Homogeneous equations

2.1 General form of the homogeneous closures

2.1.1 Incompressible flow

For an incompressible homogeneous turbulence, the equations of motion, and a second-moment closure model can be written in a general form, using the conventional notations and including possibly a rotating frame:

$$\frac{\partial \bar{V}_i}{\partial t} = -\frac{1}{\rho} P_{,i} - \bar{V}_k \bar{V}_{i,k} - 2 \varepsilon_{imk} \Omega_m \bar{V}_k \quad (2.1a)$$

$$\frac{\partial R_{ij}}{\partial t} = P_{ij} + G_{ij} + \phi_{ij} - \varepsilon_{ij} \quad (2.1b)$$

$$\frac{\partial \varepsilon}{\partial t} = P^{\varepsilon 1} + P^{\varepsilon 2} + P^{\varepsilon 4} + G^\varepsilon - E^\varepsilon + \phi^\varepsilon \quad (2.1c)$$

where, \bar{V}_i is the mean velocity vector, $P_{,i}$ is the mean pressure gradient, Ω_m is system rotation angular velocity, R_{ij} is the Reynolds stress tensor and ε is the kinetic energy dissipation rate. The terms in the transport equations for R_{ij} and ε have conventional meanings: P_{ij} is the mean strain stress production, ϕ_{ij} pressure-strain correlation and ε_{ij} stress dissipation. In the ε equation, $P^{\varepsilon 1}$, $P^{\varepsilon 2}$ and $P^{\varepsilon 4}$ are the production terms, E^ε is viscous destruction, and ϕ^ε the term with fluctuating pressure. System rotation in both equations is represented by G terms, defined as

$$G_{ij} = 2 [R_{ik} \theta_{jk} + R_{jk} \theta_{ik}] \quad (2.2a)$$

$$G^\varepsilon = 0 \quad (2.2b)$$

where $\theta_{ik} = \varepsilon_{ijm} \Omega_m$. It should be noted that the mean velocity gradients are independent of their spatial location and, therefore, the mean deformation and rotation rate tensors, S_{ij} and W_{ij} obey the following equations:

$$\frac{\partial S_{ij}}{\partial t} = -\frac{1}{\rho} P_{,ij} - S_{ik} S_{kj} - W_{ik} W_{kj} + \theta_{ik} (S_{kj} + W_{kj}) - (S_{ik} - W_{ik}) \theta_{kj} \quad (2.3a)$$

$$\frac{\partial W_{ij}}{\partial t} = S_{ik} (W_{jk} - \theta_{jk}) - (W_{ik} - \theta_{ik}) S_{kj} + (W_{ik} \theta_{jk} - \theta_{ik} W_{jk}) \quad (2.3b)$$

The pressure gradient does not explicitly appear in the rotation rate tensor equation. Consequently, only the homogeneous turbulent flows undergoing a rotation in the mean flow, can be affected by their relative rotation rate evolving in time.

The stress and dissipation equation can be written in another form, which may be more convenient when considering rotating flows

$$\frac{\partial R_{ij}}{\partial t} = -R_{ik} \tilde{V}_{aj,k} - R_{jk} \tilde{V}_{ai,k} + \phi_{ij} - \varepsilon_{ij} \quad (2.4a)$$

$$\frac{\partial \varepsilon}{\partial t} = -C_{\varepsilon 1} R_{mn} S_{mn} \frac{\varepsilon}{K} - C_{\varepsilon 2} \frac{\varepsilon^2}{K} \quad (2.4b)$$

where $\tilde{V}_{ai,j} = \bar{V}_{i,j} - 2\theta_{ij}$. Because of homogeneity, the turbulence statistical quantities are independent of their position in space.

Alternatively, the model can be reformulated in terms of Reynolds stress anisotropy tensor, $b_{ij} = R_{ij}/2K - 1/3\delta_{ij}$, and its trace, the turbulence kinetic energy $K = 1/2R_{ii}$:

$$\frac{\partial K}{\partial t} = -2K b_{mn} S_{mn} - \varepsilon \quad (2.5a)$$

$$\begin{aligned} \frac{\partial b_{ij}}{\partial t} = & -\frac{2}{3} S_{ij} + (2b_{mn} S_{mn} + \frac{\varepsilon}{K}) b_{ij} \\ & + \bar{\phi}_{ij} - {}^D\bar{\varepsilon}_{ij} - (b_{ik} S_{jk} + b_{jk} S_{ik} - \frac{2}{3} b_{mn} S_{mn} \delta_{ij}) - (b_{ik} \tilde{W}_{ajk} + b_{jk} \tilde{W}_{aik}) \end{aligned} \quad (2.5b)$$

$$\frac{\partial \varepsilon}{\partial t} = -C_{\varepsilon 1} R_{mn} S_{mn} \frac{\varepsilon}{K} - C_{\varepsilon 2} \frac{\varepsilon^2}{K} \quad (2.5c)$$

where the pressure-strain correlation tensor and the dissipation rate are nondimensionalized by the kinetic energy

$$\bar{\phi}_{ij} = \frac{1}{2K} \phi_{ij} \quad (2.6a)$$

$${}^D\bar{\varepsilon}_{ij} = \frac{1}{2K} {}^D\varepsilon_{ij} \quad (2.6b)$$

For modelling purpose, it is a common to decompose the pressure-strain correlation into the rapid and slow part. The deviatoric part of the dissipation tensor ${}^D\bar{\varepsilon}_{ij}$ is usually assumed to be closely related to the stress anisotropy tensor b_{ij} , so that it is closed together with the slow part of the pressure-strain tensor (Lumley, 1970), hence the following notations will be used

$$\bar{\phi}_{ij}^* = \bar{\phi}_{ij}^{*R} + \bar{\phi}_{ij}^{*S} \quad (2.7)$$

and

$$\bar{\phi}_{ij}^{*R} = 2\bar{V}_{ap,q} (\bar{X}_{iqpj} + \bar{X}_{jqpi}) \quad (2.8a)$$

$$\bar{\phi}_{ij}^{*S} = \bar{\phi}_{ij}^S - {}^D\bar{\varepsilon}_{ij} \quad (2.8b)$$

where

$$\overline{V}_{ap,q} = \overline{V}_{p,q} - \theta_{pq} \quad (2.9)$$

$$\overline{X}_{ijpq} = \frac{1}{2K} X_{ijpq} \quad (2.10)$$

Since the turbulence is supposed to be homogeneous, this term can be expressed as a Fourier transform of the spectral density of R_{ij} , as practiced in a spectral description of turbulence:

$$\overline{X}_{ijpq} = \frac{1}{2K} \int \frac{k_p k_q}{k^2} \Phi_{ij}(\underline{k}) d\underline{k} \quad (2.11)$$

where \underline{k} denotes the wave number and Φ_{ij} , the spectral tensor of the velocity correlations.

We consider now the general practice of closing the stress equation and modelling the unknown terms.

The rapid term is usually closed by a model for X_{ijpq} , which is assumed to depend only on the anisotropy tensor. According to the tensor representation theorem (functional theory), the most general form of this closure can be written as

$$\begin{aligned} \overline{X}_{ijpq} &= C_1 \delta_{ij} \delta_{pq} + C_2 (\delta_{ip} \delta_{jq} + \delta_{iq} \delta_{jp}) \\ &+ C_3 \delta_{ij} b_{pq} + C_4 \delta_{pq} b_{ij} \\ &+ C_5 (\delta_{ip} b_{jq} + \delta_{iq} b_{jp} + \delta_{jq} b_{ip} + \delta_{jp} b_{iq}) \\ &+ C_6 \delta_{ij} b_{.pq}^2 + C_7 \delta_{pq} b_{.ij}^2 \\ &+ C_8 (\delta_{ip} b_{.jq}^2 + \delta_{iq} b_{.jp}^2 + \delta_{jq} b_{.ip}^2 + \delta_{jp} b_{.iq}^2) \\ &+ C_9 b_{ij} b_{pq} + C_{10} (b_{ip} b_{jq} + b_{iq} b_{jp}) \\ &+ C_{11} b_{ij} b_{.pq}^2 + C_{12} b_{pq} b_{.ij}^2 \\ &+ C_{13} (b_{ip} b_{.jq}^2 + b_{iq} b_{.jp}^2 + b_{jq} b_{.ip}^2 + b_{jp} b_{.iq}^2) \\ &+ C_{14} b_{.ij}^2 b_{.pq}^2 + C_{15} (b_{.ip}^2 b_{.jq}^2 + b_{.iq}^2 b_{.jp}^2) \end{aligned} \quad (2.12)$$

Inserting the expression (2.12) in (2.8a) and rearranging yields $\overline{\phi}_{ij}^{*R}$ as a general functional in terms of b_{ij} , S_{ij} and \overline{W}_{ij} , with the coefficients β_i to be determined later:

(ANNE, PLEASE CHECK IF THIS EXPRESSION IS CORRECT: SOMETHING SEEMS TO BE INCORRECT WITH β_2 , see equation 2.20!)

$$\begin{aligned} \overline{\phi}_{ij}^{*R} &= \beta_1 b_{ij} \\ &+ \beta_2 [b_{.ij}^2 + \frac{2}{3} II \delta_{ij}] \\ &+ \beta_3 \overline{S}_{ij} \\ &+ \beta_4 [b_{ik} \overline{S}_{jk} + b_{jk} \overline{S}_{ki} - \frac{2}{3} b_{mn} \overline{S}_{mn} \delta_{ij}] \\ &+ \beta_5 [b_{.ik}^2 \overline{S}_{jk} + b_{.jk}^2 \overline{S}_{ki} - \frac{2}{3} b_{.mn}^2 \overline{S}_{mn} \delta_{ij}] \\ &+ \beta_6 [b_{ik} \overline{W}_{jk} + b_{jk} \overline{W}_{ik}] \\ &+ \beta_7 [b_{.ik}^2 \overline{W}_{jk} + b_{.jk}^2 \overline{W}_{ik}] \\ &+ \beta_8 [b_{ik} \overline{W}_{kp} b_{.pj} + b_{jp} \overline{W}_{pk} b_{.ik}] \end{aligned} \quad (2.13)$$

This expression (2.12) satisfies all symmetries properties of the tensor X_{ijpq} for a homogeneous turbulence, that is

$$\overline{X}_{ijpq} = \overline{X}_{ijqp} \quad (2.14a)$$

given by the permutation of the second derivatives, and

$$\overline{X}_{ijpq} = \overline{X}_{jipq} \quad (2.14b)$$

because of the homogeneous character of the flow.

The 15 coefficients of (2.12) are not independent. Their number can be reduced by applying the incompressibility and normalisation constraints on the anisotropy tensor. The incompressibility condition imposes:

$$\overline{X}_{n j n q} = 0 \quad (2.15)$$

which leads to the following three relations between the coefficients:

$$C_1 + 4 C_2 - 2 II C_8 + III (C_{11} + C_{12} + 2 C_{13}) = 0 \quad (2.16a)$$

$$C_3 + C_4 + 5 C_5 - II (C_{11} + C_{12} + 4 C_{13}) + III (C_{14} + C_{15}) = 0 \quad (2.16b)$$

$$C_6 + C_7 + 5 C_8 + C_9 + C_{10} - II (C_{14} + 3 C_{15}) = 0 \quad (2.16c)$$

where $II = -1/2\{b^2\} = -1/2\{b_{ij}b_{ij}\}$ and $III = 1/3\{b^3\} = 1/3\{b_{ij}b_{jk}b_{ki}\}$ are the second and third invariants of the stress anisotropy tensor b_{ij} , respectively.

The normalisation of the anisotropy tensor express the fact that the Reynolds tensor is a contraction of the fourth order tensor in the case of a homogeneous flow

$$\overline{X}_{ijpp} = b_{ij} + \frac{1}{3} \delta_{ij} \quad (2.17)$$

and this constraint must be satisfied by the model if \overline{X}_{ijpq} is to be closed by a functional depending solely on b_{ij} . This condition gives three additional equations:

$$3 C_1 + 2 C_2 - 2 II C_6 + 4 III C_{13} = \frac{1}{3} \quad (2.18a)$$

$$3 C_4 + 4 C_5 - 2 II (C_{11} + 2 C_{13}) + 2 III C_{15} = 1 \quad (2.18b)$$

$$3 C_7 + 4 C_8 + 2 C_{10} - 2 II (C_{14} + C_{15}) = 0 \quad (2.18c)$$

reducing the number of independent coefficients to 9. It is convenient (though not necessary) to choose the following unknowns of the model:

$$C_5 \quad C_8 \quad C_9 \quad C_{10} \quad C_{11} \quad C_{12} \quad C_{13} \quad C_{14} \quad C_{15} \quad (2.19)$$

The remaining 6 coefficients is then expressed in terms of the above selected 9 independent coefficients from equations (2.15) and (2.16):

$$C_1 = \frac{2}{15} - 2 II \left(\frac{5}{3} C_8 + \frac{2}{5} C_9 + \frac{2}{15} C_{10} \right) + \frac{1}{5} III (C_{11} + C_{12} - 6 C_{13}) + \frac{4}{15} II^2 (C_{14} + 7 C_{15}) \quad (2.20a)$$

$$C_2 = -\frac{1}{30} + II \left(\frac{4}{3} C_8 + \frac{1}{5} C_9 + \frac{1}{15} C_{10} \right) - \frac{1}{5} III \left[\frac{3}{2} (C_{11} + C_{12}) + C_{13} \right] \quad (2.20b)$$

$$\begin{aligned}
 & - \frac{1}{15} II^2 (C_{14} + 7 C_{15}) \\
 C_3 & = -\frac{1}{3} - \frac{11}{3} C_5 + II \left(\frac{1}{3} C_{11} + C_{12} + \frac{8}{3} C_{13} \right) - III \left(C_{14} + \frac{1}{3} C_{15} \right) \quad (2.20c)
 \end{aligned}$$

$$C_4 = \frac{1}{3} - \frac{4}{3} C_5 + \frac{2}{3} II (C_{11} + 2 C_{13}) - \frac{2}{3} III C_{15} \quad (2.20d)$$

$$C_6 = -\frac{11}{3} C_8 - C_9 - \frac{1}{3} C_{10} + \frac{1}{3} II (C_{14} + 7 C_{15}) \quad (2.20e)$$

$$C_7 = -\frac{4}{3} C_8 - \frac{2}{3} C_{10} + \frac{2}{3} II (C_{14} + C_{15}) \quad (2.20f)$$

Inserting the expressions for the coefficients C_1 to C_7 in the closure hypothesis for X_{ijpq} tensor and rearranging leads to the following model of the rapid pressure-strain term:

$$\begin{aligned}
 \overline{\Phi}_{ij}^{*R} & = [4 \{bS\} (C_9 + 2 C_{10}) + 2 \{b^2S\} (C_{11} + C_{12} + 4 C_{13})] b_{ij} \quad (2.21) \\
 & + [2 \{bS\} (C_{11} + C_{12} + 4 C_{13}) + 4 \{b^2S\} (C_{14} + 2 C_{15})] {}^D b_{ij}^2 \\
 & + \left[\frac{2}{5} - 8 II \left(C_8 + \frac{4}{5} C_9 + \frac{3}{5} C_{10} \right) - \frac{12}{5} III (C_{11} + C_{12} + 4 C_{13}) - \frac{8}{5} II^2 (2 C_{14} - C_{15}) \right] S_{ij} \\
 & + [-6 C_5 + 2 II (C_{11} + C_{12} + 4 C_{13}) - 6 III (C_{14} + C_{15})] [b_{ik} S_{jk} + b_{jk} S_{ik} - \frac{2}{3} b_{mn} S_{mn} \delta_{ij}] \\
 & + [-6 (C_8 + C_9 + C_{10}) - 2 II (C_{14} - C_{15})] [b_{ik}^2 S_{jk} + b_{jk}^2 S_{ik} - \frac{2}{3} b_{mn}^2 S_{mn} \delta_{ij}] \\
 & + \left[\frac{4}{3} + \frac{14}{3} C_5 - 2 II \left(-\frac{1}{3} C_{11} + C_{12} - \frac{4}{3} C_{13} \right) + 2 III \left(C_{14} - \frac{1}{3} C_{15} \right) \right] [b_{ik} \overline{W}_{ajk} + b_{jk} \overline{W}_{aik}] \\
 & + \left[\frac{14}{3} C_8 + 2 C_9 - \frac{2}{3} C_{10} + \frac{2}{3} II (C_{14} - 5 C_{15}) \right] [b_{ik}^2 \overline{W}_{ajk} + b_{jk}^2 \overline{W}_{aik}] \\
 & + [2 (C_{12} - C_{11})] [b_{ik} \overline{W}_{akp} b_{pj}^2 + b_{ik}^2 \overline{W}_{apk} b_{jp}]
 \end{aligned}$$

The dependency of the β_i coefficients coming from the direct expression of the functional clearly appears here. This is also clear that if the two models are tensorially similar, they are not equivalent. They do not exactly contain the same information. There exist no truncature of the polynomial development of the β_i coefficients in the II and III invariants which corresponds to the form obtained with the closure on \overline{X}_{ijpq} . Such a development gives a more important number of scalar unknown than the nine coefficients that are to be retained with the closure on \overline{X}_{ijpq} .

The slow term is closed directly by an isotropic functional depending uniquely on the anisotropy tensor of the Reynolds stresses:

$$\phi_{ij}^{*S} = \varepsilon [\beta_1^S b_{ij} + \beta_2^S {}^D b_{ij}^2] \quad (2.22)$$

or again

$$\overline{\phi}_{ij}^{*S} = [\beta_1^S b_{ij} + \beta_2^S {}^D b_{ij}^2] \quad (2.23)$$

In the following paragraph we present the most common model expressions for the rapid and for the slow term. The closures are presented separately even if the original proposition treats the rapid term jointly with the slow term.

2.1.2 Extension to a weakly compressible homogeneous flow

For compressible turbulence additional terms need to be introduced in all turbulence closure equations to account for the non-zero velocity divergence S_{kk} and density variation. In this report we consider only a case of a weakly compressed homogeneous turbulence, for which it suffices to introduce the S_{kk} term only in the dissipation equation, by which to account for the modification of the turbulence time and length scale, K/ε and $K^{3/2}/\varepsilon$ respectively. A simple way to introduce the compressibility effects in the model of stress redistribution is to replace S_{ij} in the rapid term by $S_{ij}^* = S_{ij} - 1/3 S_{kk} \delta_{ij}$. Other modifications have also been proposed, but no conclusive outcome has been reported. Even the coefficient of the divergence term in the dissipation equation is still controversial. Because in a weakly compressed homogeneous turbulence the scale modification seems most dominant, we confine our attention to the standard $K - \varepsilon$ model, with an extra term in the ε equation as proposed by Watkins (1977):

$$\frac{dK}{dt} = P - \varepsilon \quad (2.24a)$$

$$\frac{d\varepsilon}{dt} = C_{\varepsilon_1} \frac{P\varepsilon}{K} - C_{\varepsilon_2} \frac{\varepsilon^2}{K} + C_{\varepsilon_3} \varepsilon S_{kk} \quad (2.24b)$$

The coefficients have standard values, usually associated with Launder and Spalding (1974). In addition the value of C_{ε_3} proposed by Watkins (1977) is listed, hence the notation LSW. The same form of the model was also considered by Reynolds (1980), except that the values of the coefficients, denoted by R, differ substantially from the common values, as shown in the table below:

| Model | C_{ε_1} | C_{ε_2} | C_{ε_3} | C_{μ} |
|-------|---------------------|---------------------|---------------------|-----------|
| LSW | 1.44 | 1.92 | 1.00 | 0.09 |
| R | 1.0 | 1.83 | -2/3 | 0.09 |

The Boussinesq closure takes the conventional form:

$$R_{ij} = \frac{2}{3} K \delta_{ij} - 2 \nu_t (S_{ij} - \frac{1}{3} S_{kk} \delta_{ij})$$

with

$$\nu_t = C_{\mu} \frac{K^2}{\varepsilon}$$

with the standard value of $C_{\mu} = 0.09$.

A more advanced three equations eddy viscosity closure, developed by Wu *et al.* (1985) specifically for compressed flows will be considered later.

2.2 Models considered for the incompressible flow cases

2.2.1 Models of the rapid term

Naot, Shavit and Wolfshtein model

The model proposed by Naot *et al.* (1973), called "isotropization of production" (IP), is the most simple of all models for the rapid terms. Its form follows directly from the rapid distortion theory (RDT), hence this model can be regarded as a RDT limit of a general model of the rapid term. However, the first derivation of the IP term was based on the assumption that the rapid pressure-scrambling process is proportional to the negative deviatoric part of the stress production:

$$\overline{\phi}_{ij}^R = -C_2 [P_{ij} - \frac{2}{3} P \delta_{ij}] \quad (2.25)$$

or, expressed in terms of S_{ij} and \overline{W}_{aij} again:

$$\overline{\phi}_{ij}^R = C_2 \left[\frac{2}{3} S_{ij} + (b_{ik} S_{kj} + b_{jk} S_{ki} - \frac{2}{3} b_{mn} S_{mn} \delta_{ij}) + (b_{ik} \overline{W}_{ajk} + b_{jk} \overline{W}_{aik}) \right] \quad (2.26)$$

The coefficients of the functional for this model are

$$\begin{aligned} \beta_1 &= 0 & \beta_2 &= 0 \\ \beta_3 &= \frac{2}{3} C_2 & \beta_4 &= C_2 \\ \beta_5 &= 0 & \beta_6 &= C_2 \\ \beta_7 &= 0 & \beta_8 &= 0 \end{aligned} \quad (2.27)$$

where $C_2 = 0.6$.

The slow term associated with the IP model of Naot *et al.* (1973) is also linear, in the form as proposed by Rotta (to be discussed in more details in the next paragraph). but the coefficient is slightly different, i.e. $C_1 = 3.6$ instead of $C_1 = 3.0$. The dissipation rate tensor is also assumed to be isotropic and the coefficients of the dissipation transport equation are close to the standard values, $C_{\varepsilon_1} = 1.45$ and $C_{\varepsilon_2} = 1.92$.

Launder, Reece and Rodi model

This model (LRR) Launder *et al.* (1975) is the most general form of the homogeneous linear closure expressed uniquely in terms of the anisotropy of the Reynolds stress tensor. It has been derived through the closure of the fourth order tensor X_{ijpq} , satisfying all basic constraint: symmetry, incompressibility and the normalisation on b_{ij} . This model has one degree of freedom, resulting in one free coefficient C_2 . The expression satisfy the

limit of the rapid term in the case of a homogeneous isotropic turbulence, for which the exact form has been derived by Crow, see Leith (1968). The model can be written as

$$\overline{\phi}_{ij}^R = \frac{2}{5} S_{ij} + \frac{9C_2 + 6}{11} (b_{ik} S_{kj} + b_{jk} S_{ki} - \frac{2}{3} b_{mn} S_{mn} \delta_{ij}) + \frac{10 - 7C_2}{11} (b_{ik} \overline{W}_{ajk} + b_{jk} \overline{W}_{aik}) \quad (2.28)$$

where the coefficients of the functional are

$$\begin{aligned} \beta_1 &= 0 & \beta_2 &= 0 \\ \beta_3 &= \frac{2}{5} & \beta_4 &= \frac{9C_2 + 6}{11} \\ \beta_5 &= 0 & \beta_6 &= \frac{10 - 7C_2}{11} \\ \beta_7 &= 0 & \beta_8 &= 0 \end{aligned} \quad (2.29)$$

This rapid term is associated with the linear model of the slow term of Rotta (1951). The dissipation is closed in the same way as in the previous model, with the coefficients $C_{\varepsilon_1} = 1.45$ and $C_{\varepsilon_2} = 1.90$. For the coefficient C_2 , Launder *et al.* (1975) proposed $C_2 = 0.4$. This value was derived from the assumption that the asymptotic state of a homogeneous constant shear flow satisfy the energy equilibrium condition, $P = \varepsilon$, as also discussed by Speziale and Mhauris (1988).

It is now known that the linear approximation of the rapid term does not satisfy the realisability constraint when the turbulence reaches a two-component (2C) state Lumley, 1978. Therefore, we consider also some of the nonlinear closures proposed in the literature.

Speziale, Sarkar and Gatski model

The form of the Speziale *et al.* (1991) model, (SSG), has been derived by a direct modelling of the complete pressure-strain term. The rapid part needs to be associated with the slow term that will be presented in the next paragraph. The rapid part can be written as

$$\begin{aligned} \overline{\phi}_{ij}^R &= C_1^* b_{mn} S_{mn} b_{ij} \\ &+ \frac{1}{2} (C_3 - \sqrt{b_{mn} b_{mn}} C_3^*) S_{ij} + \frac{1}{2} C_4 (b_{ik} S_{kj} + b_{jk} S_{ki} - \frac{2}{3} b_{mn} S_{mn} \delta_{ij}) \\ &+ \frac{1}{2} C_5 (b_{ik} \overline{W}_{ajk} + b_{jk} \overline{W}_{aik}) \end{aligned} \quad (2.30)$$

where the coefficients of the functional are

$$\begin{aligned} \beta_1 &= C_1^* b_{mn} S_{mn} & \beta_2 &= 0 \\ \beta_3 &= \frac{1}{2} (C_3 - \sqrt{b_{mn} b_{mn}} C_3^*) & \beta_4 &= \frac{1}{2} C_4 \\ \beta_5 &= 0 & \beta_6 &= \frac{1}{2} C_5 \\ \beta_7 &= 0 & \beta_8 &= 0 \end{aligned} \quad (2.31)$$

and the free parameter, chosen by the authors, are:

$$C_1^* = 1.8 \quad C_3 = \frac{4}{5} \quad C_3^* = 1.3 \quad C_4 = 1.25 \quad C_5 = 0.4 \quad (2.32)$$

The dissipation rate tensor is assumed to be isotropic, and the coefficients of the dissipation equation are $C_{\varepsilon_1} = 1.44$ and $C_{\varepsilon_2} = 1.83$.

The Speziale *et al.* (1991) model is of a non-linear nature, and usually classified as a quasi-linear model, because the non linearity arises from the coefficients of the functional and not from its tensorial form. The calibration of the fourth coefficients, (the number resulting from the fact that the normalisation constraint is not enforced here), is done by imposing the stability limit of a homogeneous sheared flow in presence of an orthogonal rotation. This model, just as LRR, does not satisfy entirely the realisability criterion.

Fu, Launder and Tselepidakis model

The derivation of the Fu *et al.* (1987) model (FLT) was based on the same principles as the Launder *et al.* (1975) model, except that the closure of the X_{ijpq} functional is here extended to its complete form. Applying the Cayley-Hamilton theorem to the matrix expansion closes the expression at the cubic level (in terms of b_{ij} so that the resulting rapid term is cubic and can be written as:

$$\begin{aligned} \overline{\phi}_{ij}^R &= \frac{2}{3} S_{ij} \\ &+ \frac{2}{5} [b_{ik} S_{jk} + b_{jk} S_{kj} - \frac{2}{3} b_{mn} S_{mn} \delta_{ij}] \\ &+ \frac{2}{5} [b_{ik}^2 S_{jk} + b_{jk}^2 S_{kj} - 2 b_{im} S_{mn} b_{nj} - 3 b_{mn} S_{mn} b_{ij}] \\ &+ (\frac{13}{15} - 16 r II) [b_{ik} \overline{W}_{ajk} + b_{jk} \overline{W}_{aik}] \\ &+ \frac{2}{5} [b_{ik}^2 \overline{W}_{ajk} + b_{jk}^2 \overline{W}_{aik}] \\ &+ 24 r [b_{ik} \overline{W}_{akp} b_{pj}^2 + b_{ik}^2 \overline{W}_{apk} b_{jp}] \end{aligned} \quad (2.33)$$

with coefficients:

$$\begin{aligned} \beta_1 &= -2 b_{mn} S_{mn} & \beta_2 &= 0 \\ \beta_3 &= \frac{2}{5} + \frac{4}{5} II & \beta_4 &= \frac{3}{5} \\ \beta_5 &= \frac{6}{5} & \beta_6 &= \frac{13}{15} - 16 r II \\ \beta_7 &= \frac{6}{5} & \beta_8 &= 24 r \end{aligned} \quad (2.34)$$

with $r = 0.7$.

This model is closed with an anisotropic expression of the dissipation tensor:

$$\varepsilon_{ij} = 2 \varepsilon \left[(1 - \sqrt{F}) b_{ij} + \frac{2}{3} \delta_{ij} \right] \quad (2.35)$$

where $F = 1 + 9II + 27III$ is Lumley's "flatness" parameter which is zero in isotropic turbulence and takes the value 1 in the limit of two-component turbulence.

It is clear that the deviatoric part of this tensor can be grouped with the slow term of the pressure-strain correlation tensor, which leads to the following contributions to the slow term coefficients:

$$\beta_1^S = 2(1 - \sqrt{F}) \quad \beta_2^S = 0 \quad (2.36)$$

The slow term associated to this model, proposed by Fu *et al.* (1987) is described in the next paragraph. The equation for the dissipation rate is in the standard form, with $C_{\varepsilon_1} = 1.45$ and $C_{\varepsilon_2} = 1.90$.

This cubic rapid term has only one degree of freedom. The model of X_{ijpq} satisfies all basic constraints and the 2C limit, and is fully realisable.

Shih and Lumley model

The model of Shih and Lumley (1985) (SL) is quadratic, but the coefficients are expressed in terms of invariants of the anisotropy tensor, so that it has in fact a cubic character. Therefore, this model is sometimes classified as a quasi-quadratic one. It can be written as

$$\begin{aligned}
 \overline{\phi}_{ij}^R &= \frac{2}{5} S_{ij} \\
 &+ 6 \alpha_5 [b_{ik} S_{jk} + b_{jk} S_{kj} - \frac{2}{3} b_{mn} S_{mn} \delta_{ij}] \\
 &+ \frac{2}{5} [b_{ik}^2 S_{jk} + b_{jk}^2 S_{kj} - 2 b_{im} S_{mn} b_{nj} - 3 b_{mn} S_{mn} b_{ij}] \\
 &+ \frac{2}{3} (2 - 7 \alpha_5) [b_{ik} \overline{W}_{ajk} + b_{jk} \overline{W}_{aik}] \\
 &+ \frac{2}{5} [b_{ik}^2 \overline{W}_{ajk} + b_{jk}^2 \overline{W}_{aik}]
 \end{aligned} \tag{2.37}$$

The coefficients are summarized as:

$$\begin{aligned}
 \beta_1 &= -2 b_{mn} S_{mn} & \beta_2 &= 0 \\
 \beta_3 &= \frac{2}{5} S_{ij} S_{ij} + \frac{4}{5} II & \beta_4 &= 6 \alpha_5 \\
 \beta_5 &= \frac{2}{5} S_{ij} S_{ij} & \beta_6 &= \frac{2}{3} (2 - 7 \alpha_5) \\
 \beta_7 &= \frac{2}{5} S_{ij} S_{ij} & \beta_8 &= 0
 \end{aligned} \tag{2.38}$$

with

$$\alpha_5 = \frac{1}{10} (1 + 0.8 \sqrt{F}) \tag{2.39}$$

The dissipation tensor is assumed to be isotropic and the coefficients of the dissipation rate equation are modified in order to take account for the turbulent Reynolds number and stress invariant.

$$C_{\varepsilon 1} = 1.2 \tag{2.40a}$$

$$C_{\varepsilon 2} = \frac{7}{5} + 0.49 \exp\left(2.83 \frac{1}{\sqrt{R_t}}\right) [1 - 0.33 \ln(1 - 55 II)] \tag{2.40b}$$

where

$$R_t = \frac{4}{9} \frac{K^2}{\nu \varepsilon} \tag{2.41}$$

The slow term associated to this closure is that proposed by Lumley (1978), and will be outlined in the next chapter.

This model satisfy the 2C realisability limit.

Ristorcelli, Lumley and Abid model

The model proposed by Ristorcelli *et al.* (1994), (RLA), has been derived from the same general tensorial expansion principle, but to satisfy the realisability constraint on X_{ijpq} proposed by Lumley. In addition to the constraints used in most of the previously outlined models, here also the joint realisability constraint Ristorcelli *et al.* (1994), has been imposed to satisfy the material indifference principle in the limit of a two-component

turbulence. This yields an additional condition to derive the coefficients of the functional. This last condition leads to the application of the Taylor-Proudman theorem in the case of a rotating turbulence. The coefficients can be summarized as:

$$\begin{aligned}
 \beta_1 &= 2(C_6 b_{mn} S_{mn} + C_4''' b_{,mn}^2 S_{mn}) & \beta_2 &= 2C_4''' b_{mn} S_{mn} \\
 \beta_3 &= 2(C_3 - 2II C_3'' + 3III C_3''') & \beta_4 &= 2C_4 \\
 \beta_5 &= 2C_7 & \beta_6 &= -2C_5 \\
 \beta_7 &= -2C_8 & \beta_8 &= -2C_9
 \end{aligned} \tag{2.42}$$

All C coefficients, denoted here as C_i , can be written in a general form:

$$C_i = B_i + F A_i^c \tag{2.43}$$

where the B_i coefficients satisfy the basic constraint, and the A_i^c coefficients allow the C_i to satisfy the asymptotic equilibrium of a shear flow. Introducing

$$II_d = \frac{(1 + 3II)}{(7 + 12II)} \tag{2.44}$$

yields the following expressions for C_i coefficients:

$$C_3 = B_3 - \frac{2}{5} F (10A_8^c + 3A_9^c + A_{10}^c) II - \frac{1}{5} F (A_{11}^c + A_{12}^c + 14A_{13}^c) III \tag{2.45a}$$

$$C_3'' = B_3'' + F (A_9^c + A_{10}^c) \tag{2.45b}$$

$$C_3''' = B_3''' - \frac{1}{3} F (A_{11}^c + A_{12}^c + 2A_{13}^c) \tag{2.45c}$$

$$C_4 = B_4 + F [-3A_5^c + II (A_{11}^c + A_{12}^c + 4A_{13}^c)] \tag{2.45d}$$

$$C_4''' = B_4''' + F (A_{11}^c + A_{12}^c + 4A_{13}^c) \tag{2.45e}$$

$$C_5 = B_5 + F [-\frac{7}{3} A_5^c + \frac{1}{3} II (-A_{11}^c + 3A_{12}^c + 4A_{13}^c)] \tag{2.45f}$$

$$C_6 = B_6 + F (2A_9^c + 4A_{10}^c) \tag{2.45g}$$

$$C_7 = B_7 - 3F (A_8^c + A_9^c + A_{10}^c) \tag{2.45h}$$

$$C_8 = B_8 - \frac{1}{3} F (7A_8^c + 3A_9^c - A_{10}^c) \tag{2.45i}$$

$$C_9 = B_9 + F (A_{11}^c - A_{12}^c) \tag{2.45j}$$

The coefficients A_i^c are determined by three constraints. The first one is given by the incompressibility condition, which imposes:

$$A_1^c + 4A_2^c - 2A_8^c II + III (A_{11}^c + A_{12}^c + 2A_{13}^c) = 0 \tag{2.46a}$$

$$A_3^c + A_4^c + 5A_5^c - II (A_{11}^c + A_{12}^c + 4A_{13}^c) = 0 \tag{2.46b}$$

$$A_6^c + A_7^c + 5A_8^c + A_9^c + A_{10}^c = 0 \tag{2.46c}$$

The second condition is imposed by the normalisation constraint on b_{ij} :

$$3A_1^c + 2A_2^c - 2A_6^c II + 4A_{13}^c III = 0 \tag{2.47a}$$

$$3A_4^c + 4A_5^c - 2II (A_{11}^c + 2A_{13}^c) = 0 \tag{2.47b}$$

$$3A_7^c + 4A_8^c + 2A_{10}^c = 0 \tag{2.47c}$$

The last condition presumes the linear modelling of the slow term, associated to the rapid term, and is imposed to satisfy the asymptotic state of a pure sheared flow. This condition yields the following relations:

$$A_5^c = -0.29 - 0.06 (A_{10}^c - A_8^c) \quad (2.48a)$$

$$A_{11}^c = -3.6 + 5 A_{10}^c - 2 A_{13}^c - 12.7 A_8^c - 3.8 A_9^c \quad (2.48b)$$

$$A_{12}^c = -24.5 - 44.2 A_{10}^c - 2 A_{13}^c + 29 A_8^c - 8 A_9^c \quad (2.48c)$$

where

$$A_8^c = 0.8 \quad A_9^c = -1.0 \quad A_{10}^c = -0.01 \quad A_{13}^c = 0. \quad (2.49)$$

The solution of this system determines entirely the A_i^c coefficients. The B_i coefficients are given by

$$B_3 = \frac{2}{27} \frac{1}{II_d} [41 + 42 II - 0.1 F (221 + 420 II)] \quad (2.50a)$$

$$B_3'' = -\frac{14}{3} \frac{1}{II_d} (1 + 3 II) + 0.6 F \frac{1}{(1 + 3 II)} \quad (2.50b)$$

$$B_3''' = \frac{1}{3} \frac{1}{II_d} (55 + 84 II) \quad (2.50c)$$

$$B_4 = \frac{3}{II_d} - 0.9 F \frac{1}{(1 + 3 II)} \quad (2.50d)$$

$$B_4''' = -\frac{9}{II_d} \quad (2.50e)$$

$$B_5 = -\frac{1}{30} (10 + 21 F) \frac{1}{(1 + 3 II)} \quad (2.50f)$$

$$B_6 = -18 \frac{II}{II_d} + 3 F \frac{1}{(1 + 3 II)} \quad (2.50g)$$

$$B_7 = -\frac{9}{II_d} - 1.8 F \frac{1}{(1 + 3 II)} \quad (2.50h)$$

$$B_8 = \frac{1}{5} (3 F - 5) \frac{1}{(1 + 3 II)} \quad (2.50i)$$

$$B_9 = -\frac{3}{(1 + 3 II)} \quad (2.50j)$$

The equation for the dissipation rate is closed in the conventional manner, with $C_{\varepsilon_1} = 1.44$ and $C_{\varepsilon_2} = 1.83$.

2.2.2 Models of the slow term

Rotta model

The model proposed by Rotta (1951) is linear, and simply proportional to the anisotropy tensor:

$$\overline{\phi}_{ij}^S = -C_1 b_{ij} \quad (2.51)$$

with $C_1 = 3.0$. This formulation corresponds to the first term in the expansion of the isotropic functional depending only on the Reynolds stress anisotropy tensor, with the following coefficients:

$$\beta_1^S = -C_1 \quad \beta_2^S = 0 \quad (2.52)$$

In the computations reported here, this model is associated with the LRR model and used with their rapid term model. Even though it does not give non-physical solutions, it does not allow the turbulence to reach a 2C state.

Lumley model

The non-linearities can be introduced in the slow term through the coefficients defined as functions of stress anisotropy itself, or by taking into account the quadratic term of the functional. In fact the Cayley-Hamilton theorem closes this term at the quadratic level, if expressed only in terms of stress anisotropy tensor, so that the quadratic expression is the most complete tensorial expansion. The model proposed by Lumley (1978) adopts the first possibility and therefore can be characterized as quasi-linear:

$$\overline{\phi}_{ij}^S = -\beta b_{ij} - \gamma {}^D b_{.ij}^2 \quad (2.53)$$

where

$$\beta = 2 + \frac{F}{9} \exp\left(-\frac{7.77}{\sqrt{R_t}}\right) \left[\frac{72}{\sqrt{R_t}} + 80.1 \ln(1 + 62.4(-II + 2.3 III)) \right] \quad (2.54a)$$

$$\gamma = 0 \quad (2.54b)$$

and $R_t = 4K^2/9\nu\varepsilon$. Recalling that the ${}^D b_{.ij}^2$ denotes the deviator $b_{.ij}^2 + 2/3 II \delta_{ij}$, this above model expression corresponds to the functional with the following coefficients:

$$\beta_1^S = -\beta \quad \beta_2^S = -\gamma \quad (2.55)$$

This model was calibrated on the experiment of Comte-Bellot and Corrsin (1966) for configurations where the structures of the turbulence are of the disk type, that is $III < 0$.

Sarkar and Speziale model

The Sarkar and Speziale (1990) model is defined by a quadratic functional with constants coefficients. The coefficients have been adjusted with reference to the behaviour of the invariants of the anisotropy tensor in the case of return to isotropy of an homogeneous turbulence, yielding:

$$\overline{\phi}_{ij}^S = -C_1 b_{ij} + 3(C_1 - 2) {}^D b_{.ij}^2 \quad (2.56)$$

with $C_1 = 3.4$. Although this models satisfies the realisability condition in the invariant map, just as Rotta (1951) model it still does not allow the turbulence to reach a 2C state e.g. in the immediate vicinity of walls. This model is associated to the Speziale *et al.* (1991) model.

Fu, Launder et Tselepidakis model

The slow term of Fu *et al.* (1987), that includes the deviator of the dissipation rate tensor, is in full quadratic form:

$$\overline{\phi}_{ij}^S = -2 C_1 \sqrt{F} [b_{ij} + \gamma {}^D b_{.ij}^2] - 2 (1 - \sqrt{F}) b_{ij} \quad (2.57)$$

so that the coefficients can be written as:

$$\beta_1^S = -2 C_1 \sqrt{F} - 2 (1 - \sqrt{F}) \quad \beta_2^S = -2 \gamma C_1 \sqrt{F} \quad (2.58)$$

with $C_1 = -60 II$ and $\gamma = 1.2$.

This model has been developed in order to comply with the 2C realisable limit.

Ristorcelli, Lumley and Abid model

The slow term, associated to the Ristorcelli *et al.* (1994) model, also includes the deviator of the dissipation rate tensor, and is of the same type as the Lumley (1978) model: the nonlinearity is included through the coefficient of the linear term, which is expressed as a function of the stress anisotropy invariants:

$$\overline{\phi}_{ij}^S = \beta_1^S b_{ij} + \beta_2^S {}^D b_{.ij}^2 \quad (2.59)$$

with

$$\beta_1^S = -2 + 31 II \sqrt{F} \quad \beta_2^S = 0 \quad (2.60)$$

For simplicity, the non-linear term is not taken into account, and the value of β_1^S is tuned to satisfy the isotropic limit where $\beta_1^S = -2$, as well as the asymptotic state in a pure shear flow, where $\beta_1^S = -3.4$.

2.3 Models considered for the compressible cases

2.3.1 Wu, Ferziger and Chapman model

The closure developed by Wu *et al.* (1985) is derived from an inspection of the scale behaviour in the spectral space for homogeneous flows. This model is defined by the following set of model equations: :

$$\frac{dK}{dt} = P - \varepsilon \quad (2.61a)$$

$$\frac{d\varepsilon}{dt} = -\varepsilon/K + C_1 P \varepsilon/K - (C_4 - C_1) \frac{2}{3} S_{kk} \varepsilon \quad (2.61b)$$

$$\frac{d\tau}{dt} = \frac{5}{11} + C_5 \left(\frac{\varepsilon\tau}{K} - \frac{6}{11} \right) + C_6 \frac{1}{3} S_{kk}\tau \quad (2.61c)$$

where $C_1 = 2$, $C_4 = 1.0$, $C_5 = -1.1$ and $C_6 = -0.5$.

Chapter 3

Homogeneous test cases

The performance of the homogeneous closures can be compared in various homogeneous turbulent flows of distinct characteristics. The focus of our study is the treatment of the pressure-strain correlation and of the turbulent scale, the latter provided by the standard dissipation rate transport equation. It should be noted that the decomposition of the pressure-strain correlations into a slow and a rapid term originates from the character of various terms in the Poisson equation for the fluctuating pressure, where some terms are associated with the mean flow deformation (rapid term) and some only with the fluctuating turbulence properties (slow term). However, the decomposed terms do not correspond strictly to two distinct processes so that there is no real justification of assessing their behaviour separately in a general flow (Speziale *et al.*, 1992). The closure of the slow and of the rapid terms can, however, be individually validated by considering selected flows where each of these parts represent the physical processes associated with the pressure-strain term in a preponderant manner. It is therefore justified to compare models for the rapid term whenever the turbulent is subjected to rapid distortions of the mean flow, and the models for the slow term when the flow, without any mean deformation, evolves toward an isotropic turbulent state.

The homogeneous test cases can, therefore, be classified into three types: flows that reach the rapid distortion limit, flows that are allowed to relax towards the isotropic state, and flows that are in an intermediate state.

The return to isotropy belongs to the test cases for which the turbulence is initially non isotropic. Here it is necessary to know the initial values of every variable that appears in the considered closure level. For example, for the second moment closure, we need to know initial Reynolds stress components and the dissipation rate of the kinetic energy. We can further distinguish the cases according to whether or not the initial variables were obtained from the application of a rapid distortion to an initially isotropic turbulence.

Two of the flow types are particularly illustrative

flows subjected to irrotational deformations, such as flow in axisymmetric contraction, axisymmetric expansion, and the plane deformation: these three modes of deformation all lead to very different turbulent structures. For all these three flows direct numerical simulations are available (Lee and Reynolds, 1985), covering a wide

range of conditions, including mild deformations that have also been investigated experimentally, to the rapidly distorted ones. Analytical solutions for some of the cases are also available (Lee, 1990). flows with a mean rotation, possibly imposed by a rotating frame. The pure shear flows subjected to an orthogonal rotation, as well as nonrotating ones have been calculated by large eddy simulations by Bardina *et al.* (1983). Kassinos and Reynolds (1995) also reported on rapid approximation of these flows. Pure rotation applied to an initially axisymmetric turbulence has also been considered using the rapid distortion approach by (Cadiou and Piquet, 1994).

For comparison, it is useful to express the equations in non-dimensional form. The characteristic parameter defining the intensity of the deformation of the mean flow is denoted as S . This allows to compare each distortion reduced to the same nondimensional time, defined by

$$t^* = S t \quad (3.1)$$

except for the pure rotation case, where the nondimensional time is given by

$$t^* = \Omega t \quad (3.2)$$

The mean flow equations can now be written in the nondimensional form:

$$\frac{\partial W_{ij}^*}{\partial t^*} = S_{ik}^* (W_{jk}^* - R_o \theta_{jk}^*) - (W_{ik}^* - R_o \theta_{ik}^*) S_{kj}^* + (W_{ik}^* R_o \theta_{jk}^* - R_o \theta_{ik}^* W_{jk}^*) \quad (3.3a)$$

$$\begin{aligned} \frac{\partial R_{ij}}{\partial t^*} &= -R_{ik} (\bar{V}_{aj,k}^* - 2 R_o \theta_{jk}^*) - R_{jk} (\bar{V}_{ai,k}^* - 2 R_o \theta_{ik}^*) \\ &+ \phi_{ij}^R(R_{mn}, S_{mn}^*, W_{amn}^*) + \phi_{ij}^S(R_{mn}, \varepsilon/S, R_t) - \varepsilon_{ij}(R_{mn}, \varepsilon/S, R_t) \end{aligned} \quad (3.3b)$$

$$\frac{\partial(\varepsilon/S)}{\partial t^*} = -C_{\varepsilon 1} R_{mn} S_{mn}^* \frac{(\varepsilon/S)}{K} - C_{\varepsilon 2} \frac{(\varepsilon/S)^2}{K} \quad (3.3c)$$

However, in the discussion that follows we will omit the star (*) for simplicity!

ANNE: ARE YOU SIMPLY OMITTING THE STAR, switching again to DIMENSIONAL EQUATIONS?

The non-dimensional parameter that characterises the time scale of turbulent motion is defined by:

$$\tau = \frac{\varepsilon}{S K} \quad (3.4)$$

This allows to characterise various distortions according to their intensities. Another nondimensional parameter can be used also when irrotational strain is considered, that is the total strain parameter, defined by:

$$c = \exp \left(\int_0^t S(t') dt' \right) \quad (3.5)$$

The expression and the value of c varies then according to the considered configuration.

In the case of a homogeneous flow, the dissipation rate of kinetic turbulent energy can be directly written in terms of the vorticity and the dynamic viscosity as:

$$\varepsilon = \nu \omega^2 \quad (3.6)$$

so that the turbulence Reynolds number defined as:

$$R_t = \frac{K^2}{\nu \varepsilon} \quad (3.7)$$

can also be expressed as

$$R_t = \left(\frac{K \omega}{\varepsilon} \right)^2 \quad (3.8)$$

The description of the test cases and their characteristic parameters are given in the tables below.

3.1 Decay of isotropic turbulence

Homogeneous isotropic turbulence is the simplest state that a turbulent flow can have. The flows investigated by Lee and Reynolds (1985) corresponds to

| | ν_0 | ε_0 | K_0 | b_{11} | b_{22} | b_{33} | b_{12} | b_{13} | b_{23} |
|-----|----------|-----------------|--------|----------|----------|----------|----------|----------|----------|
| HIA | 0.004299 | 2.264 | 0.4735 | 0 | 0 | 0 | 0 | 0 | 0 |
| HIB | 0.001706 | 0.898 | 0.4735 | 0 | 0 | 0 | 0 | 0 | 0 |
| HIC | 0.004299 | 2.350 | 0.4830 | 0 | 0 | 0 | 0 | 0 | 0 |
| HID | 0.004299 | 2.344 | 0.4775 | 0 | 0 | 0 | 0 | 0 | 0 |
| HIE | 0.001377 | 0.570 | 0.4975 | 0 | 0 | 0 | 0 | 0 | 0 |

In this case the equations are very simple and only the dissipation of the turbulence kinetic energy remains to be defined in order to close the system. The direct numerical simulation give an exponential law of decay, i.e. a constant slope in $\log\text{-}\log k - t$ diagram. This has also been observed by experiments with the grid turbulence, Comte-Bellot and Corrsin (1966).

3.2 Irrotational mean deformations

The intensity of the deformation of the mean flow defined by Lee and Reynolds (1985) is:

$$S_d = \sqrt{\frac{1}{2} S_{mn} S_{mn}} \quad (3.9)$$

and the characteristic parameter of the turbulent time is given by:

$$S^* = 2 \frac{K}{\varepsilon} S_d \quad (3.10)$$

or again

$$\tau = 2 \frac{S_d}{S} \frac{1}{S^*} \quad (3.11)$$

The simulations of Lee and Reynolds (1985) are performed for various values of S^* , covering the plane distortions investigated also experimentally by Tucker and Reynolds (1968) or Mills and Corrsin (1959), as well as rapidly distorted axisymmetric and plane flow cases.

3.2.1 Axisymmetric deformation

The mean deformation rate S_{ij} is here identical to the imposed mean velocity gradient, and can be defined by

$$S_{ij} = \begin{bmatrix} S & 0 & 0 \\ 0 & -\frac{1}{2}S & 0 \\ 0 & 0 & -\frac{1}{2}S \end{bmatrix} \quad (3.12)$$

where the characteristic parameter $S = S_{11}$ is related to the intensity of the deformation of the mean flow by

$$|S| = \frac{2}{\sqrt{3}} S_d \quad (3.13)$$

S is positive in the case of a contraction and negative in the case of an expansion. The nondimensional deformation time scale is given by

$$\tau = \sqrt{3} \frac{1}{S^*} \quad (3.14)$$

Even if these two cases differ only by the sign of S , they lead to two very different behaviour of the turbulence. The evolution of the anisotropy of the Reynolds stress tensor depends, however, in both cases on the total deformation parameter c , defined by:

$$c = e^{|S|t} \quad (3.15)$$

and not on the mean deformation.

Axisymmetric contraction

The eddy structures of various scales, initially randomly oriented in the isotropic turbulent state, tend to become aligned and stretched in the positive direction of the deformation, and to decrease in the lateral directions. Therefore, at high values of the total deformation rate, the turbulence reaches an organised pattern with cigar-like structures of circular cross-sections. The components of the pressure-strain tensor decrease under the influence of the axisymmetric contraction. The behaviour of the turbulent flow, described by Lee (1990) in the rapid distortion case, shows clearly that the orientation of the structures depend solely on the imposed total deformation rate. The larger the deformation rate, the more aligned become the structures with the positive deformation axis. The rapid distortion assumption also allows to determine an asymptotic state of the 3D-2C type around this symmetry axis. This state is reached at $c = 3.0$ (Lee, 1990).

Among several cases considered by Lee and Reynolds (1985), we have selected two test cases, defined by the following parameters:

| | S_d | S^* | ε_0 | K_0 | ω_0 | b_{11} | b_{22} | b_{33} | b_{12} | b_{13} | b_{23} |
|-----|-------|-------|-----------------|---------|------------|----------|----------|----------|----------|----------|----------|
| AXL | 8.66 | 9.653 | 0.2117 | 0.11795 | 7.0167 | 0 | 0 | 0 | 0 | 0 | 0 |
| AXM | 86.6 | 96.53 | 0.2117 | 0.11795 | 7.0167 | 0 | 0 | 0 | 0 | 0 | 0 |

with $\nu_0 = 0.004299$, or equivalently:

| | $ S $ | τ_0 | ε_0 | K_0 | R_{t_0} | b_{11} | b_{22} | b_{33} | b_{12} | b_{13} | b_{23} |
|-----|-------|----------|-----------------|---------|-----------|----------|----------|----------|----------|----------|----------|
| AXL | 10.00 | 0.179 | 0.2117 | 0.11795 | 15.28 | 0 | 0 | 0 | 0 | 0 | 0 |
| AXM | 100.0 | 0.0179 | 0.2117 | 0.11795 | 15.28 | 0 | 0 | 0 | 0 | 0 | 0 |

The first test case, AXL, has an evolution of the kinetic energy close the the experiment of Mills and Corrsin (1959). The second one, AXM, with a strong deformation, corresponds to the rapid distortion approximation.

Figures (3.1) to (3.4) show the evolution of the turbulent kinetic energy and the Reynolds stress anisotropy tensor for AXL given by the various models. In order to facilitate the reading of these results, the graphs are grouped in two groups, the first one corresponds to the tensorially linear formulations (IP, LRR, SSG) and the second the non linear ones (FLT,SL,RLA). It is clear here that in the AXL flow, the SSG model does not bring any amelioration over the LRR model. The FLT model has also a similar behaviour, whereas the RLA formulation gives clearly inferior performance. The SL model gives here undoubtedly better results. The next figures show the evolution of the anisotropy in the invariant map for each model. All models reproduce the evolution of the models along the axisymmetric contraction limit and clearly show the intensity of the anisotropy that is reached at the end of the contraction.

The same sort of conclusion can be reached for the AXM case. Figures(3.11) to (3.14) show again the evolution of the Reynolds stress anisotropies and the turbulent kinetic energy. The models are compared to the analytical solution for the rapid distortion.

A general conclusion emerging from this test case is that the only model that is able to correctly predict the anisotropy levels is the SL model. All other closures underestimate

the anisotropy intensity imposed by the axisymmetric contraction. It can be pointed out that the RLA model, even though it is the most recent one, performs less well than than the LRR or SSG models.

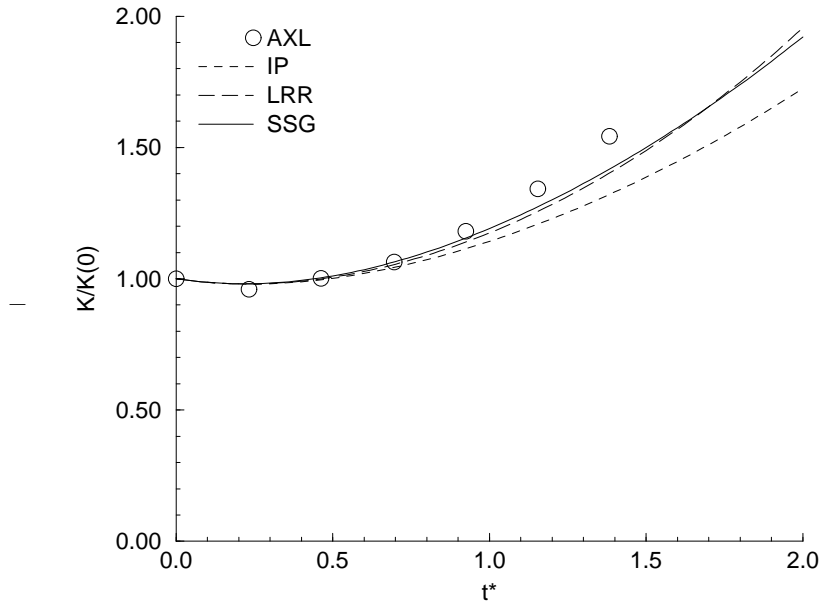


Figure 3.1: *Turbulent kinetic energy evolution for the axisymmetric contraction AXL.*

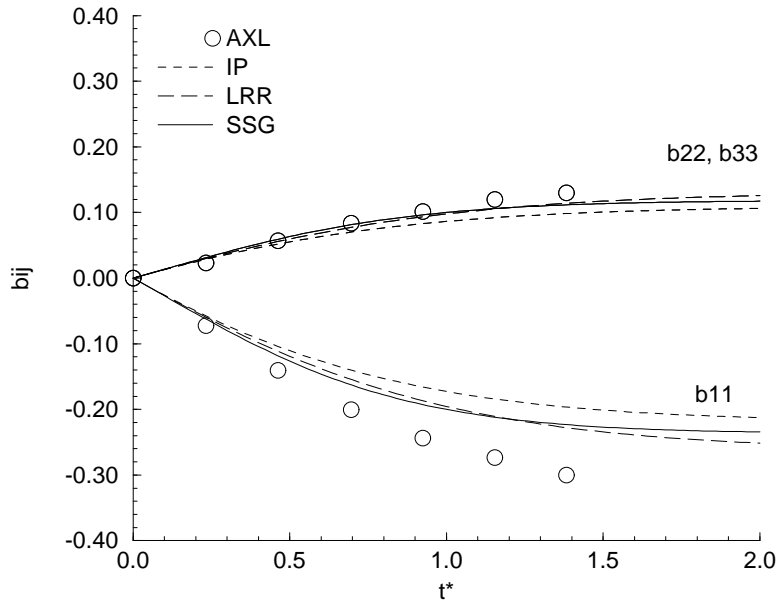
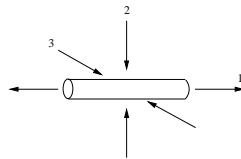


Figure 3.2: *Anisotropy tensor evolution for the axisymmetric contraction AXL.*



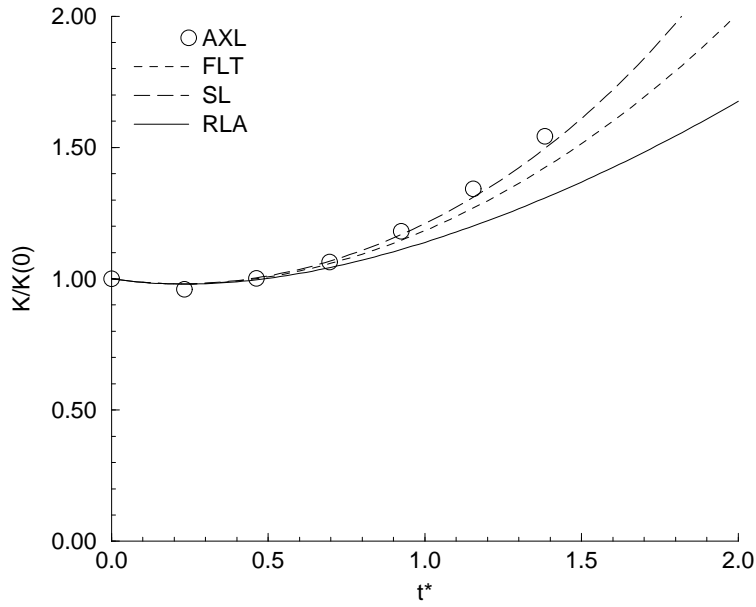


Figure 3.3: *Turbulent kinetic energy evolution for the axisymmetric contraction AXL.*

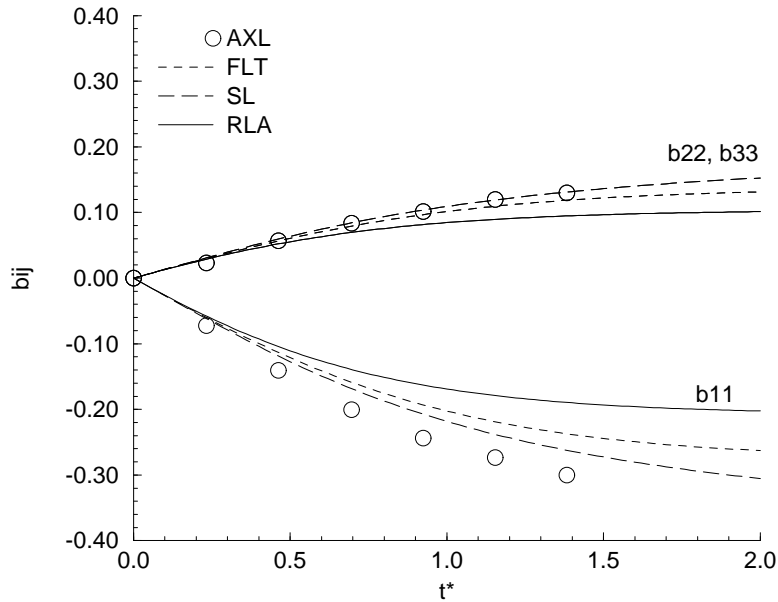
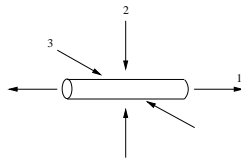


Figure 3.4: *Anisotropy tensor evolution for the axisymmetric contraction AXL.*



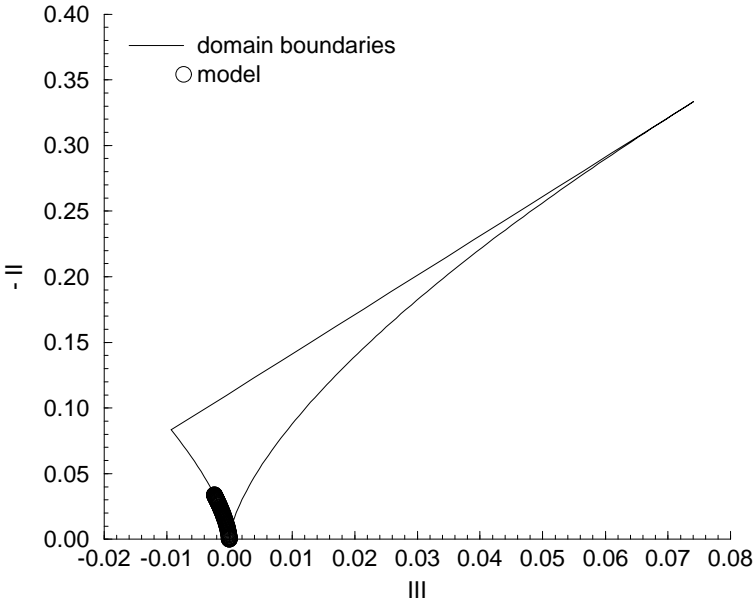


Figure 3.5: *Axisymmetric contraction AXL. IP model.*

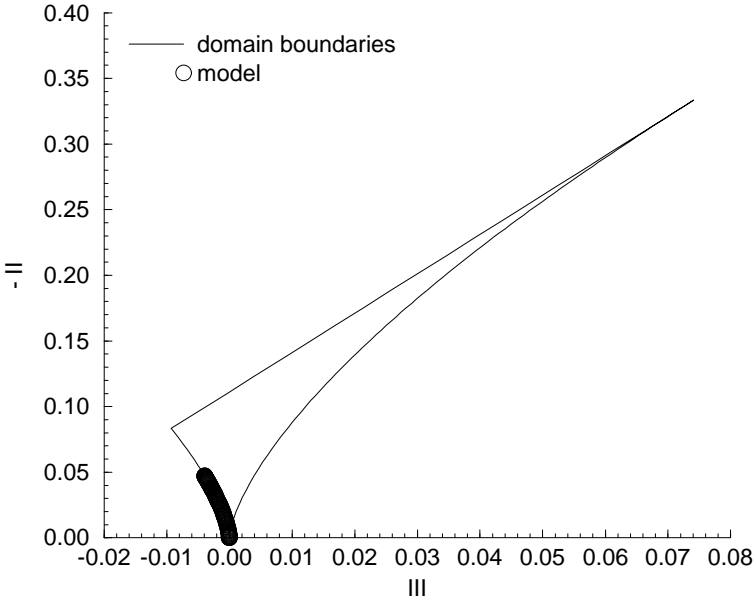
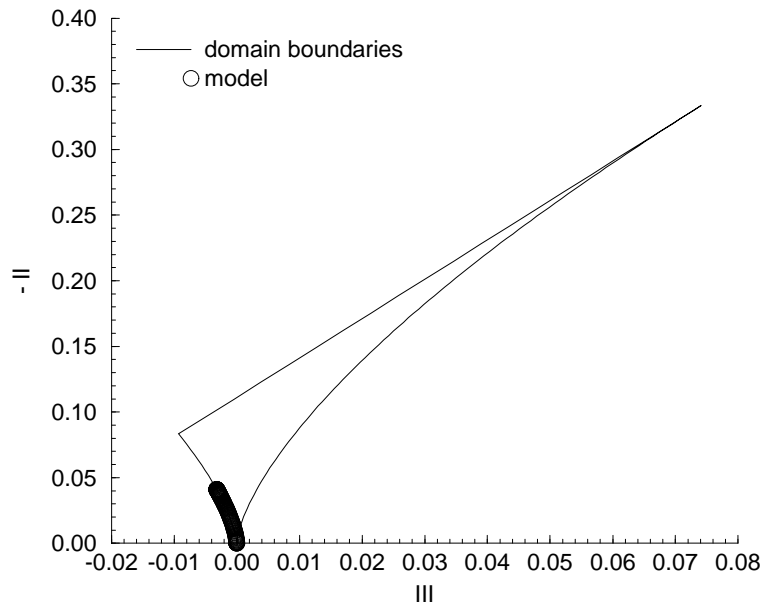
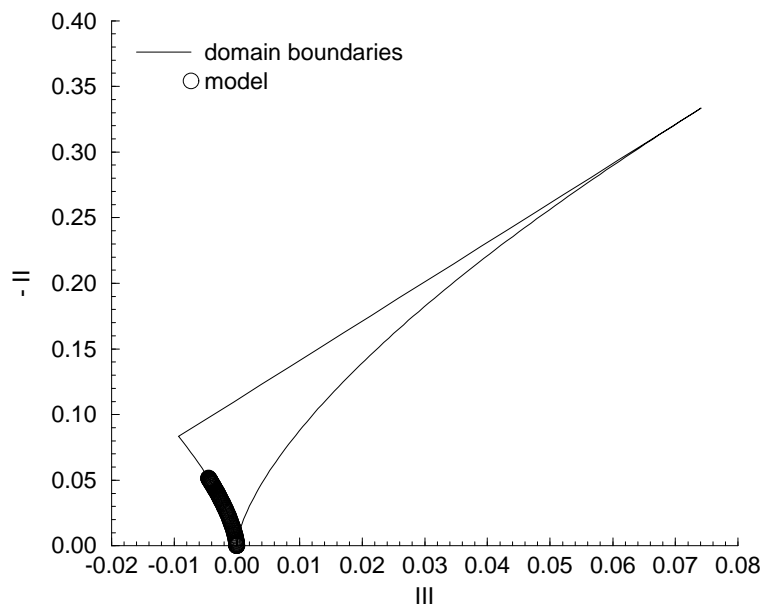


Figure 3.6: *Axisymmetric contraction AXL. LRR model.*

Figure 3.7: *Axisymmetric contraction AXL. SSG model.*Figure 3.8: *Axisymmetric contraction AXL. FLT model.*

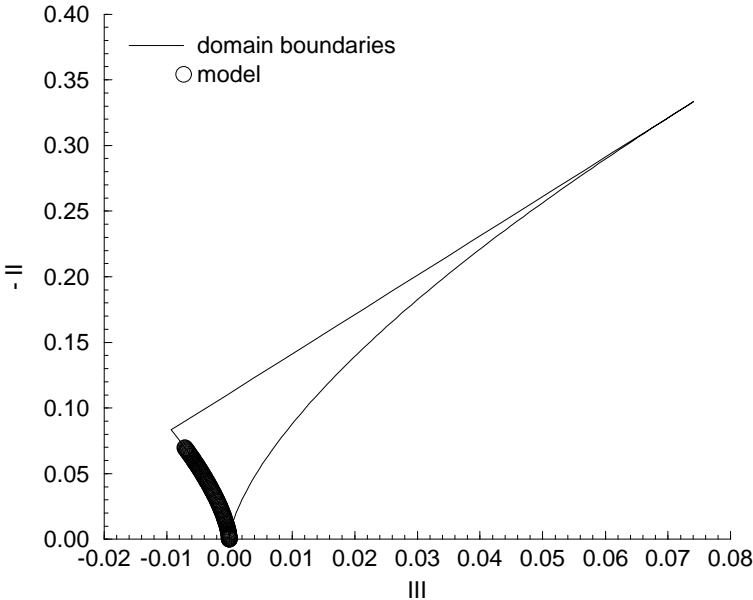


Figure 3.9: *Axisymmetric contraction AXL. SL model.*

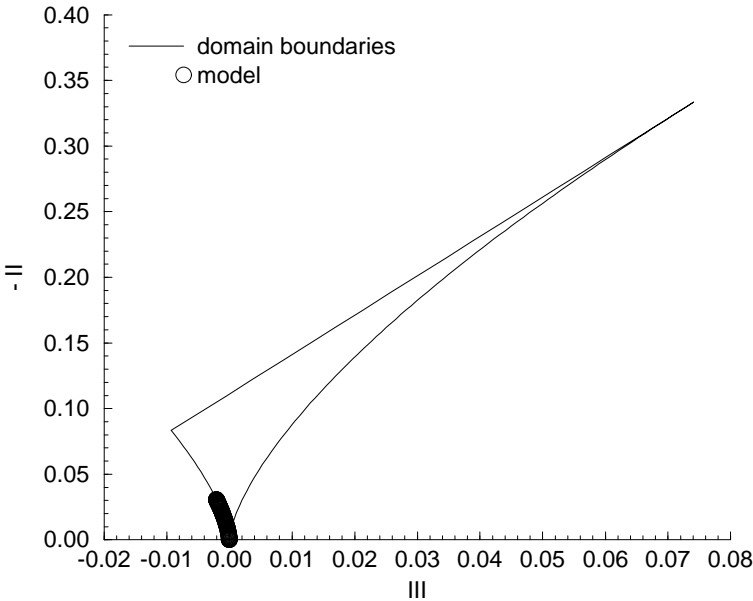


Figure 3.10: *Axisymmetric contraction AXL. RLA model.*

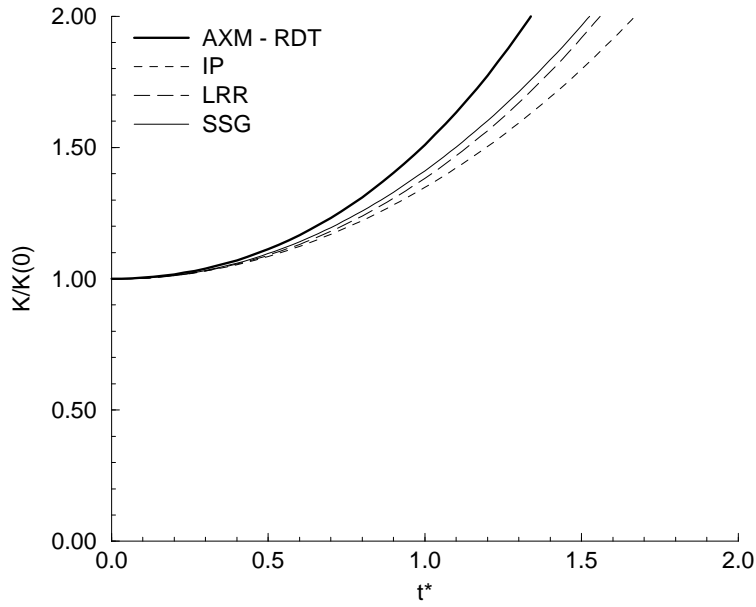


Figure 3.11: *Turbulent kinetic energy evolution for the axisymmetric contraction AXM.*

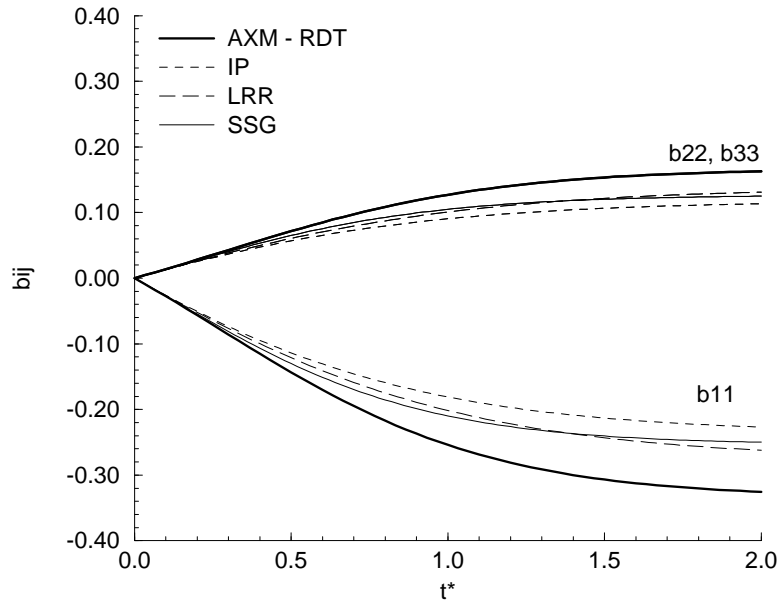
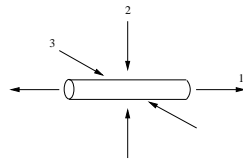


Figure 3.12: *Anisotropy tensor evolution for the axisymmetric contraction AXM.*



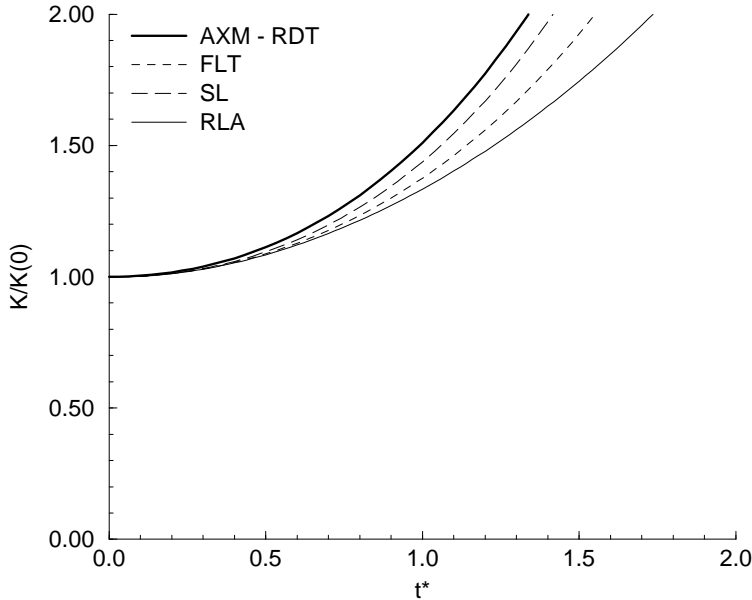


Figure 3.13: *Turbulent kinetic energy evolution for the axisymmetric contraction AXM.*

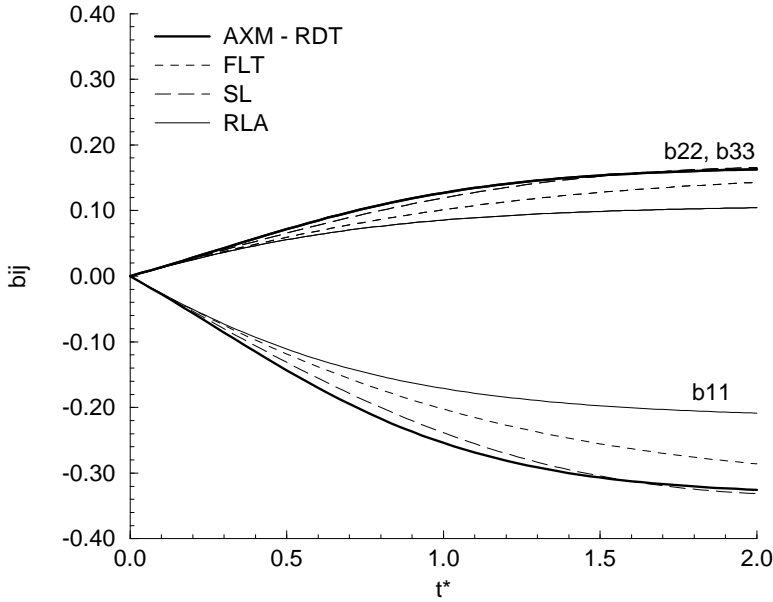
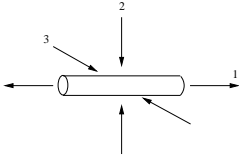
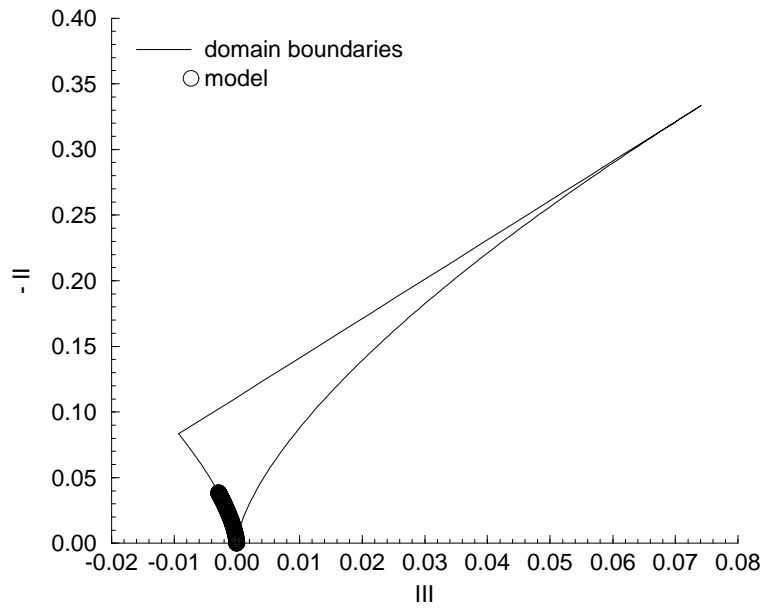
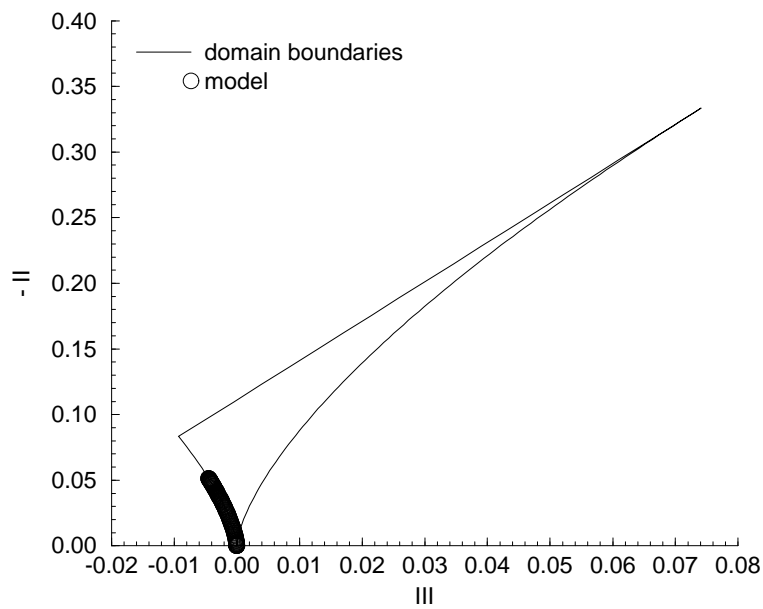


Figure 3.14: *Anisotropy tensor evolution for the axisymmetric contraction AXM.*



Figure 3.15: *Axisymmetric contraction AXM. IP model.*Figure 3.16: *Axisymmetric contraction AXM. LRR model.*

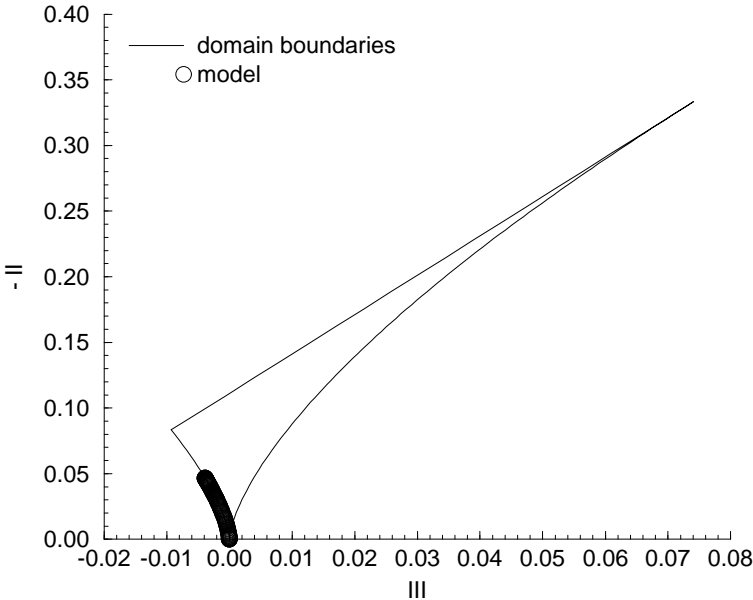


Figure 3.17: *Axisymmetric contraction AXM. SSG model.*

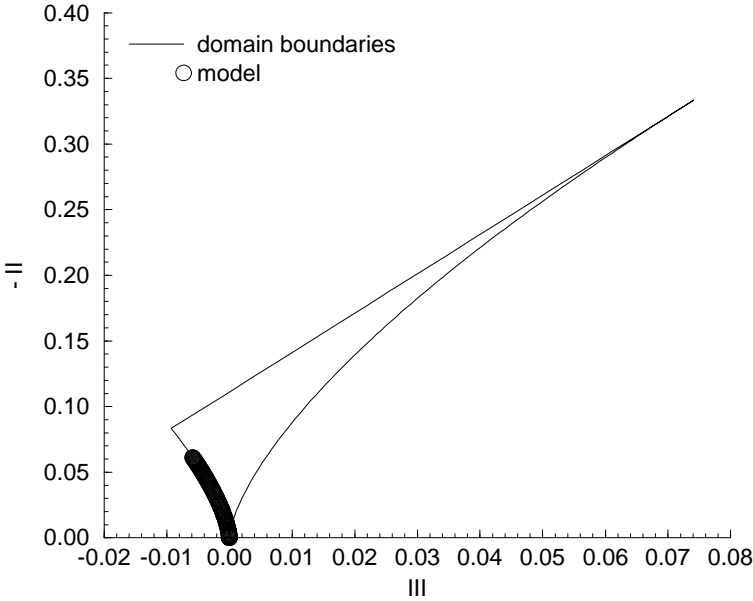
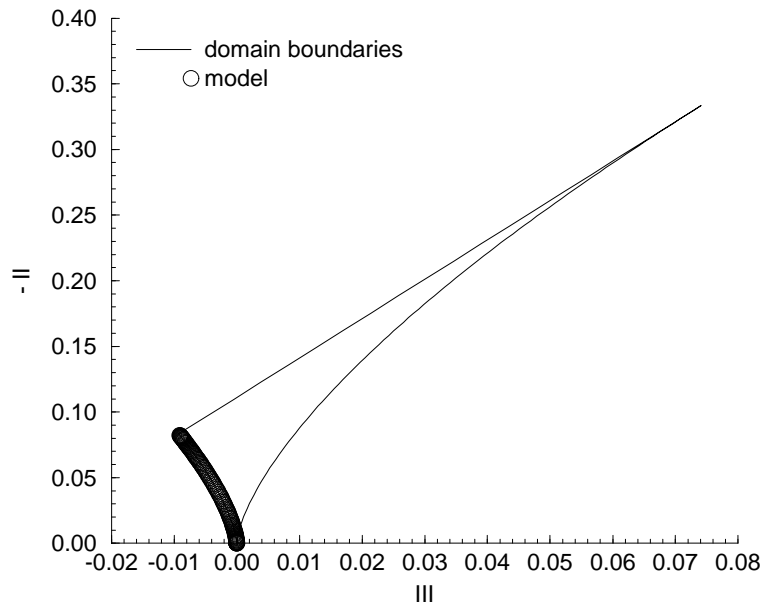
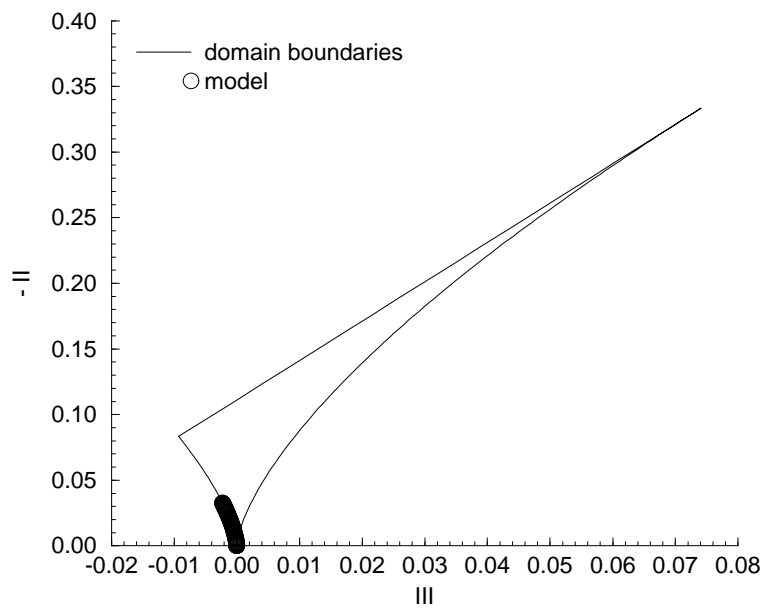


Figure 3.18: *Axisymmetric contraction AXM. FLT model.*

Figure 3.19: *Axisymmetric contraction AXM. SL model.*Figure 3.20: *Axisymmetric contraction AXM. RLA model.*

Axisymmetric expansion

When the turbulence is subjected to an axisymmetric expansion, the negative deformation rate deforms the vortical structures into relatively flat disks, orthogonal to the symmetry axis. In the same time the positive (weaker) components of the deformation rate tensor, stretch them in the radial directions. This reduced axial vorticity tends to decrease the lateral velocity fluctuations in the plan orthogonal to the symmetry axis. This decay is, however, counterbalanced by the general increase of the anisotropy level. The components of the pressure-strain tensor are augmented during the fluid motion. The asymptotic limit in the rapid distortion approximation is of the 3D-3C type, which is *a priori* less difficult to capture by the models than the rapid axisymmetric contraction limit, because it does not take place on the 2C realisability boundary.

The axisymmetric expansion cases, considered here, are taken from Lee and Reynolds (1985), and are defined by the following parameters:

| | S_d | S^* | ε_0 | K_0 | ω_0 | b_{11} | b_{22} | b_{33} | b_{12} | b_{13} | b_{23} |
|-----|--------|--------|-----------------|--------|------------|----------|----------|----------|----------|----------|----------|
| EXO | 0.6213 | 0.7071 | 0.1931 | 0.1099 | 6.702 | 0 | 0 | 0 | 0 | 0 | 0 |
| EXQ | 62.13 | 70.71 | 0.1931 | 0.1099 | 6.702 | 0 | 0 | 0 | 0 | 0 | 0 |

with again $\nu_0 = 0.004299$, or alternatively by:

| | $ S $ | τ_0 | ε_0 | K_0 | R_{t_0} | b_{11} | b_{22} | b_{33} | b_{12} | b_{13} | b_{23} |
|-----|--------|----------|-----------------|--------|-----------|----------|----------|----------|----------|----------|----------|
| EXO | 0.7174 | 2.45 | 0.1931 | 0.1099 | 14.54 | 0 | 0 | 0 | 0 | 0 | 0 |
| EXQ | 71.74 | 0.0245 | 0.1931 | 0.1099 | 14.54 | 0 | 0 | 0 | 0 | 0 | 0 |

The EXQ simulation corresponds to the rapid distortion approximation (Lee, 1990).

For the two flows in axisymmetric contraction, the models considered gave roughly the same and consistent hierarchy of performance.

For the two flows in axisymmetric expansion the performance of the models considered is different and not conclusive. In the EXO case, where the slow term has a significant role, the SL model behaves again relatively well as compared with others, but the best performance is achieved by the SSG model. In the EXQ case, where the rapid term is the major process, none of the closures is able to correctly predict the level of the final anisotropy.

It is difficult to qualify the various closures in the EXQ case, since the evolutions of the anisotropy and the kinetic energy do not follow the same tendencies in all models. Generally, we can conclude that the simplest formulations, LRR and SSG respond better to this type of deformation than more complex models.

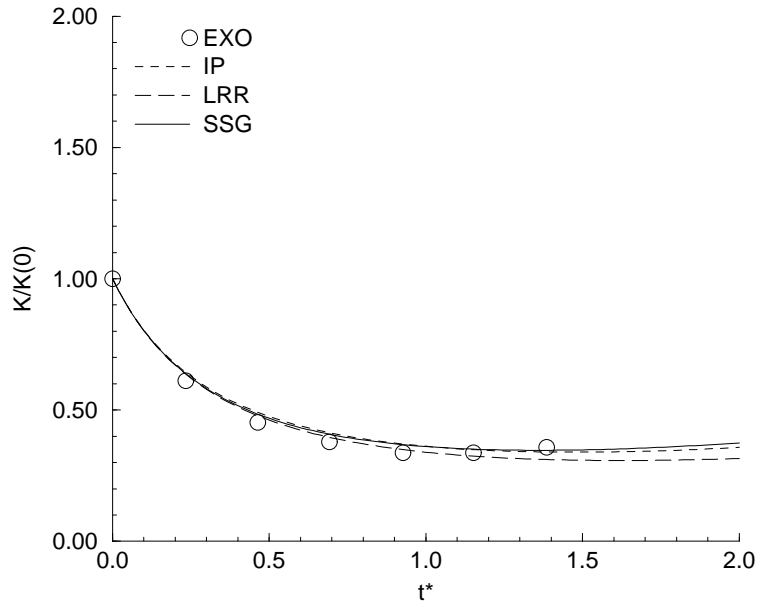


Figure 3.21: *Turbulent kinetic energy evolution for the axisymmetric expansion EXO.*

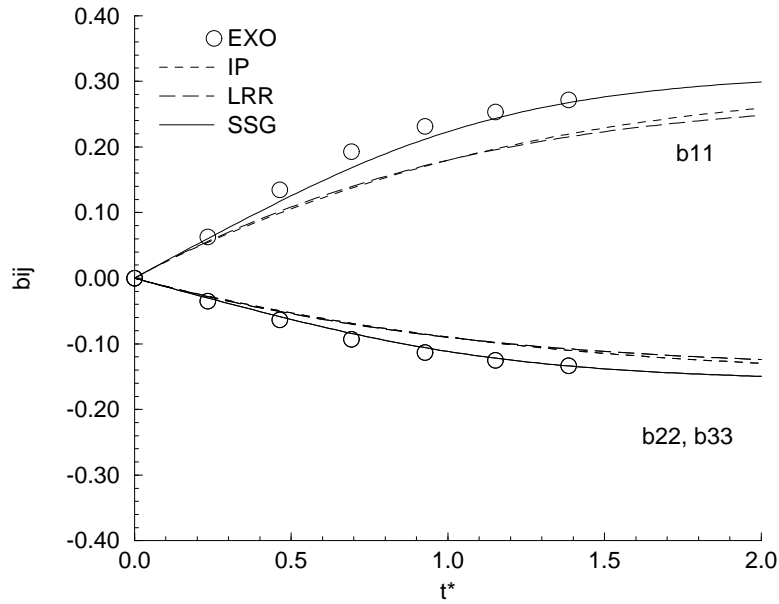
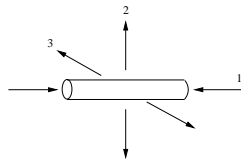


Figure 3.22: *Anisotropy tensor evolution for the axisymmetric expansion EXO.*



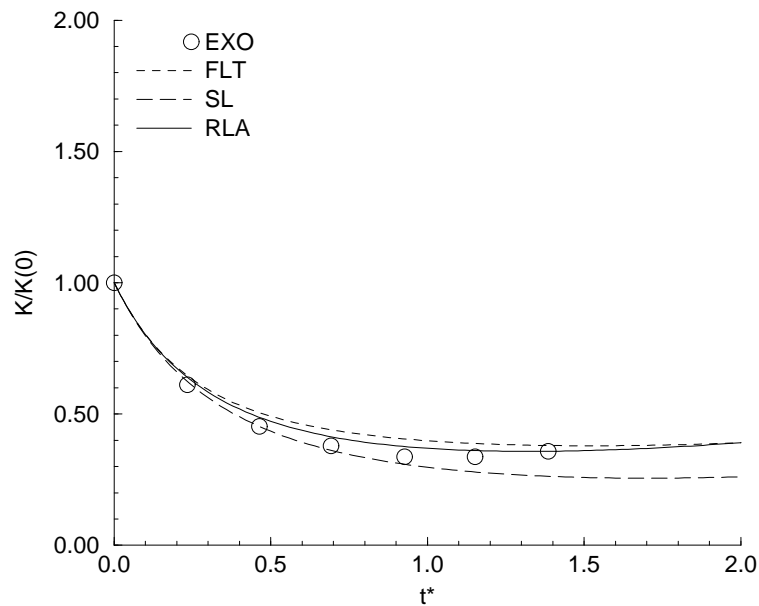


Figure 3.23: *Turbulent kinetic energy evolution for the axisymmetric expansion EXO.*

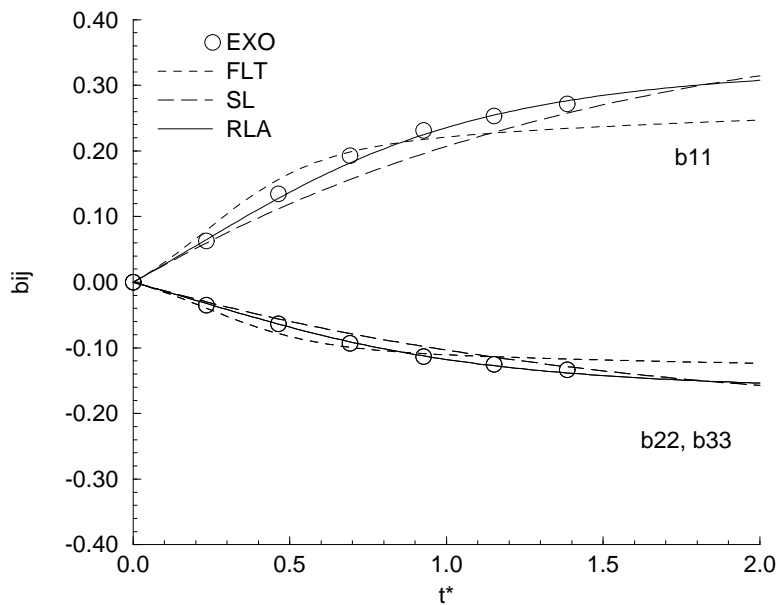
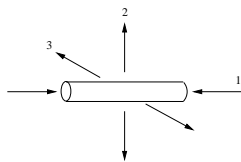
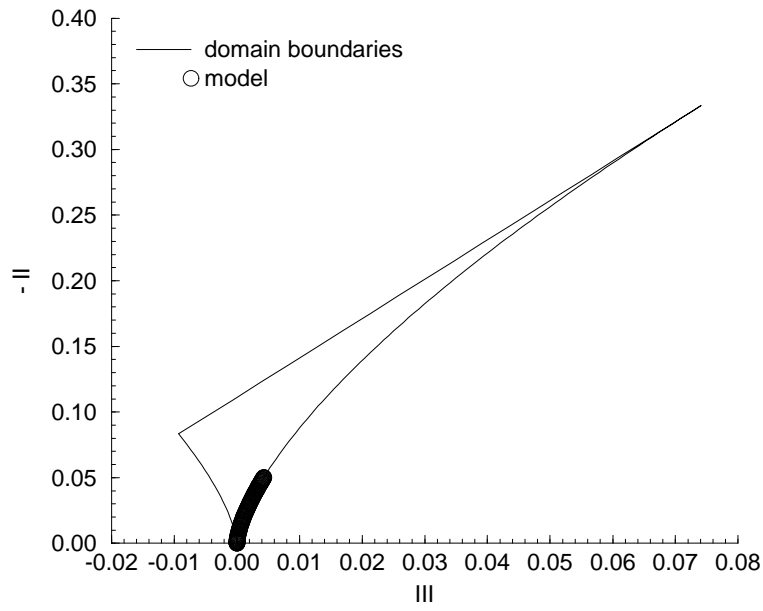
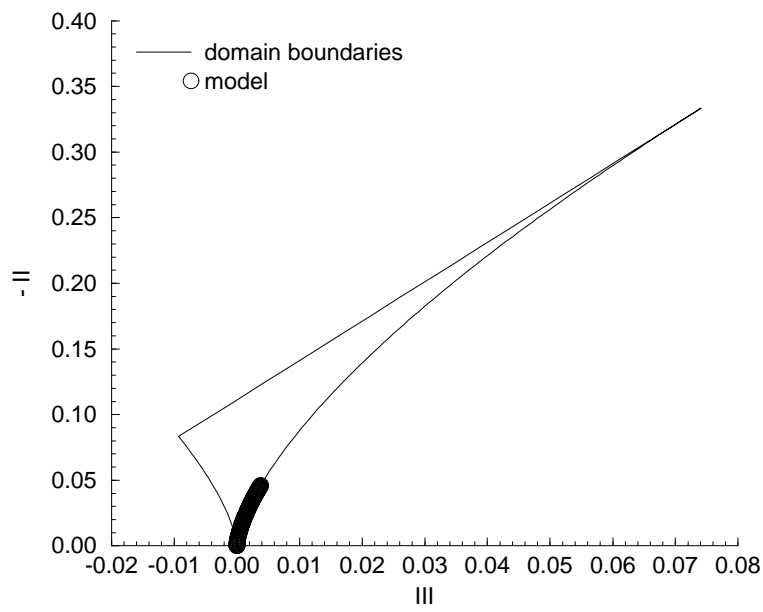


Figure 3.24: *Anisotropy tensor evolution for the axisymmetric expansion EXO.*



Figure 3.25: *Axisymmetric expansion EXO. IP model.*Figure 3.26: *Axisymmetric expansion EXO. LRR model.*

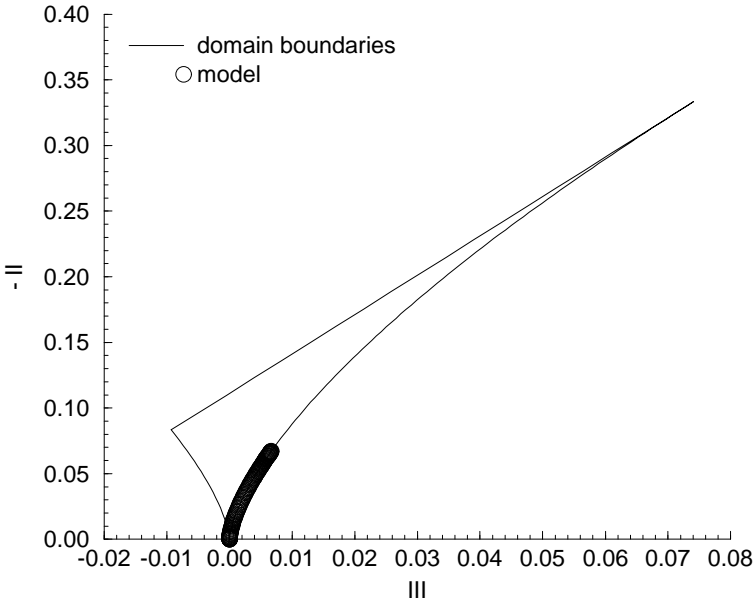


Figure 3.27: *Axisymmetric expansion EXO. SSG model.*

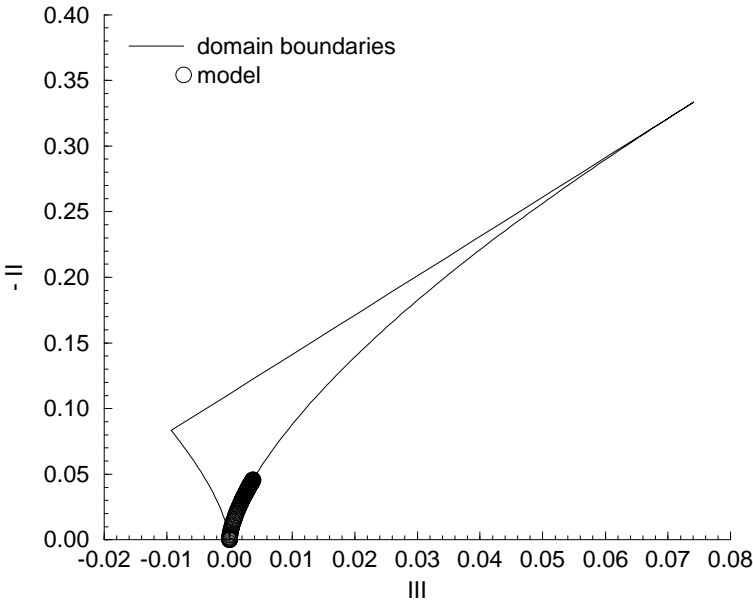
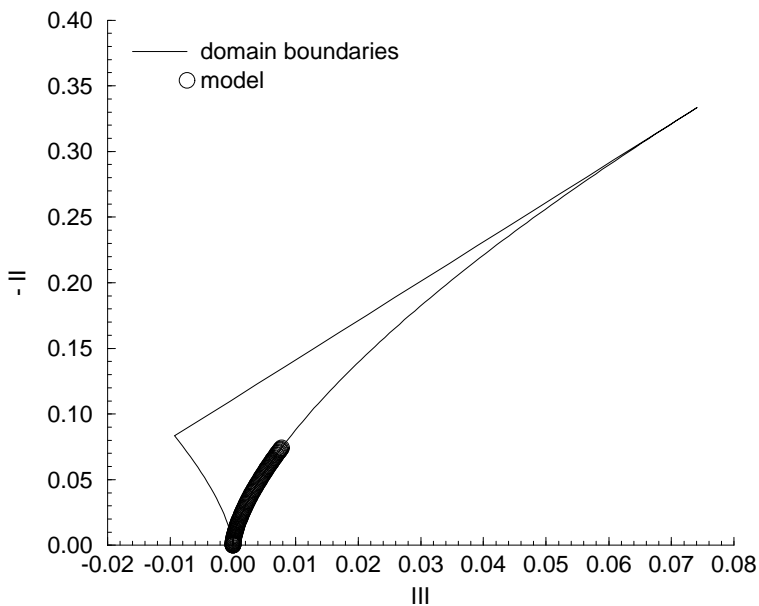
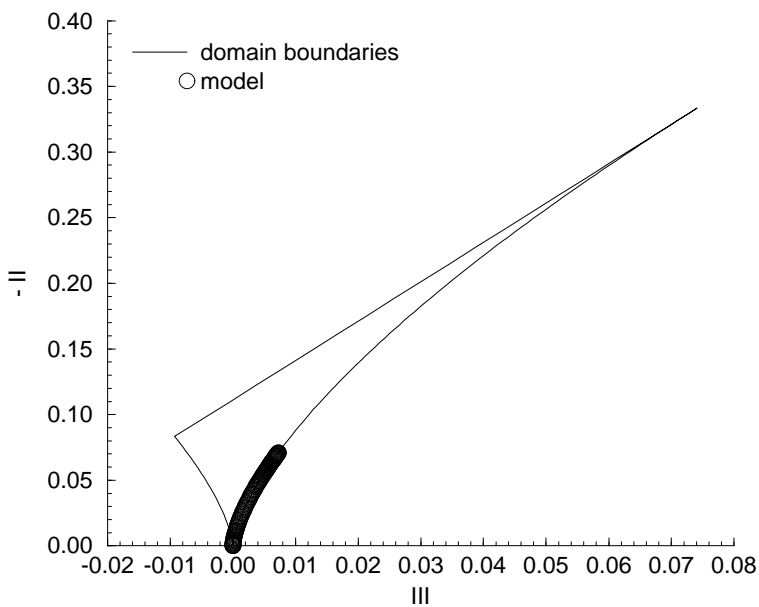


Figure 3.28: *Axisymmetric expansion EXO. FLT model.*

Figure 3.29: *Axisymmetric expansion EXO. SL model.*Figure 3.30: *Axisymmetric expansion EXO. RLA model.*

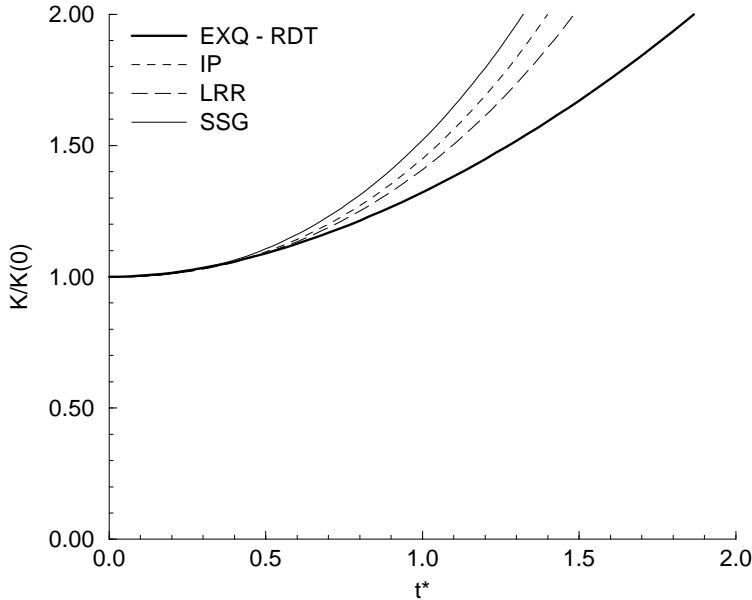


Figure 3.31: *Turbulent kinetic energy evolution for the axisymmetric expansion EXQ.*

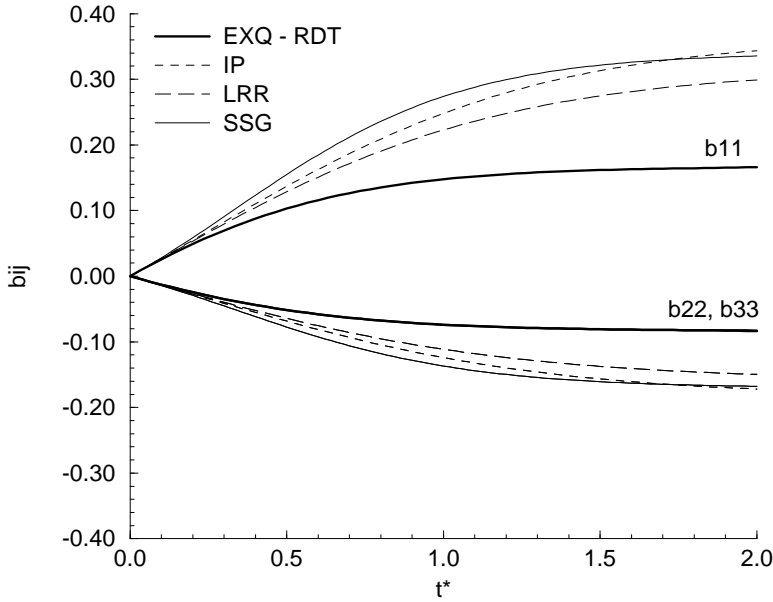
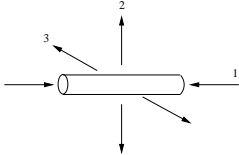


Figure 3.32: *Anisotropy tensor evolution for the axisymmetric expansion EXQ.*



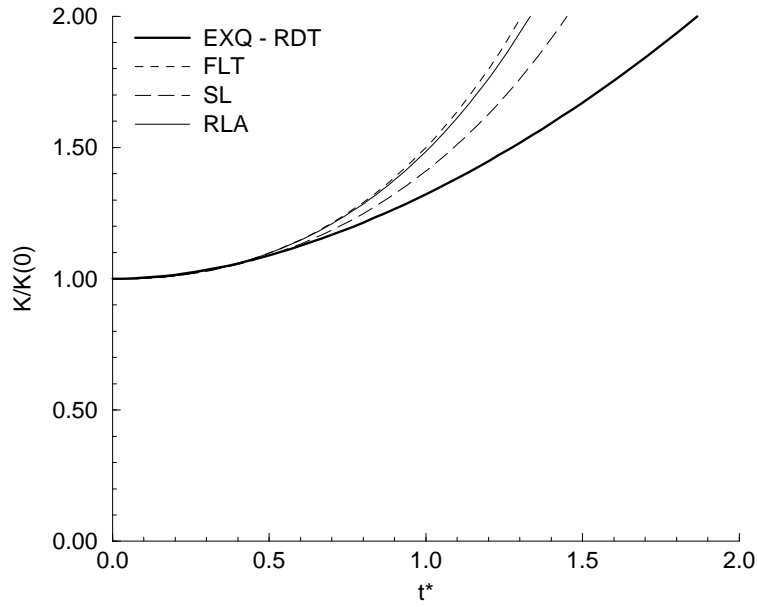


Figure 3.33: *Turbulent kinetic energy evolution for the axisymmetric expansion EXQ.*

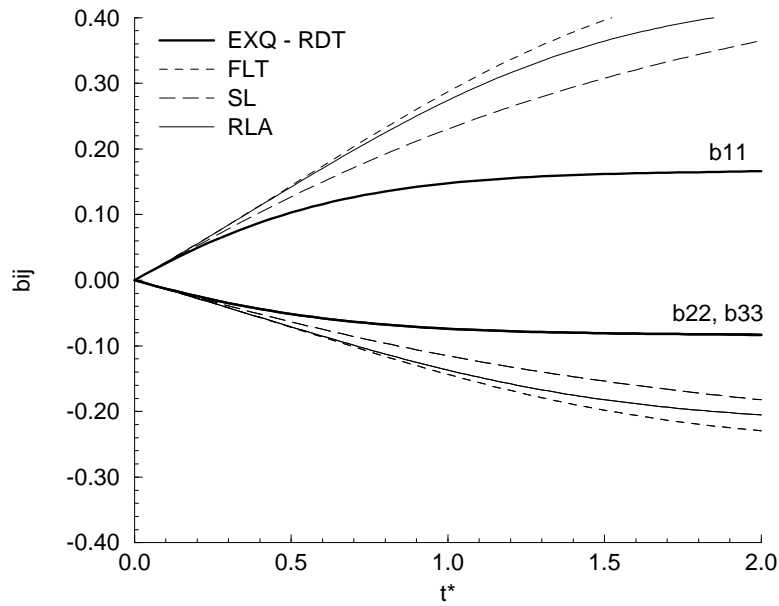
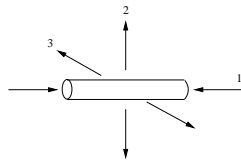


Figure 3.34: *Anisotropy tensor evolution for the axisymmetric expansion EXQ.*



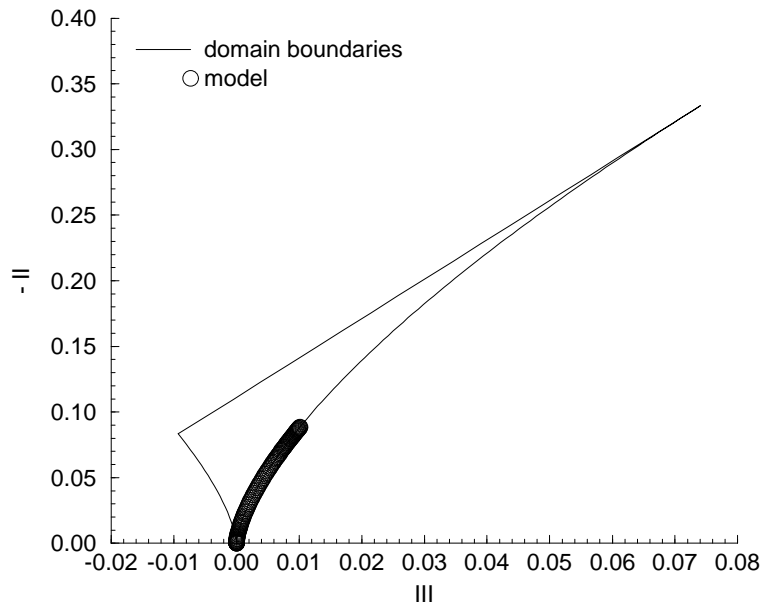


Figure 3.35: *Axisymmetric expansion EXQ. IP model.*

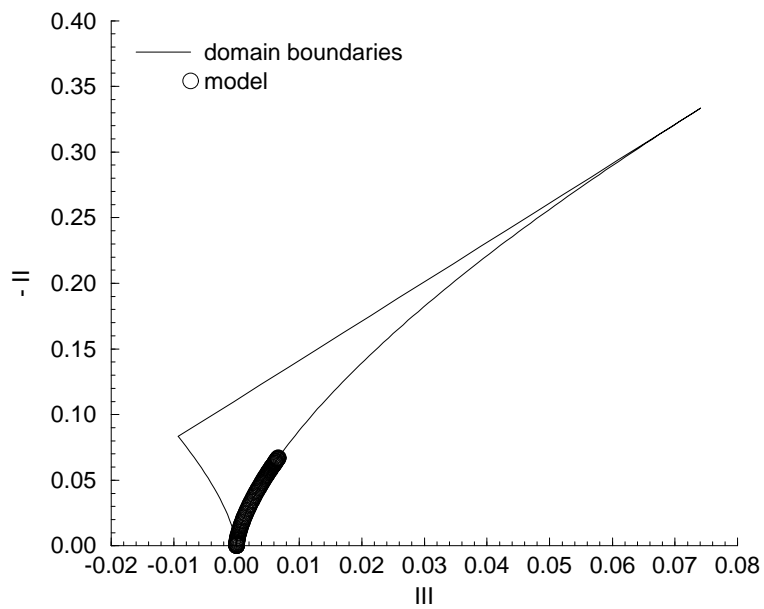
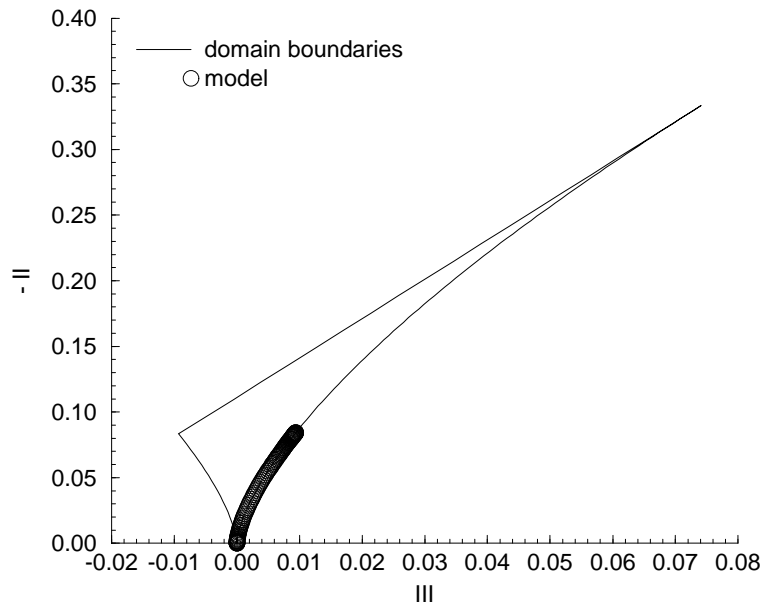
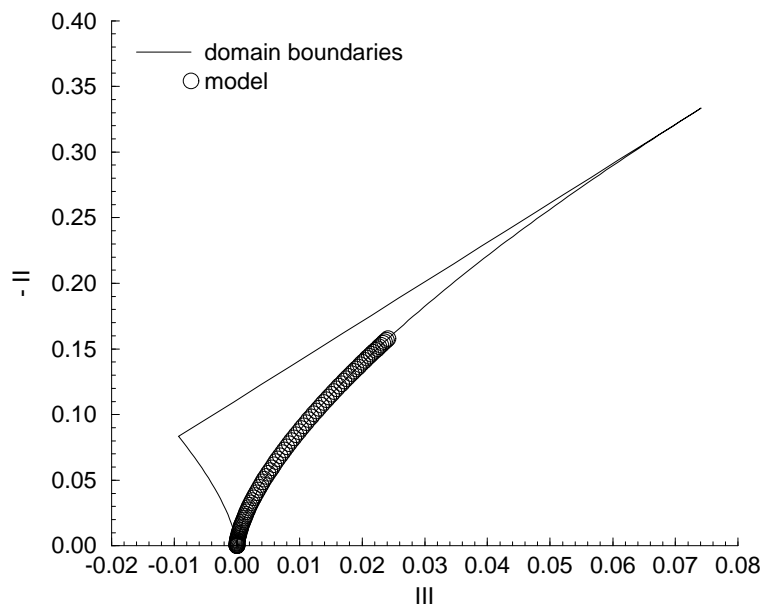


Figure 3.36: *Axisymmetric expansion EXQ. LRR model.*

Figure 3.37: *Axisymmetric expansion EXQ. SSG model.*Figure 3.38: *Axisymmetric expansion EXQ. FLT model.*

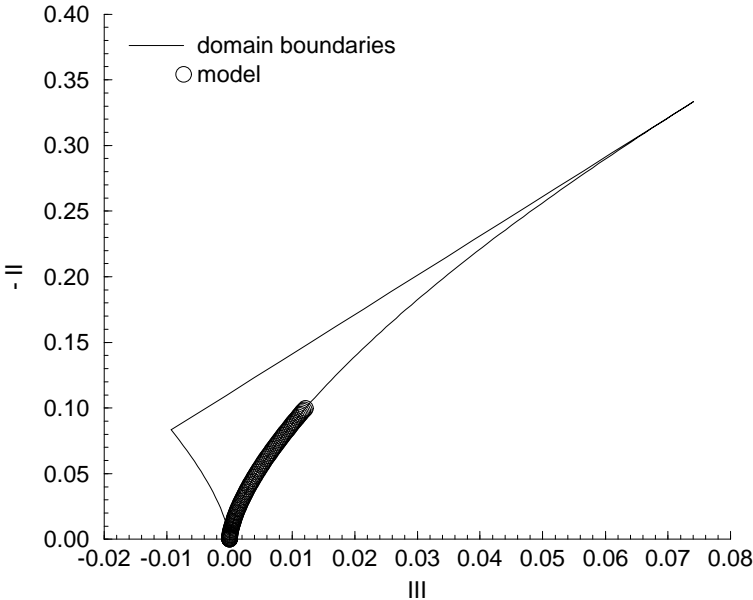


Figure 3.39: *Axisymmetric expansion EXQ. SL model.*

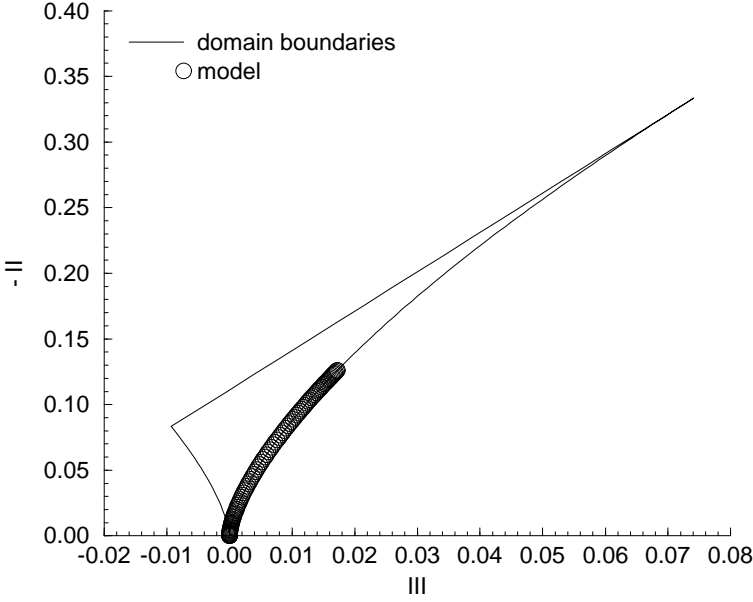


Figure 3.40: *Axisymmetric expansion EXQ. RLA model.*

3.2.2 Plane deformation.

The mean rate of strain in this type of flow is defined by the following matrix:

$$S_{ij} = \begin{bmatrix} 0 & 0 & 0 \\ 0 & -S & 0 \\ 0 & 0 & S \end{bmatrix} \quad (3.16)$$

with $S > 0$. In this case it is obvious that $|S| = S_d$ and $\tau = 2/S^*$.

The evolution of the kinetic energy and the Reynolds stress anisotropy are very sensitive to the deformation rate, especially in the direction of the contraction axis. The rapid distortion limit is similar to the case of an axisymmetric contraction.

Only two simulations has been considered, corresponding to the two extreme cases. The first one has the same evolution of the turbulence kinetic energy as in the experiment of Tucker and Reynolds (1968), though the initial parameters (particularly the dissipation rate and the imposed strain rate) are different. The second case corresponds to the rapid distortion approximation. The two flows considered are defined by the following set of parameters:

| | S_d | S^* | ε_0 | K_0 | ω_0 | b_{11} | b_{22} | b_{33} | b_{12} | b_{13} | b_{23} |
|-----|-------|-------|-----------------|--------|------------|----------|----------|----------|----------|----------|----------|
| PXA | 0.65 | 1.0 | 0.08469 | 0.0652 | 4.438 | 0 | 0 | 0 | 0 | 0 | 0 |
| PXF | 100. | 154.0 | 0.08469 | 0.0652 | 4.438 | 0 | 0 | 0 | 0 | 0 | 0 |

or, with again $\nu_0 = 0.004299$:

| | $ S $ | τ_0 | ε_0 | K_0 | R_{t_0} | b_{11} | b_{22} | b_{33} | b_{12} | b_{13} | b_{23} |
|-----|-------|----------|-----------------|--------|-----------|----------|----------|----------|----------|----------|----------|
| PXA | 0.65 | 2.0 | 0.08469 | 0.0652 | 11.67 | 0 | 0 | 0 | 0 | 0 | 0 |
| PXF | 100. | 0.0129 | 0.08469 | 0.0652 | 11.67 | 0 | 0 | 0 | 0 | 0 | 0 |

It should be pointed out how the PXA case is close to the Tucker and Reynolds (1968) experiment, which has been widely referred to in the validation of homogeneous models. In contrast to the direct numerical simulation, the initial state is not fully isotropic. For the same initial dynamic viscosity, the flow is defined with the following parameters:

| | $ S $ | τ_0 | ε_0 | K_0 | R_{t_0} | b_{11} | b_{22} | b_{33} | b_{12} | b_{13} | b_{23} |
|------|-------|----------|-----------------|--------|-----------|----------|----------|----------|----------|----------|----------|
| TR68 | 4.45 | 2.91 | 0.6300 | 0.0486 | 0.872 | 0.0859 | -0.0239 | -0.0636 | 0 | 0 | 0 |

Despite obvious similarities between the two cases (see figures 3.41 and 3.42), there are differences. The major source of difference comes from the fact that the initial state of turbulence in the experimental case is not fully isotropic. It is, therefore, interesting to inspect the performance of the models in both cases. The turbulent kinetic energy and the anisotropy tensor are given first for the experimental flow TR68 in figures 3.43 to 3.46). The behaviour of the models however follows roughly the same hierarchy of quality as in PXA flow, though some differences appear.

As in the preceding case, the presence of the slow and rapid term allows the different models to reproduce the first DNS configuration, PXA, as well as TR68, closer to the

direct numerical simulation results, than the PXF case, which is in the rapid distortion limit.

All models give a good behaviour of the turbulent kinetic energy in both the PXA and TR68 cases. The predictions of the anisotropies in the PXA flow by the LRR and SSG models are relatively close and it is difficult to decide which is better, since SSG predict b_{22} better than LRR, but LRR captures b_{11} better than SSG. Both closures, however, predict very similar b_{33} (direction of the stretching), though not in good agreement with DNS. Because b_{11} corresponds to the non-constrained direction and b_{22} is in the direction of the compression, SSG might be considered as marginally better. However, in the experimental case TR68, both the LRR and SSG give excellent reproduction of b_{33} , but LRR reproduces better both b_{11} and b_{22} than SSG.

The predictions of the first flow case with the non-linear models are easier to rank. The SL model captures a good level of all components of the Reynolds stress anisotropy in the PXA flow, but performs worst of all in the TR68 flow, where FLT is superior. It should be noted that in these flow cases the slow term is important. The FLT and RLA models give solutions which are relatively close to each other, but that their performance is not clearly superior to SSG or LRR. The differences between predictions with various models can also be observed on the invariant maps.

The above discussion does not lead to a conclusive model ranking because no model performs superior in both flows. However, if a choice is to be made, the performance in PXA flow should serve as a more reliable basis simply because the DNS results should be regarded as more reliable than the TR68 experiment. Some inaccuracies, particular in measuring the stress anisotropy, in those days (thirty years ago) are possible, but also there is some uncertainty in defining the initial dissipation rate ε_0 which has a strong influence on the flow predictions.

The second case seems to be even more challenging for all models. It should be noted that the sign of b_{11} changes, but this feature is not captured by any of the models. They all give the same sort of predictions of the normal Reynolds stress in the non-constrained direction. On the whole the non-linear models, do not show any superiority over the three linear models.

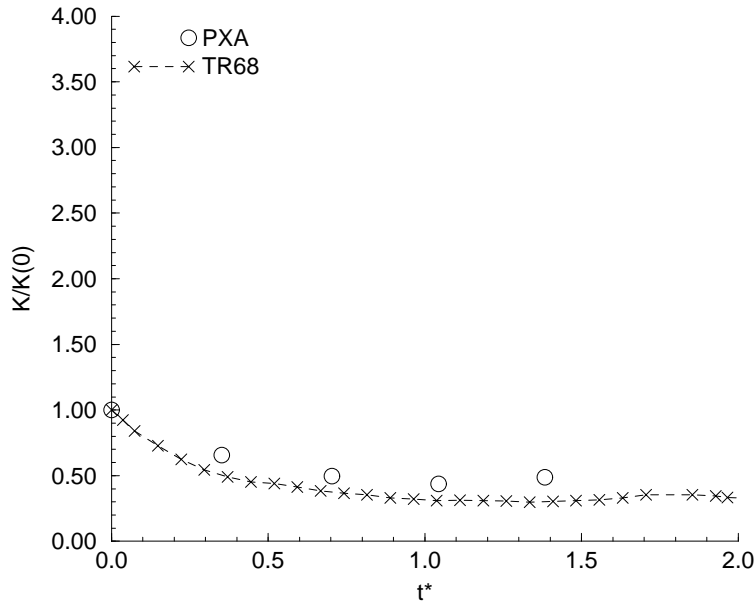


Figure 3.41: Comparison of the turbulent kinetic energy evolution for the plane deformations PXA and TR68.

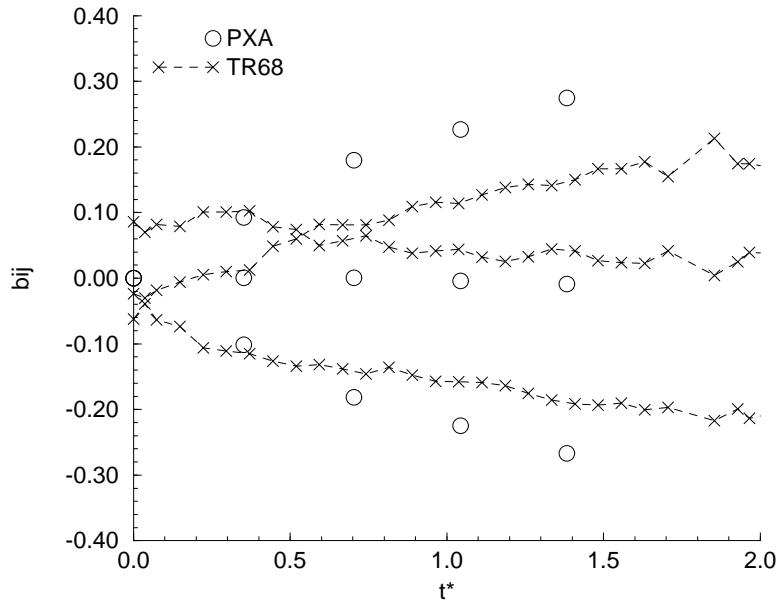
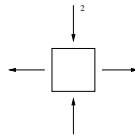


Figure 3.42: Comparison of the anisotropy tensor evolution for the plane deformations PXA and TR68.



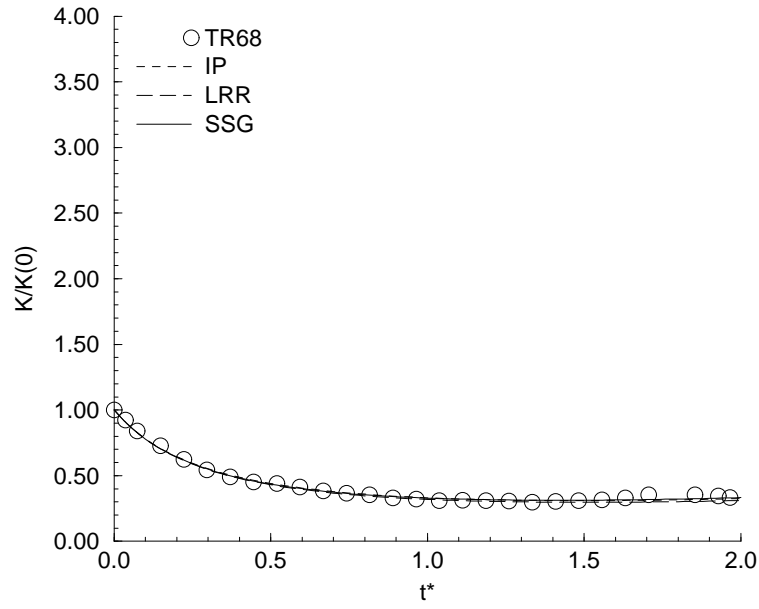


Figure 3.43: *Turbulent kinetic energy evolution for the plane deformation TR68.*

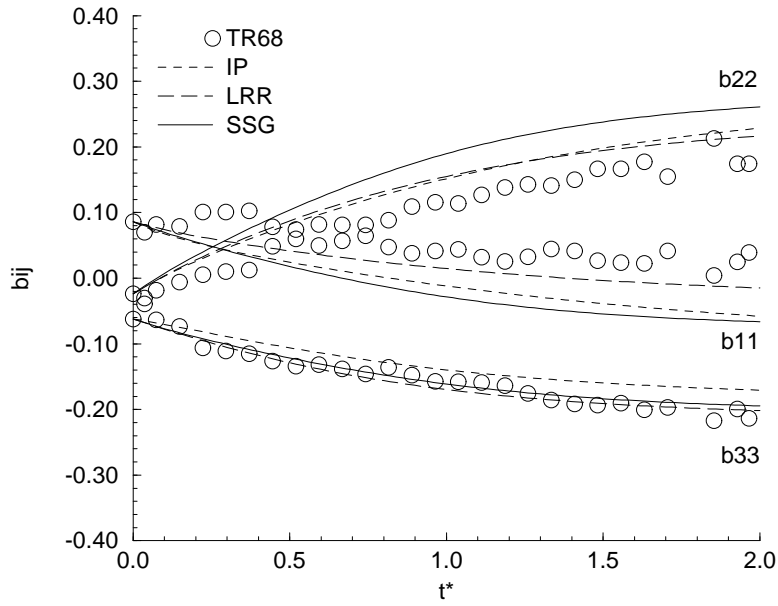
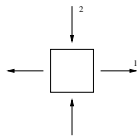


Figure 3.44: *Anisotropy tensor evolution for the plane deformation TR68.*



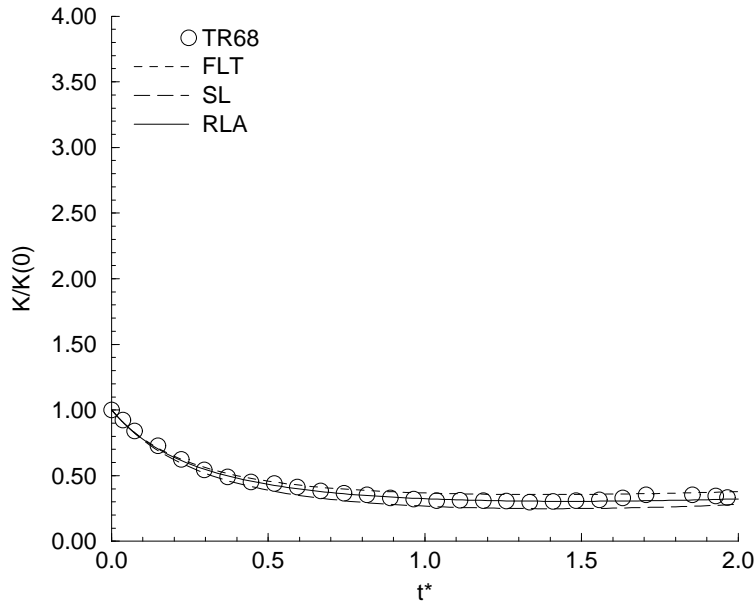


Figure 3.45: *Turbulent kinetic energy evolution for the plane deformation TR68.*

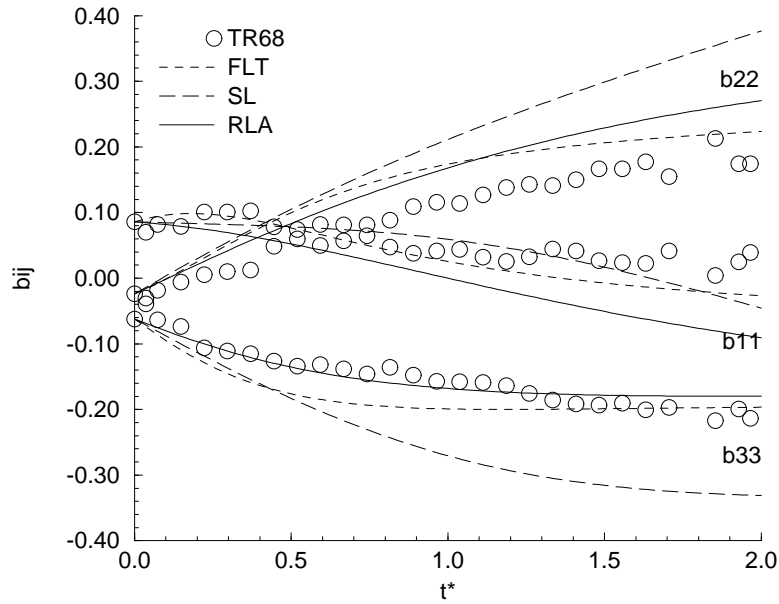
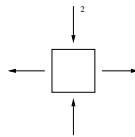


Figure 3.46: *Anisotropy tensor evolution for the plane deformation TR68.*



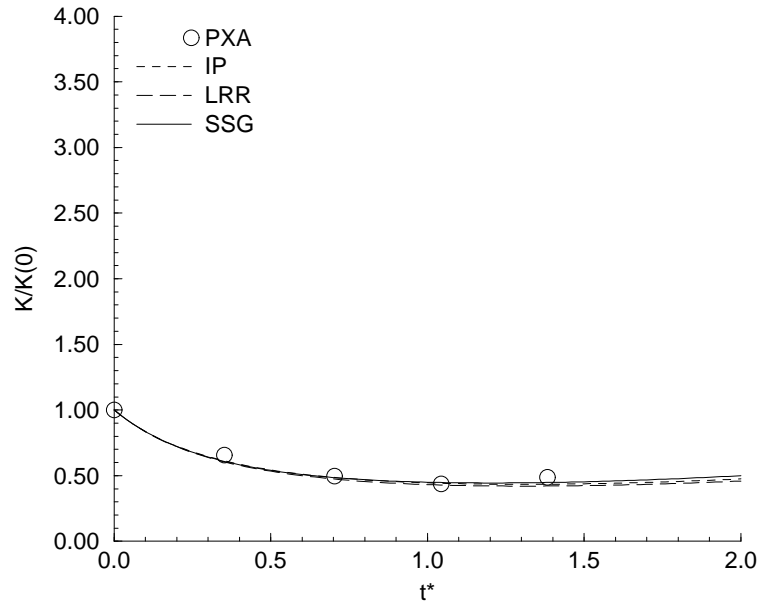


Figure 3.47: *Turbulent kinetic energy evolution for the plane deformation PXA.*

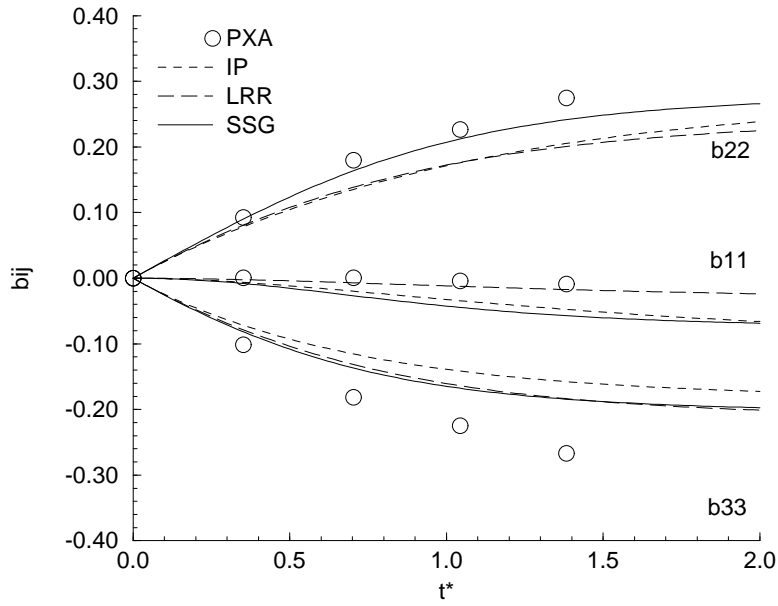
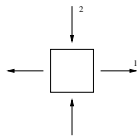


Figure 3.48: *Anisotropy tensor evolution for the plane deformation PXA.*



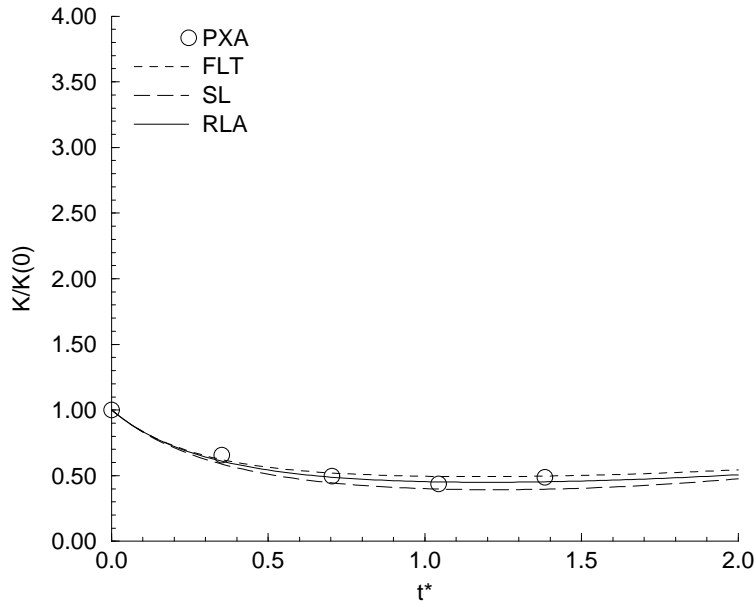


Figure 3.49: *Turbulent kinetic energy evolution for the plane deformation PXA.*

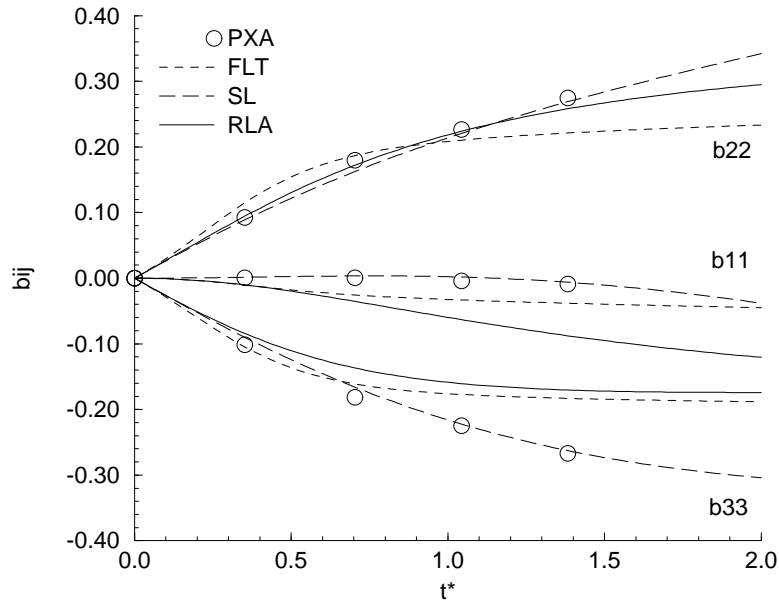
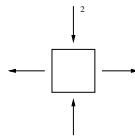


Figure 3.50: *Anisotropy tensor evolution for the plane deformation PXA.*



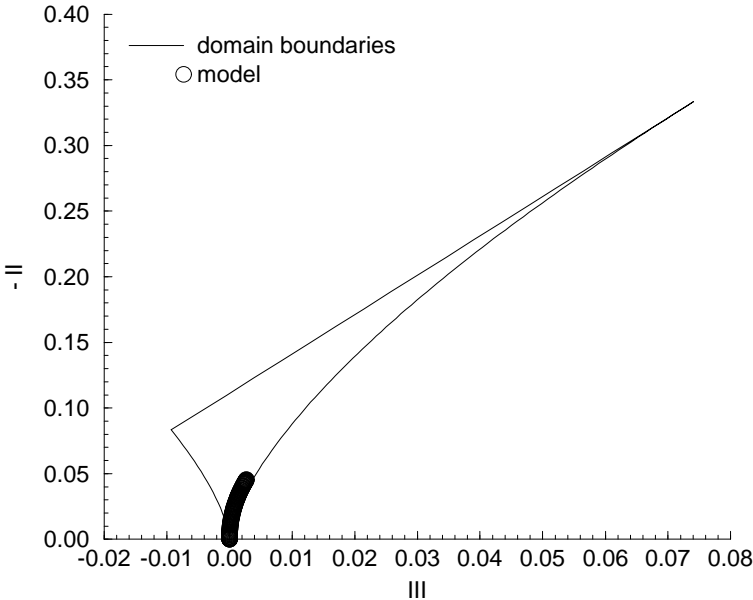


Figure 3.51: *Plane deformation PXA. IP model.*

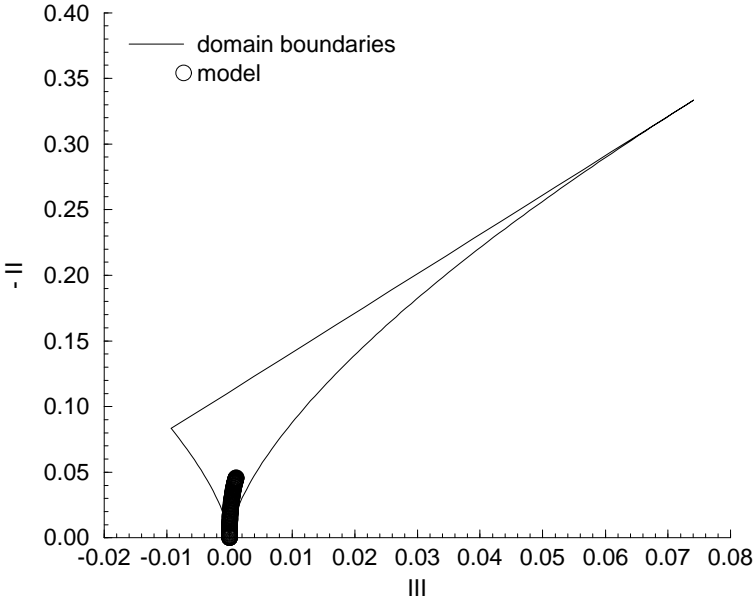
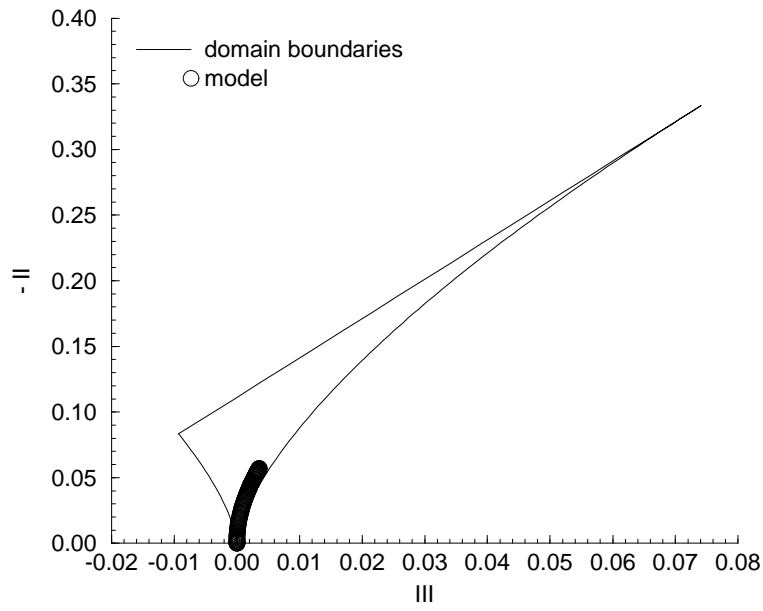
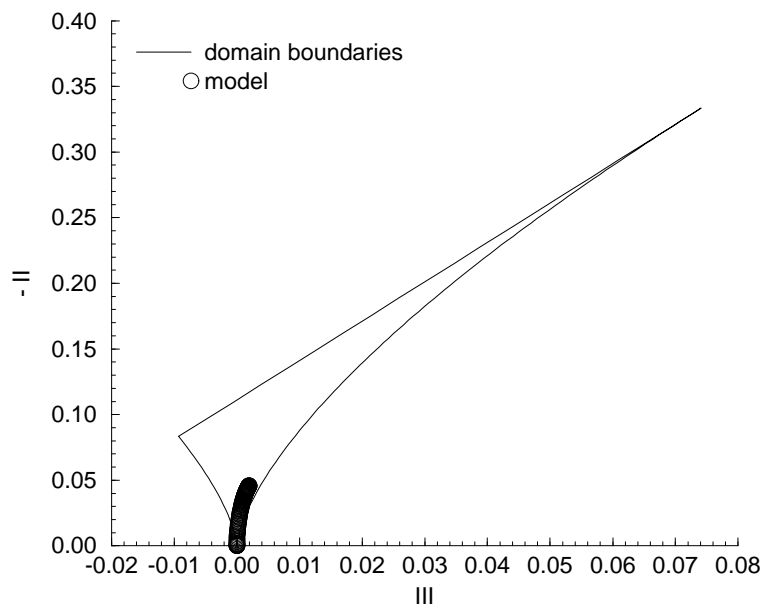


Figure 3.52: *Plane deformation PXA. LRR model.*

Figure 3.53: *Plane deformation PXA. SSG model.*Figure 3.54: *Plane deformation PXA. FLT model.*

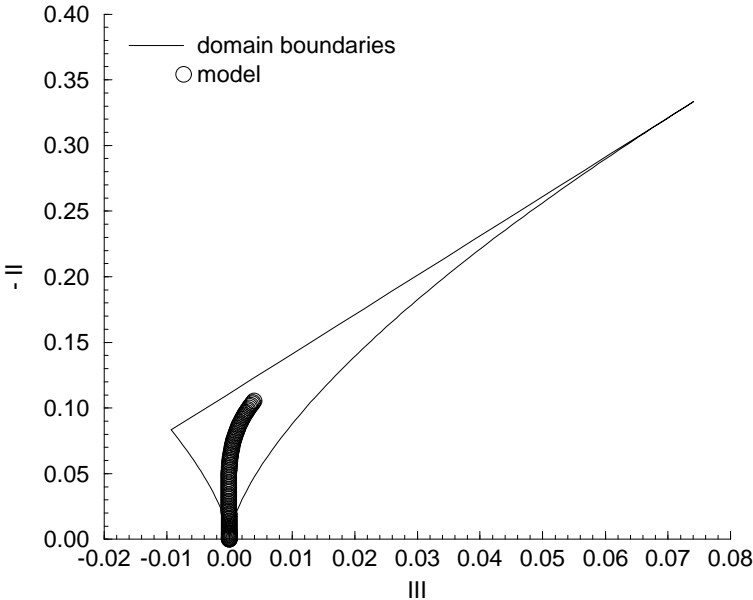


Figure 3.55: *Plane deformation PXA. SL model.*

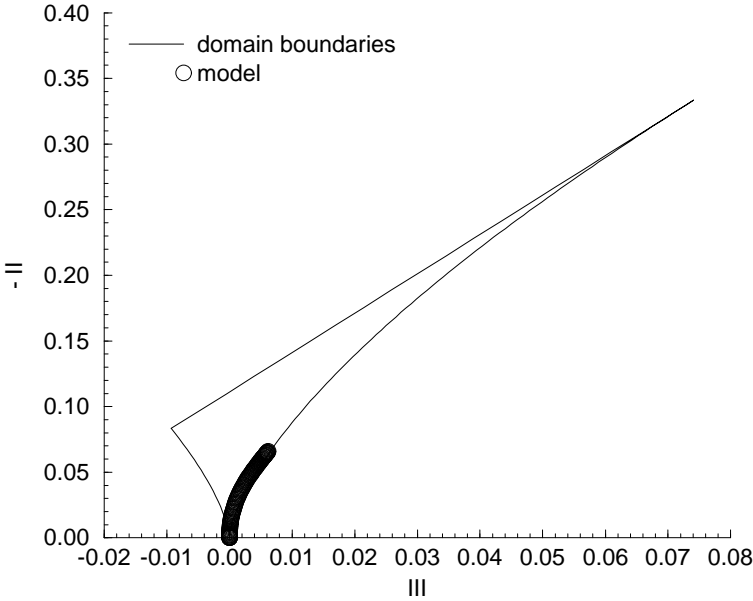


Figure 3.56: *Plane deformation PXA. RLA model.*

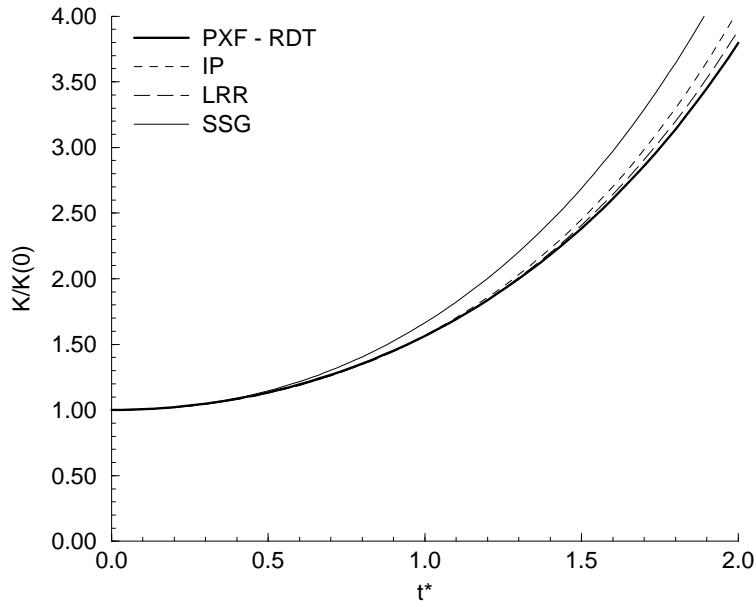


Figure 3.57: *Turbulent kinetic energy evolution for the plane deformation PXF.*

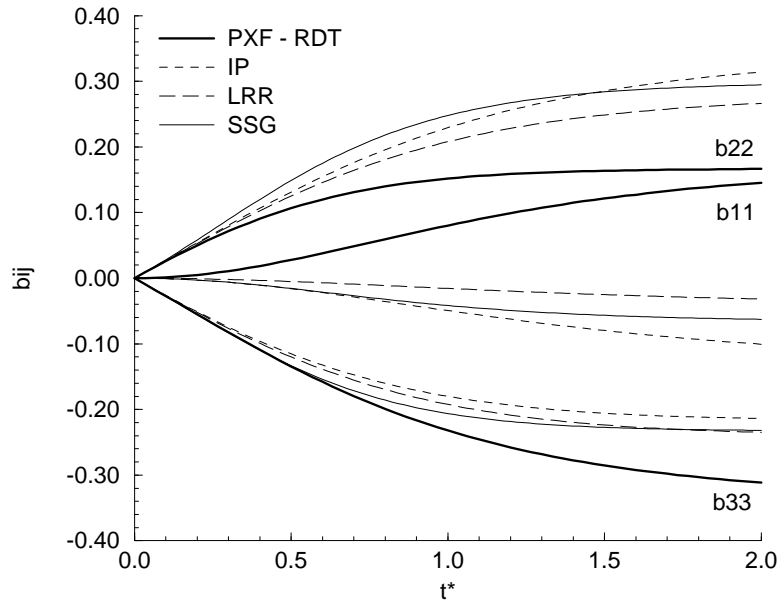
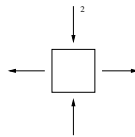


Figure 3.58: *Anisotropy tensor evolution for the plane deformation PXF.*



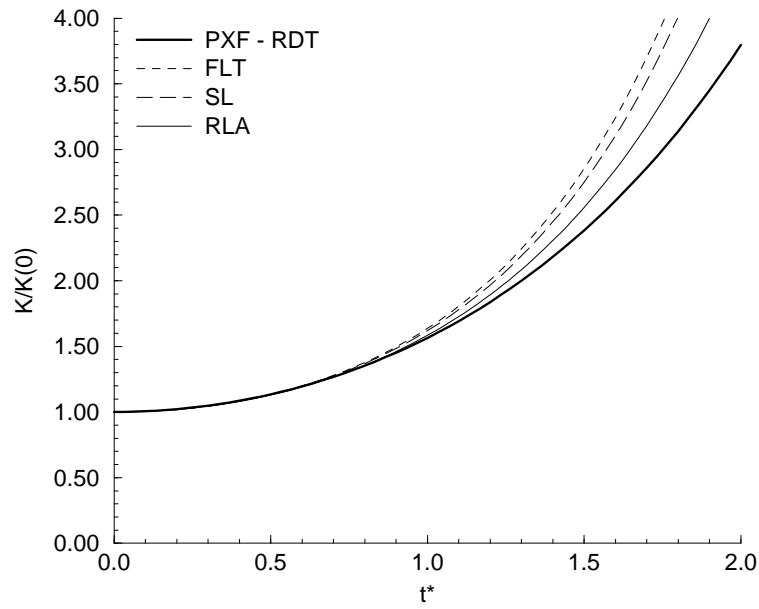


Figure 3.59: *Turbulent kinetic energy evolution for the plane deformation PXF.*

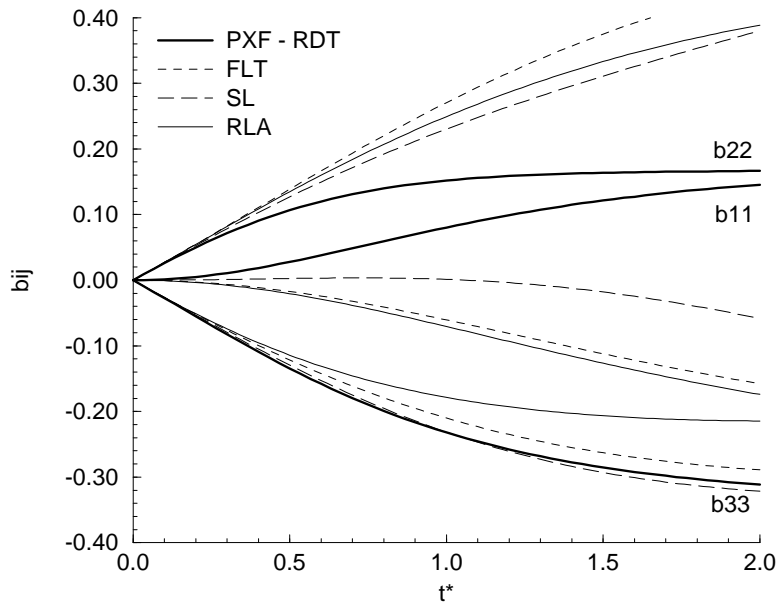
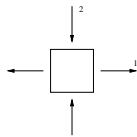
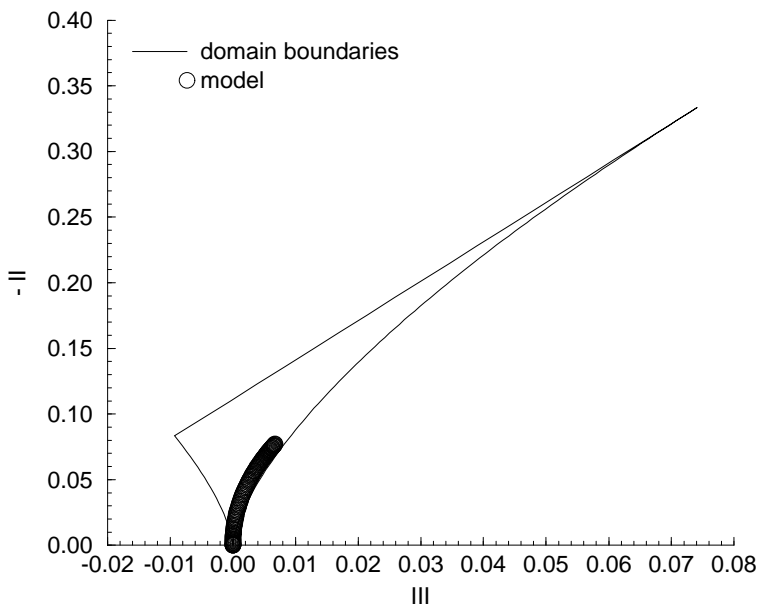
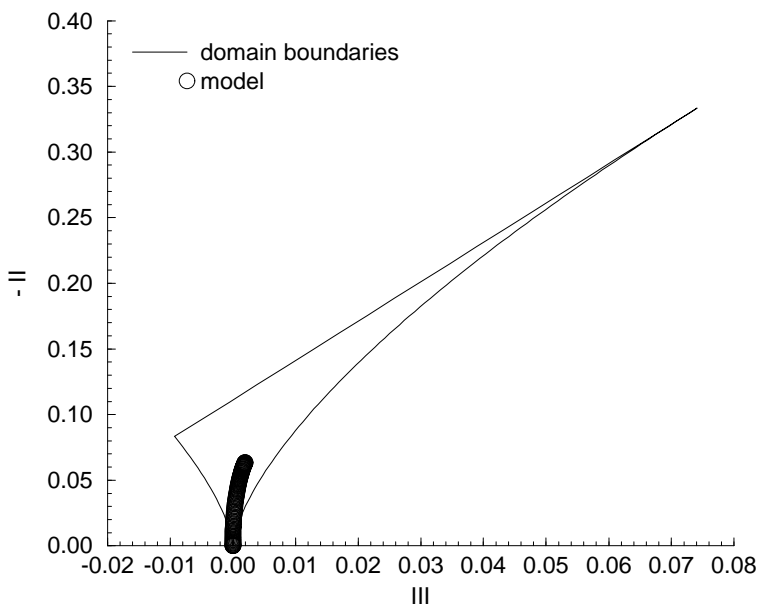


Figure 3.60: *Anisotropy tensor evolution for the plane deformation PXF.*



Figure 3.61: *Plane deformation PXF. IP model.*Figure 3.62: *Plane deformation PXF. LRR model.*

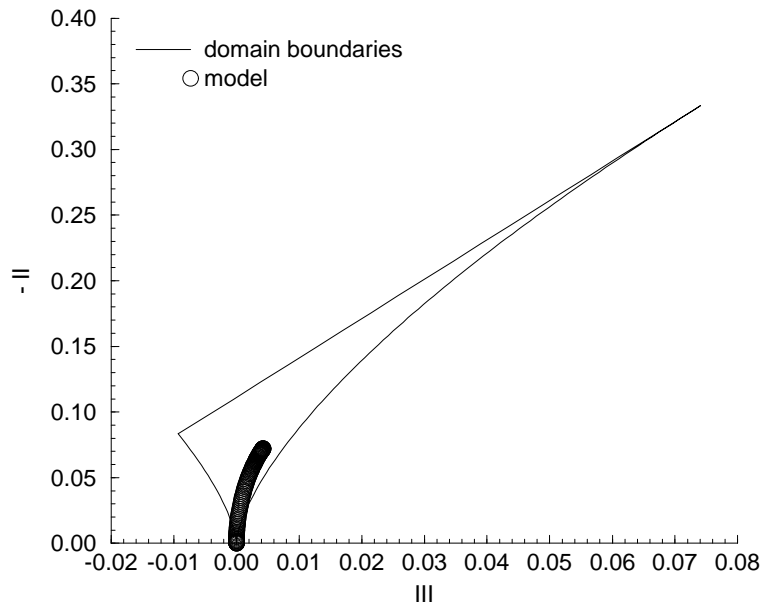


Figure 3.63: *Plane deformation PXF. SSG model.*

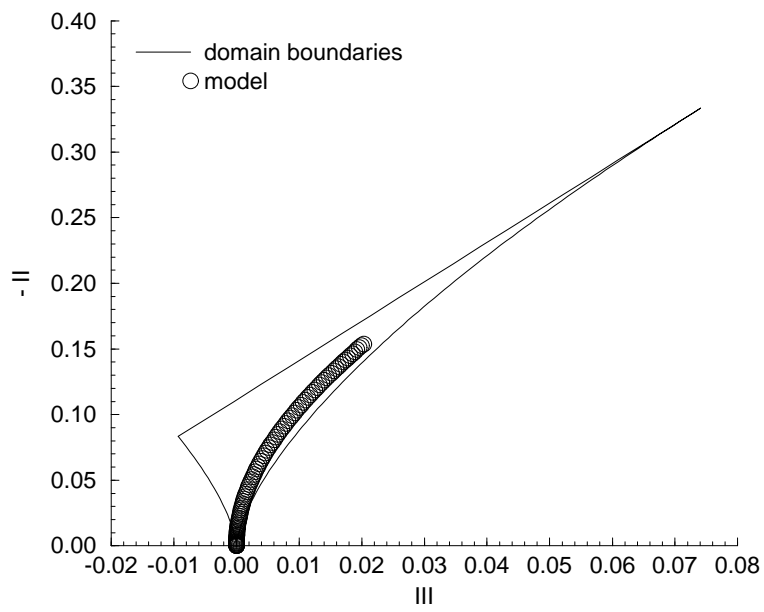
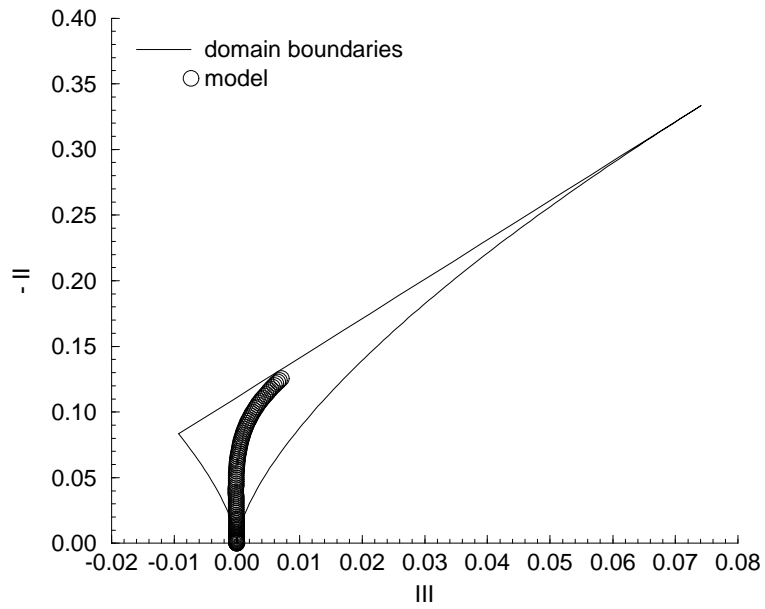
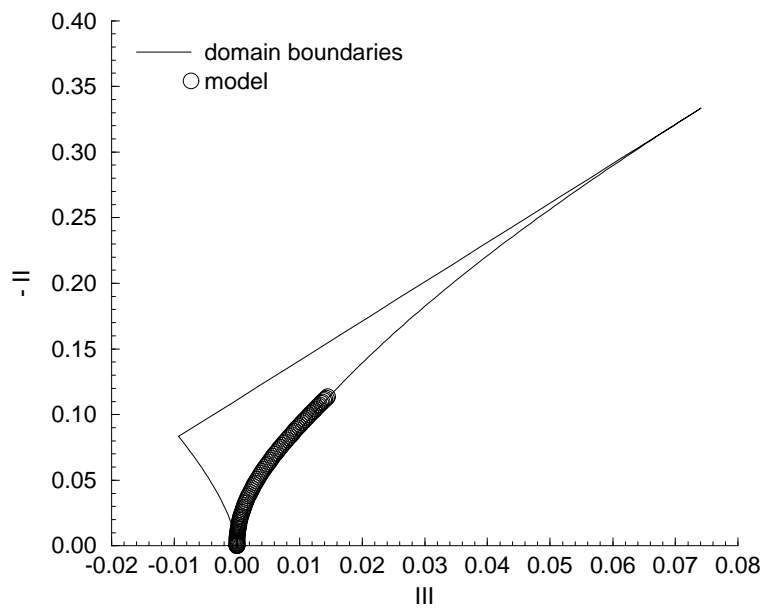


Figure 3.64: *Plane deformation PXF. FLT model.*

Figure 3.65: *Plane deformation PXF. SL model.*Figure 3.66: *Plane deformation PXF. RLA model.*

3.2.3 Successive plane deformations

The next test case is a turbulent flow subjected to two successive plane deformations. After the first deformation, the second one is imposed by rotating the principal axes by an angle of 45 degrees. The flow is defined by the mean rate of strain with the following matrix patterns: the first plane deformation, PS1, has a matrix:

$$S_{ij} = \begin{bmatrix} S & 0 & 0 \\ 0 & -S & 0 \\ 0 & 0 & 0 \end{bmatrix} \quad (3.17a)$$

applied to an initially isotropic turbulence, until $c = 2.72$. The second one, noted PS2 is defined by:

$$S_{ij} = \begin{bmatrix} 0 & \frac{1}{2}S & 0 \\ \frac{1}{2}S & 0 & 0 \\ 0 & 0 & 0 \end{bmatrix} \quad (3.17b)$$

Calculation of this type of flows in the rapid distortion approximation was reported by Kassinos and Reynolds (1995). Experiments have also been done for this configurations by Gence and Mathieu (1980). Only the results of the rapid distortion approximation are given here for reference.

For the first deformation PS1, the results are obtained numerically using the rapid distortion approximation, whereas for the second one the results have been obtained in a digitalized form from the Kassinos and Reynolds (1995) report; that explain the less smoothed form of the lines. The evolutions in the invariant map are also presented. They are, however, identical to the PXF case. The kinetic energy was not available in the second case.

It is interesting to note that none of the models correctly predicts the second deformation.

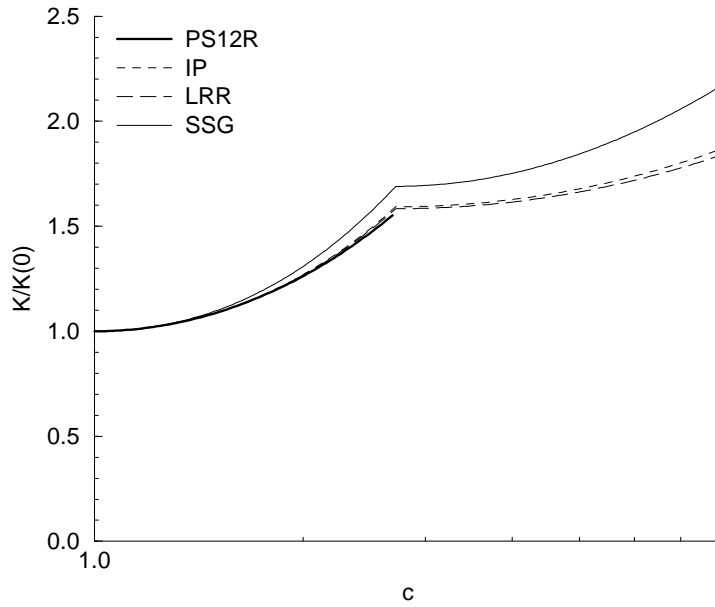


Figure 3.67: *Kinetic energy evolution for two successive plane deformation PS12R.*

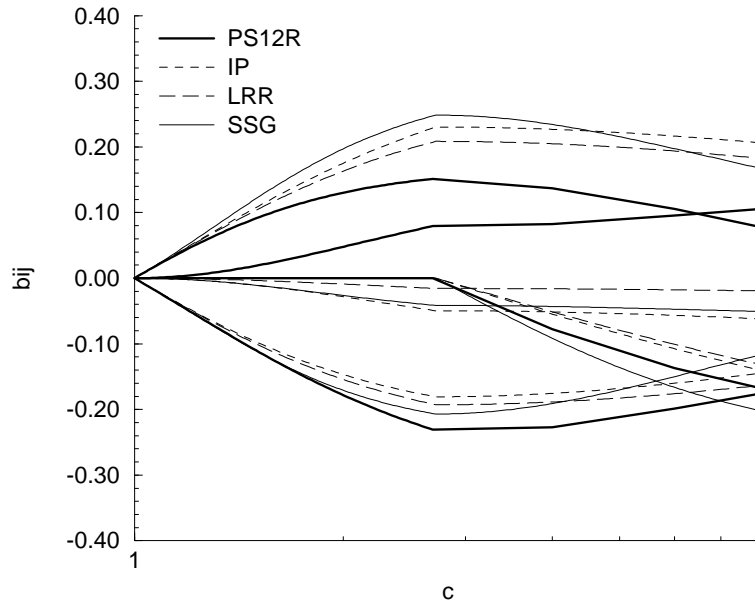
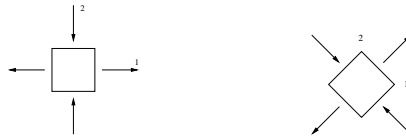


Figure 3.68: *Anisotropy evolution for two successive plane deformation PS12R.*



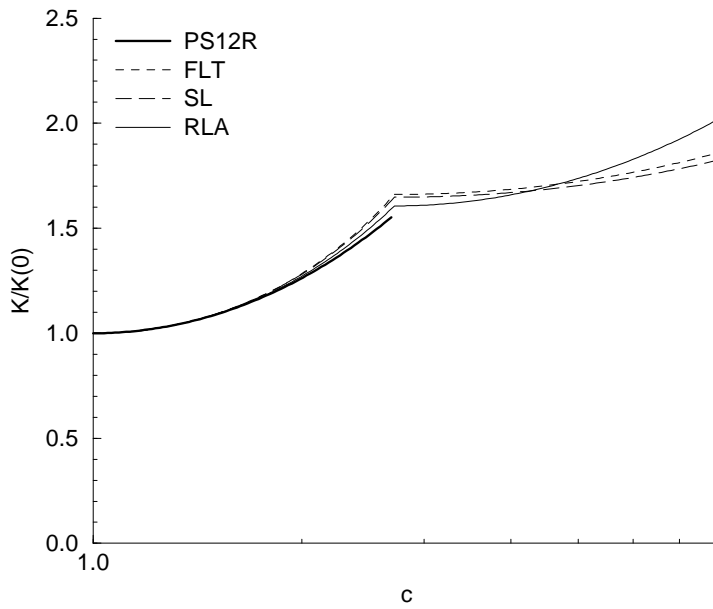


Figure 3.69: *Kinetic energy evolution for two successive plane deformation PS12R.*

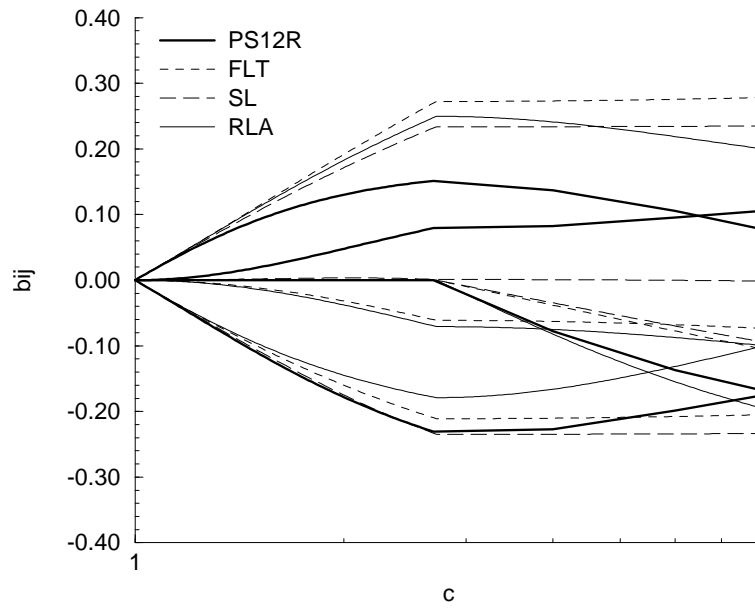
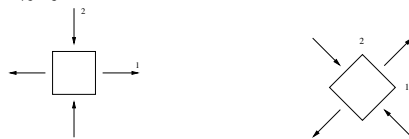


Figure 3.70: *Anisotropy evolution for two successive plane deformation PS12R.*



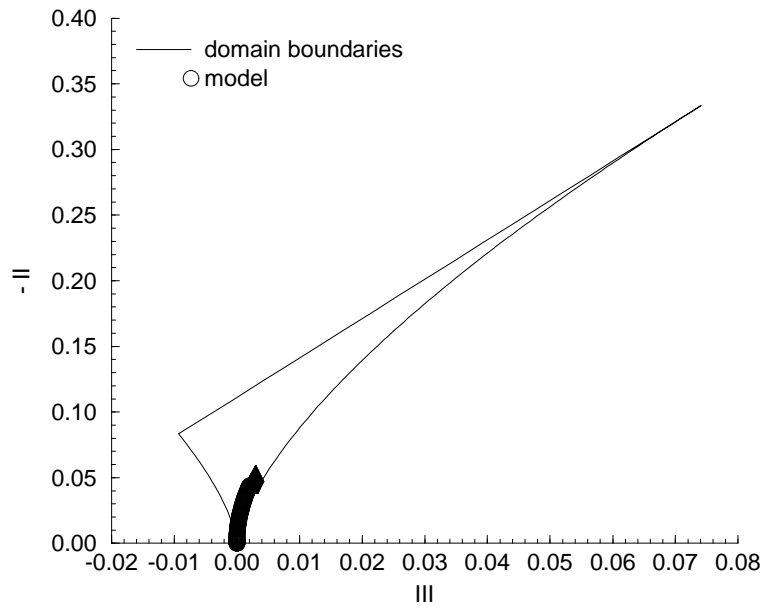


Figure 3.71: *Successive plane deformations PS12R. IP model.*

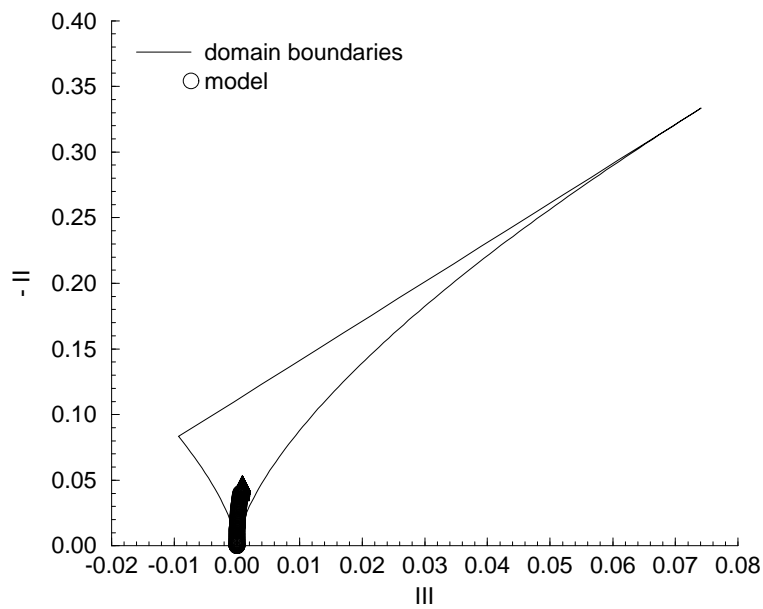


Figure 3.72: *Successive plane deformations PS12R. LRR model.*

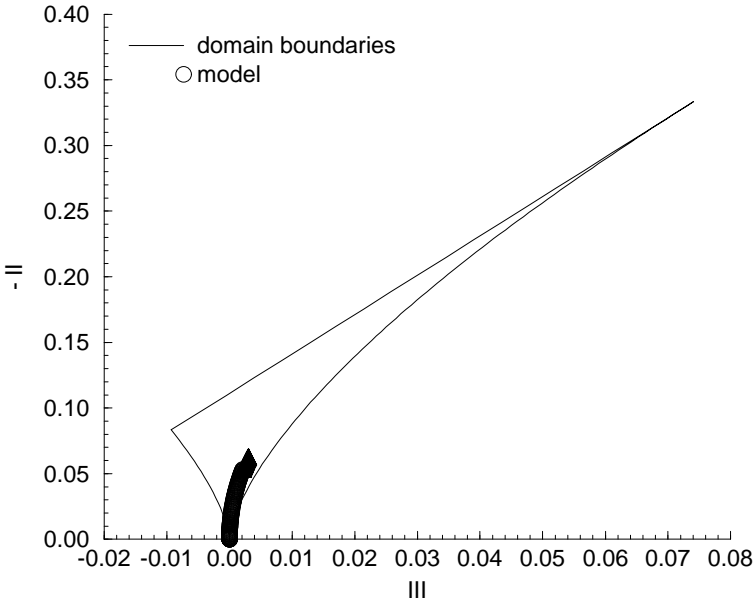


Figure 3.73: *Successive plane deformations PS12R. SSG model.*

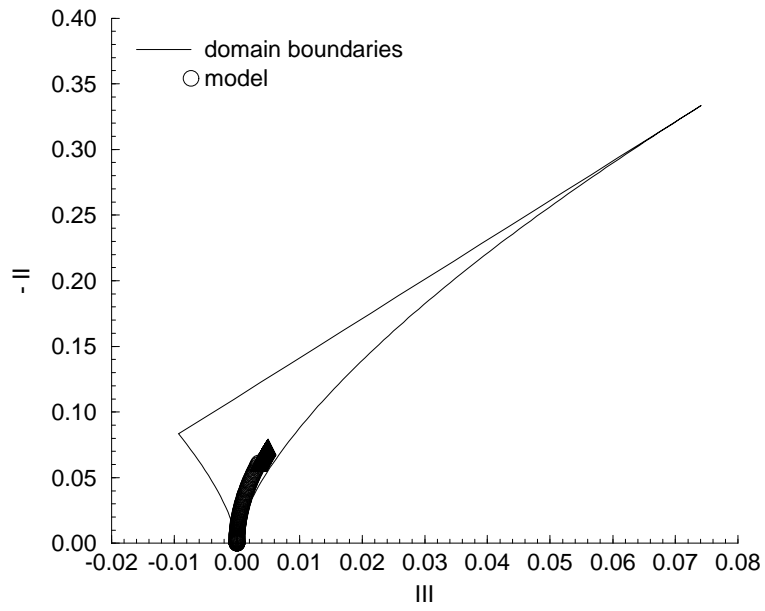


Figure 3.74: *Successive plane deformations PS12R. FLT model.*

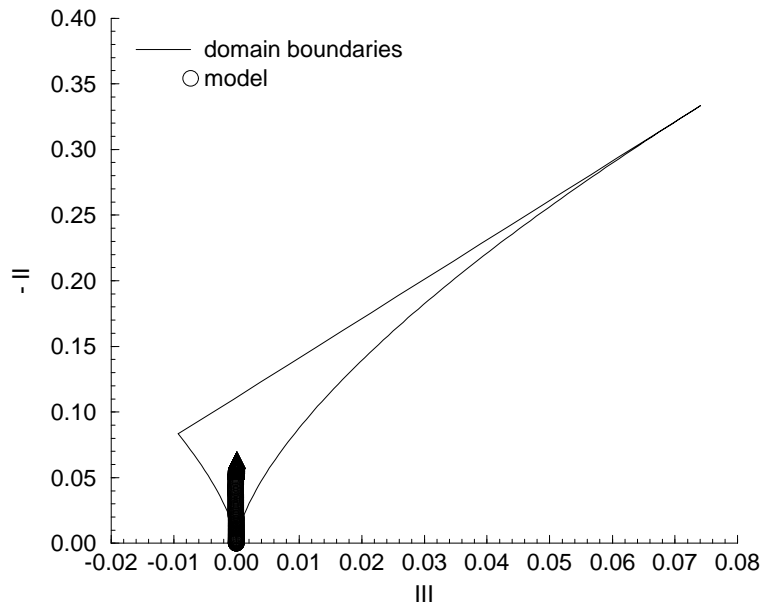


Figure 3.75: *Successive plane deformations PS12R. SL model.*

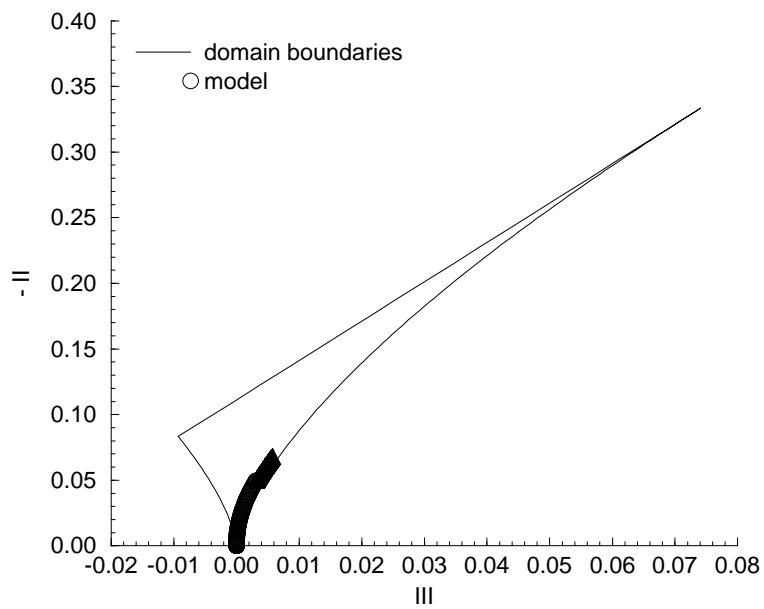


Figure 3.76: *Successive plane deformations PS12R. RLA model.*

3.3 Flows with mean rotation effect

3.3.1 Homogeneous shear

The simple homogeneous shear is defined by the velocity gradient matrix

$$\overline{V}_{i,j} = \begin{bmatrix} 0 & S & 0 \\ 0 & 0 & 0 \\ 0 & 0 & 0 \end{bmatrix} \quad (3.18)$$

In the rapid distortion limit the flow should reach a 2D-1C state.

3.3.2 Homogeneous shear in a rotating frame

The case of a homogeneous rotating shear flow is interesting because it constitutes an arbitrary combination of a plane deformation and a rotation. It represents, therefore, in a simplified form a relatively general class of turbulent homogeneous flows. The relative mean velocity gradient is defined by

$$\overline{V}_{i,j} = \begin{bmatrix} 0 & S & 0 \\ 0 & 0 & 0 \\ 0 & 0 & 0 \end{bmatrix} \quad (3.19)$$

with

$$\Omega = [0, 0, \Omega] \quad (3.20)$$

being the rotation rate of the rotating frame, relatively to an inertial reference frame.

Starting from an initially isotropic state, a turbulent flow subjected to a pure shear reaches rapidly an asymptotic state, in a monotonic manner (Speziale *et al.*, 1992). The correct prediction of this asymptotic state is not particularly challenging test of the complete model because most of the closures are calibrated by enforcing them to restore the asymptotic values of the Reynolds stress anisotropy tensor. The non dimensional form of the equations shows that the evolution of the components of the stress anisotropy depends only on the ratio $\varepsilon_0/S K_0$.

The performances of the models are compared with the large eddy simulations of Bardina *et al.* (1983), calculated for an initially isotropic turbulence, subjected to a shear of the following strength:

$$\frac{\varepsilon_0}{S K_0} = 0.296 \quad (3.21)$$

The evolution of the turbulent kinetic energy are compared to the result of those simulations, even though the latter are not defiltered. According to Speziale *et al.* (1990) the differences between the filtered and defiltered results can be considered as negligible, at least for the turbulent kinetic energy.

The addition of the Coriolis inertial forces bring a stabilising or destabilising effect on the flow (Speziale and Mhuiris, 1988). This effect appears explicitly in the momentum

equations, as well as an additional mechanism of production in the transport equation for the Reynolds stress. The large eddy simulations (Bardina *et al.*, 1983), as well as the linear theory (Bertoglio, 1982), show that the kinetic energy and its dissipation rate grow exponentially when the ratio of the rotation of the frame to the shear intensity R_o is located between 0 et 0.5. The most energetic case corresponds to $R_o = 0.25$. All intermediate state $0 < R_o < 0.5$ correspond to a destabilising action of the rotation on the shear flow. The turbulent models are generally not calibrated for such mechanisms, except the SSG model (Speziale *et al.*, 1991). It is, therefore, interesting to see how are the models able to predict the stability interval, without introducing any explicit corrections to take into account the rotation of the frame.

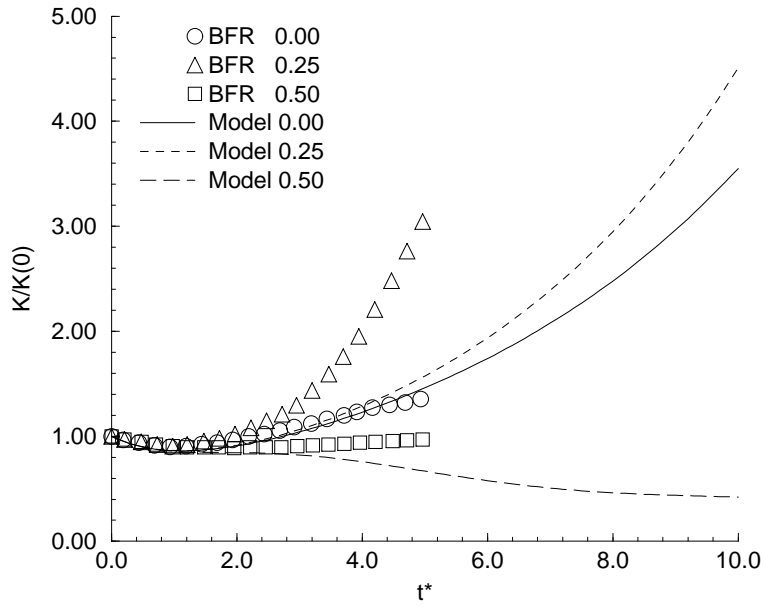


Figure 3.77: Kinetic energy evolution in the case of rotating shear. IP model.

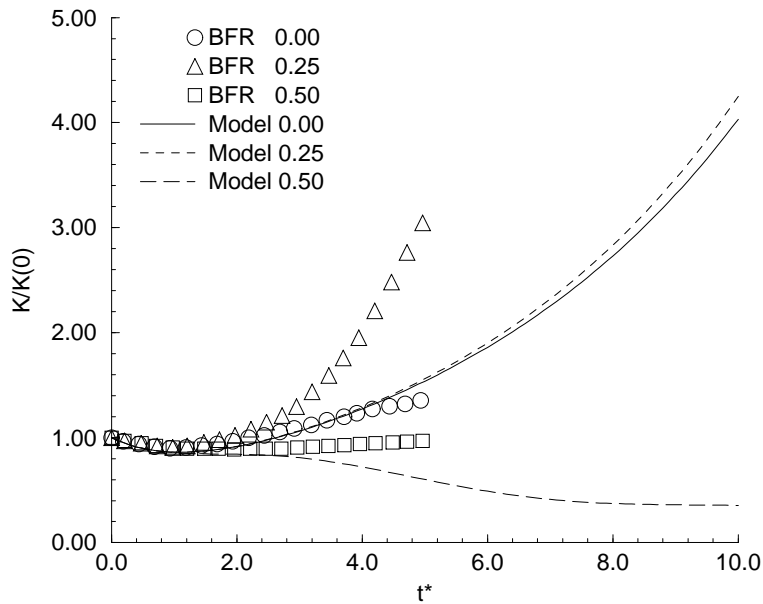
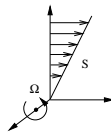


Figure 3.78: Kinetic energy evolution in the case of rotating shear. LRR model.



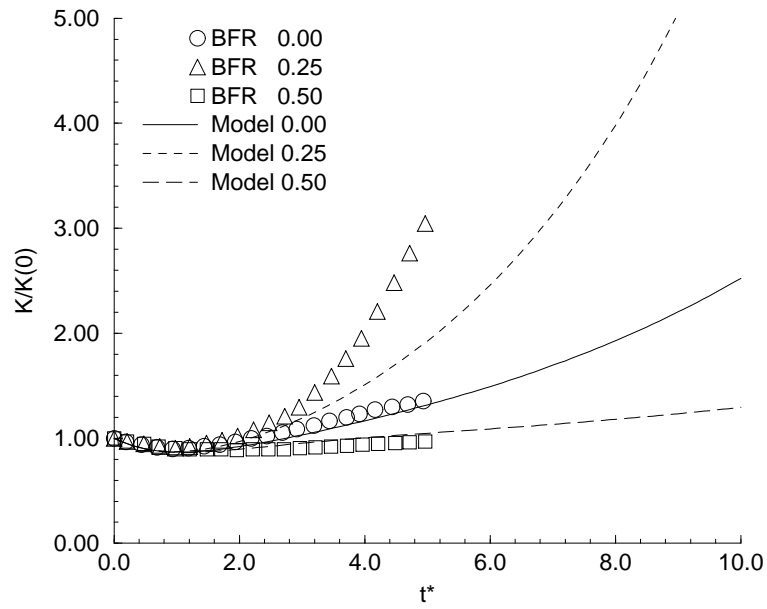


Figure 3.79: *Kinetic energy evolution in the case of rotating shear. SSG model.*

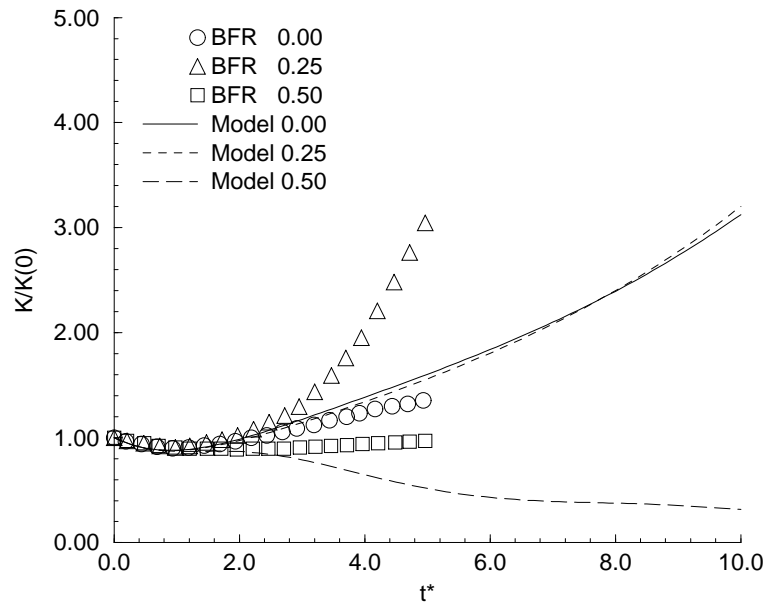
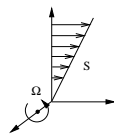


Figure 3.80: *Kinetic energy evolution in the case of rotating shear. FLT model.*



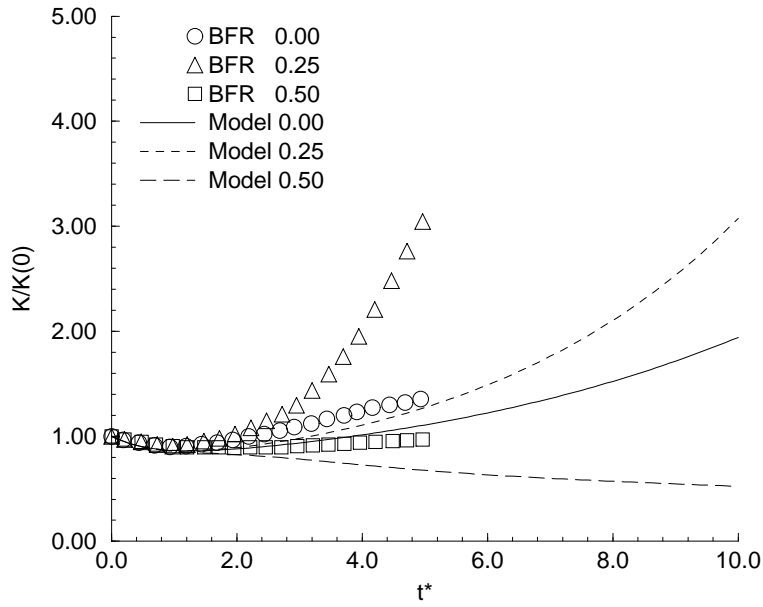


Figure 3.81: *Kinetic energy evolution in the case of rotating shear. SL model at high Reynolds number.*

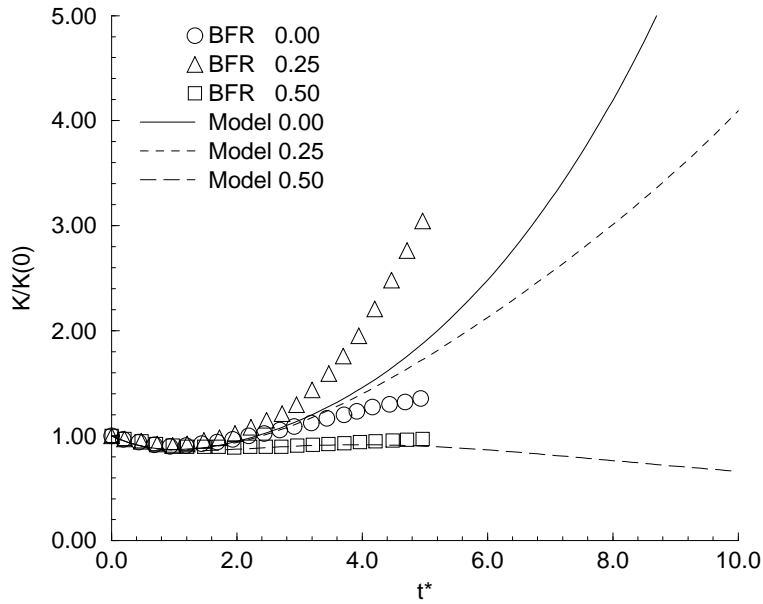
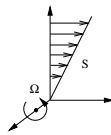


Figure 3.82: *Kinetic energy evolution in the case of rotating shear. RLA model.*



The asymptotic solutions in the pure shear case are compared with the results evaluated by averaging the experimental data of Tavoularis and Corrsin (1981), Tavoularis and Karnik (1989), and the results of Rogers *et al.* (1986) direct numerical simulations. The asymptotic values of the characteristic turbulence quantities are:

$$b_{11}^{\infty} = 0.203 \quad b_{22}^{\infty} = -0.143 \quad b_{33}^{\infty} = -0.06 \quad b_{12}^{\infty} = -0.156 \quad \left(\frac{\varepsilon}{SK}\right)_{\infty} = 0.180 \quad \left(\frac{P}{\varepsilon}\right)_{\infty} = 1.73$$

Each model reaches an asymptotic state. The asymptotic values of the characteristic parameters obtained by different models are given in the next table:

| Model | b_{11}^{∞} | b_{22}^{∞} | b_{33}^{∞} | b_{12}^{∞} | $\left(\frac{\varepsilon}{SK}\right)_{\infty}$ | $\left(\frac{P}{\varepsilon}\right)_{\infty}$ |
|-------|-------------------|-------------------|-------------------|-------------------|--|---|
| IP | 0.192 | -0.096 | -0.096 | -0.185 | 0.177 | 2.09 |
| LRR | 0.155 | -0.121 | -0.034 | -0.187 | 0.183 | 2.04 |
| SSG | 0.218 | -0.145 | -0.073 | -0.163 | 0.180 | 1.82 |
| FLT | 0.210 | -0.196 | -0.647 | -0.145 | 0.141 | 2.04 |
| SL | 0.192 | -0.186 | -0.054 | -0.090 | 0.055 | 3.24 |
| RLA | 0.207 | -0.143 | -0.061 | -0.248 | 0.263 | 1.88 |

The calculations show that the SSG model captures relatively well the tendencies of the Bardina *et al.* (1983) simulations. The linear models IP and LRR restore a too large level of turbulent kinetic energy in the case without rotation. They also predict a relaminarization in the stability limit at $R_o = 0.5$. Those tendencies can be also observed with the non linear model FLT which perform similar to LRR, as well as with RLA. All the models give a too low level of turbulent kinetic energy in the most energetic case at $R_o = 0.25$.

3.4 Return to isotropy

$$S_{ij} = 0 \tag{3.22}$$

ANNE: DO YOU WANT TO PUT ONE OR TWO SENTENCES HERE.

3.4.1 Relaxation form irrotational strains

| | ε_0 | K_0 | b_{11} | b_{22} | b_{33} | b_{12} | b_{13} | b_{23} |
|---------|-----------------|---------|----------|----------|----------|----------|----------|----------|
| U56 | 0.0339 | 0.0016 | -0.272 | 0.136 | 0.136 | 0 | 0 | 0 |
| LGC85 P | 0.0423 | 0.02241 | -0.140 | -0.041 | 0.181 | 0 | 0 | 0 |
| LGC85 M | 0.0101 | 0.00403 | -0.198 | 0.061 | 0.137 | 0 | 0 | 0 |

3.5 Homogeneous flows with dilatation effects

The study of homogeneous compressed flows is of interest for the analysis of the response of the turbulence to the mean flow perturbations as encountered in a piston-engine configuration. The homogeneous approximation allows to simplify the configuration by neglecting the presence of solid boundaries. It also allows to uncouple the mean flow evolution from the state of the turbulence field. These are idealised cases, which enable to focus on the sole effect of compression on turbulence.

Two configurations are particularly of interest here. The first one is a uniform isotropic compression, which can be seen as a simulation of the squish effect of an engine with a cup-in-piston design. The second one is a one-dimensional compression which represents the compression stroke in an internal combustion engine with a flat piston.

In this study the fluid is supposed to satisfy the ideal gas law and the compression is adiabatic. The Mach number is furthermore supposed to be sufficiently small to neglect the role of sound waves. The fluid density is, therefore, independent in space coordinates. The fluctuation of temperature can also be neglected so that the fluid properties are only functions of time.

Direct numerical simulations are available for both cases. The computations by Wu *et al.* (1985) are interesting also because they covers the same range of irrotational deformation, as in the cases studied before. For the description of the mean flow, therefore, the same notations as in Wu *et al.* (1985) are used.

The compression speed is assumed to be constant and is denoted by V_p . The homogeneous turbulent box has initially a size of L_0 whereas the instantaneous box length is x_p .

3.5.1 Isotropic compression

For an isotropic compression, the mean velocity gradient can be written as

$$S_{ij} = \begin{bmatrix} S & 0 & 0 \\ 0 & S & 0 \\ 0 & 0 & S \end{bmatrix} \quad (3.23)$$

where $S < 0$. With the notations introduced above, the strain rate can be expressed as:

$$S = \frac{V_p}{x_p} \quad \text{or again} \quad S = \frac{V_p}{L_0 + V_p t} \quad (3.24)$$

It can be noted that the total strain rate c , which can be expressed as

$$c = \frac{L_0 + V_p t}{L_0} \quad (3.25)$$

can be used here as a basis for comparison of results obtained by different models. From the assumed thermodynamic conditions we can express the time evolution of the fluid properties, e.g.

$$\frac{\rho(t)}{\rho(0)} = \left(\frac{L_0}{x_p} \right)^3 \quad (3.26a)$$

$$\frac{\nu(t)}{\nu(0)} = \left(\frac{L_0}{x_p} \right)^{-2.1} \quad (3.26b)$$

The test cases considered are defined by the following parameters (Wu *et al.* (1985)):

| (| L_0 | V_p | ε_0 | K_0 | ν_0 | b_{11} | b_{22} | b_{33} | b_{12} | b_{13} | b_{23} |
|-----|-------|--------|-----------------|--------|---------|----------|----------|----------|----------|----------|----------|
| SQF | 0.3 | -5.6 | 0.0324 | 0.0407 | 0.01 | 0 | 0 | 0 | 0 | 0 | 0 |
| SQG | 1.0 | -1.0 | 0.0324 | 0.0407 | 0.01 | 0 | 0 | 0 | 0 | 0 | 0 |
| SQH | 0.3 | -0.06 | 0.0324 | 0.0407 | 0.01 | 0 | 0 | 0 | 0 | 0 | 0 |
| SQI | 0.3 | -0.012 | 0.0324 | 0.0407 | 0.01 | 0 | 0 | 0 | 0 | 0 | 0 |

or, in terms of non-dimensional parameters,

| | $ S_0 $ | τ_0 | ε_0 | K_0 | R_{t_0} | b_{11} | b_{22} | b_{33} | b_{12} | b_{13} | b_{23} |
|-----|---------|----------|-----------------|--------|-----------|----------|----------|----------|----------|----------|----------|
| SQF | 18.66 | 0.0425 | 0.0324 | 0.0407 | 5.133 | 0 | 0 | 0 | 0 | 0 | 0 |
| SQG | 1.0 | 0.7944 | 0.0324 | 0.0407 | 5.133 | 0 | 0 | 0 | 0 | 0 | 0 |
| SQH | 2.0 | 3.9721 | 0.0324 | 0.0407 | 5.133 | 0 | 0 | 0 | 0 | 0 | 0 |
| SQI | 0.04 | 19.860 | 0.0324 | 0.0407 | 5.133 | 0 | 0 | 0 | 0 | 0 | 0 |

The first case represents the fastest compression and is close to the rapid distortion approximation. On the other hand, the last case, with the extremely slow compression exhibits negligible effect of the strain, so that the flow evolves like in an isotropic turbulence decay.

Figures 3.83 to 3.90 show a clear superiority of the Wu *et al.* (1985) model in comparison with other two, LSW (Launder and Spalding 1974, with Watkins modifications 1977) and R model (Reynolds, 1980). However, this performance is expected since the the Wu *et al.* (1985) model was tuned specifically for this flow. It is interesting to note that all three models considered reproduce very well the evolution of the turbulence kinetic energy in the fast compression case SQF, despite poor reproduction of ε by LSW and R models. In the case of a very weak compression, SQI, the model LSW gives non-physical increase of the kinetic energy in the later stage.

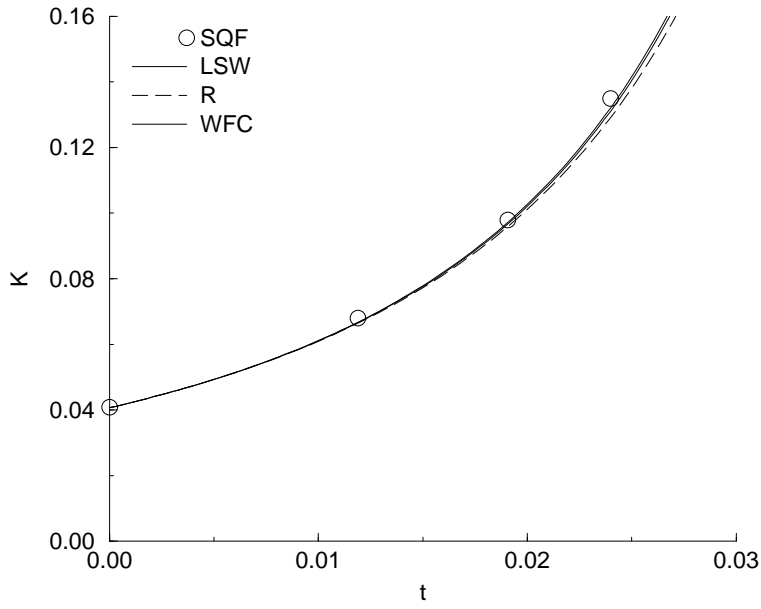


Figure 3.83: *Kinetic energy evolution for the SQF isotropic compression.*

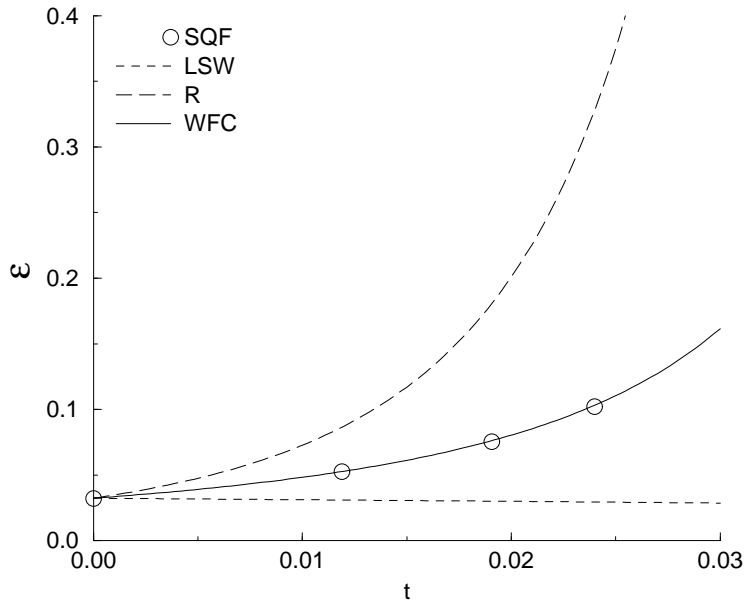
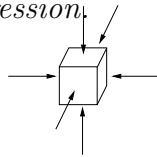


Figure 3.84: *Dissipation of the kinetic energy evolution for the SQF isotropic compression.*



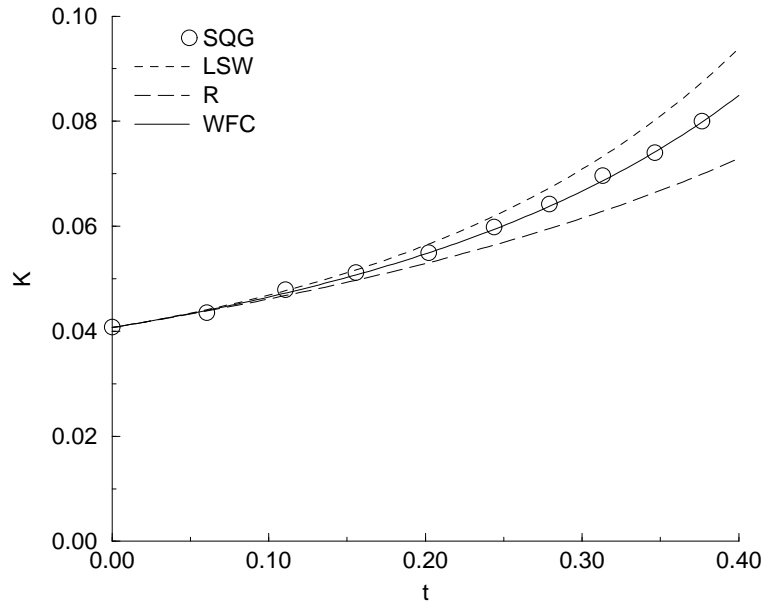


Figure 3.85: *Kinetic energy evolution for the SQG isotropic compression.*

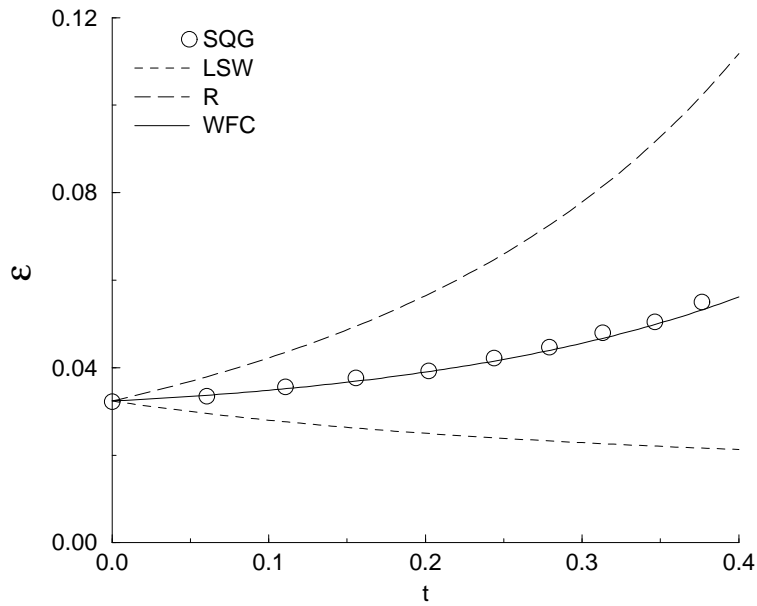
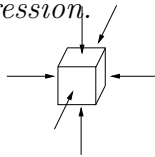


Figure 3.86: *Dissipation of the kinetic energy evolution for the SQG isotropic compression.*



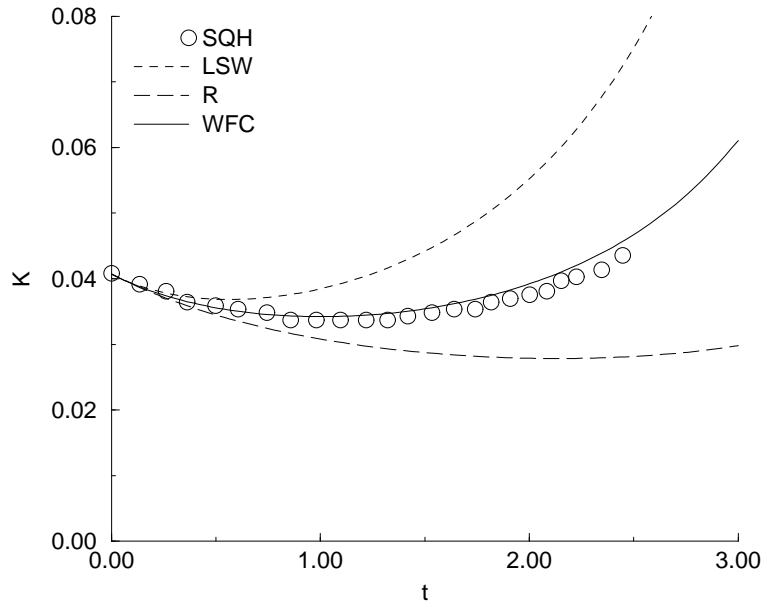


Figure 3.87: *Kinetic energy evolution for the SQH isotropic compression.*

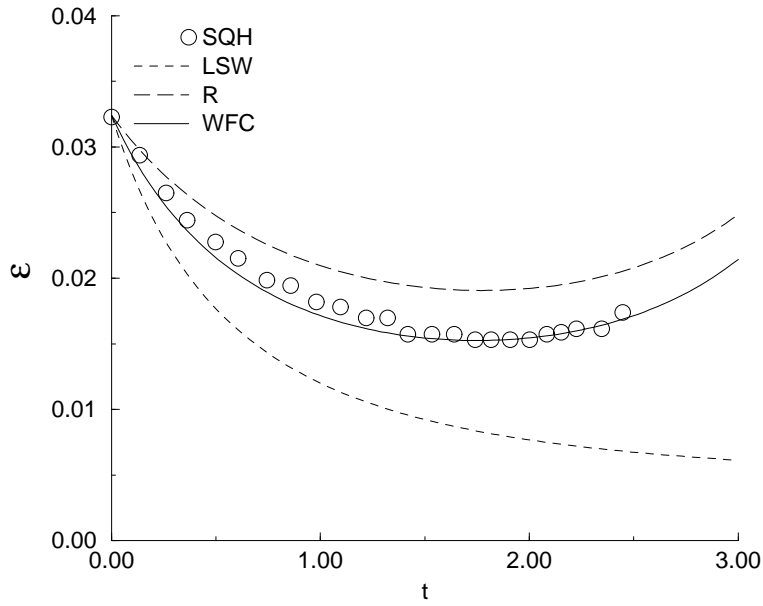
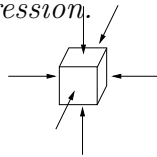


Figure 3.88: *Dissipation of the kinetic energy evolution for the SQH isotropic compression.*



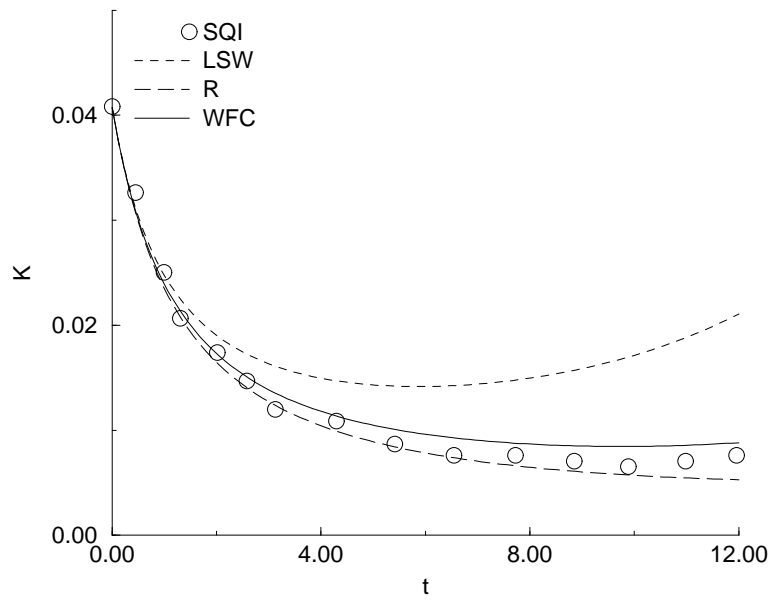


Figure 3.89: *Kinetic energy evolution for the SQI isotropic compression.*

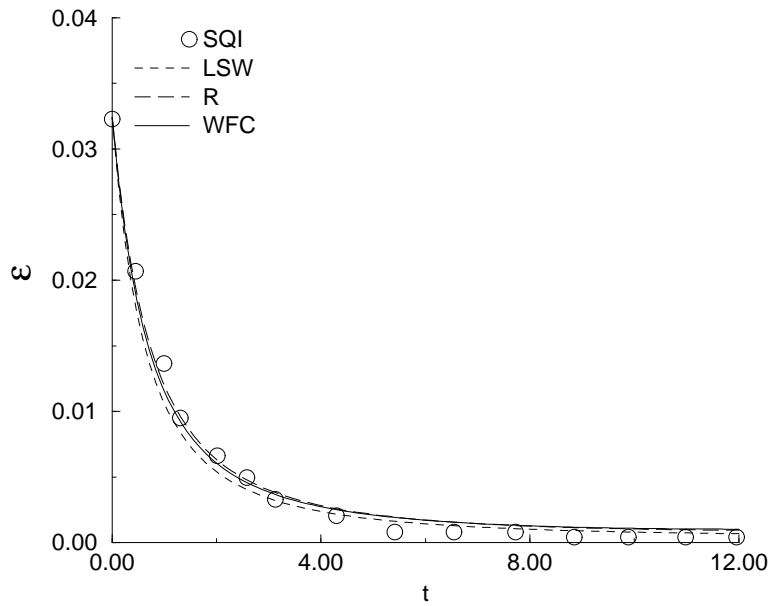
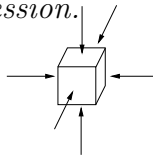


Figure 3.90: *Dissipation of the kinetic energy evolution for the SQI isotropic compression.*



3.5.2 One-dimensional compression

In the case of an one-dimensional compression, the mean strain rate is:

$$S_{ij} = \begin{bmatrix} S & 0 & 0 \\ 0 & 0 & 0 \\ 0 & 0 & 0 \end{bmatrix} \quad (3.27)$$

For comparison with the incompressible flows subjected to irrotational strain, it is convenient to decompose S_{ij} into isotropic and anisotropic dilatation:

$$S_{ij} = \underbrace{\begin{bmatrix} \frac{2}{3}S & 0 & 0 \\ 0 & -\frac{1}{3}S & 0 \\ 0 & 0 & -\frac{1}{3}S \end{bmatrix}}_{\text{anisotropic strain}} + \underbrace{\begin{bmatrix} \frac{1}{3}S & 0 & 0 \\ 0 & \frac{1}{3}S & 0 \\ 0 & 0 & \frac{1}{3}S \end{bmatrix}}_{\text{isotropic dilatation}} \quad (3.28)$$

An one-dimensional compression, for which $S < 0$, corresponds to an incompressible axisymmetric expansion while a one-dimensional expansion, for which $S > 0$, corresponds to an incompressible axisymmetric contraction.

With Wu *et al.* (1985) notations, it can be written

$$S = \frac{V_p}{x_p} \quad \text{or again} \quad S = \frac{V_p}{L_0 + V_p t} \quad (3.29)$$

and the total strain rate is again

$$c = \frac{L_0 + V_p t}{L_0} \quad (3.30)$$

The evolution of the density and molecular viscosity are given by

$$\frac{\rho(t)}{\rho(0)} = \left(\frac{L_0}{x_p} \right) \quad (3.31a)$$

$$\frac{\mu(t)}{\mu(0)} = \left(\frac{L_0}{x_p} \right)^{-0.7} \quad (3.31b)$$

The flow cases considered are defined by the following parameters:

| | L_0 | V_p | ε_0 | K_0 | ν_0 | b_{11} | b_{22} | b_{33} | b_{12} | b_{13} | b_{23} |
|-----|-------|--------|-----------------|--------|---------|----------|----------|----------|----------|----------|----------|
| ODB | 0.3 | -24.3 | 1.5369 | 0.4462 | 0.015 | 0 | 0 | 0 | 0 | 0 | 0 |
| ODC | 0.3 | -1.29 | 1.5369 | 0.4462 | 0.015 | 0 | 0 | 0 | 0 | 0 | 0 |
| ODD | 0.3 | -0.26 | 1.5369 | 0.4462 | 0.015 | 0 | 0 | 0 | 0 | 0 | 0 |
| ODE | 0.3 | -0.052 | 1.5369 | 0.4462 | 0.015 | 0 | 0 | 0 | 0 | 0 | 0 |

or, again using the previously defined non-dimensional parameters:

| | S_0 | τ_0 | ε_0 | K_0 | R_{t_0} | b_{11} | b_{22} | b_{33} | b_{12} | b_{13} | b_{23} |
|-----|--------|----------|-----------------|--------|-----------|----------|----------|----------|----------|----------|----------|
| ODB | -81.00 | 0.0425 | 1.5369 | 0.4462 | 8.637 | 0 | 0 | 0 | 0 | 0 | 0 |
| ODC | -4.3 | 0.8009 | 1.5369 | 0.4462 | 8.637 | 0 | 0 | 0 | 0 | 0 | 0 |
| ODD | -0.866 | 3.974 | 1.5369 | 0.4462 | 8.637 | 0 | 0 | 0 | 0 | 0 | 0 |
| ODE | -0.173 | 0.050 | 1.5369 | 0.4462 | 8.637 | 0 | 0 | 0 | 0 | 0 | 0 |

Again the first case. ODB, corresponds to the rapid distortion limit, whereas the last case corresponds to a very weak compression.

These test case were computed using the LSW and R models. Figures 3.92-3.94 show that none of the model can deal with a very rapid one-dimensional compression. More moderate compressions seem to be tractable, with R-model performing generally much better than the LSW in reproducing the evolution of kinetic energy, stress component R_{11} and dissipation rate. The exception is the stress anisotropy for weak compressions, cases ODD and ODE, where LSW is slightly better, but still far from the DNS results.

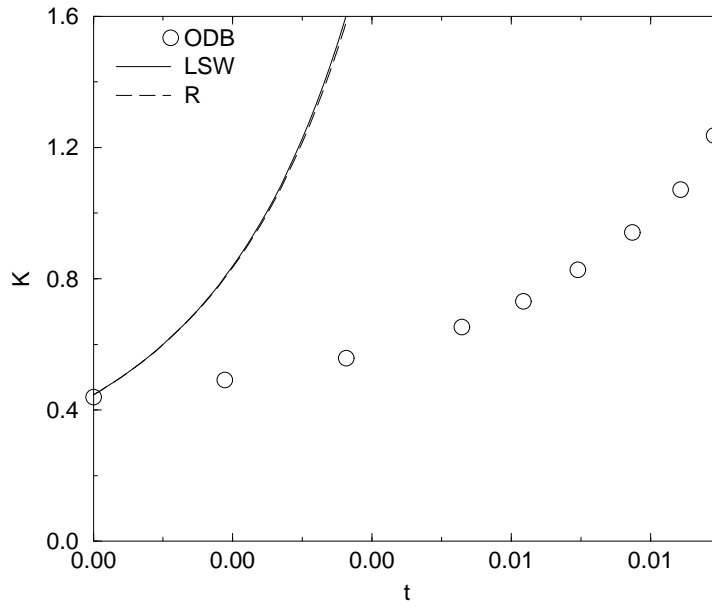


Figure 3.91: *Kinetic energy evolution for the ODB one-dimensional compression.*

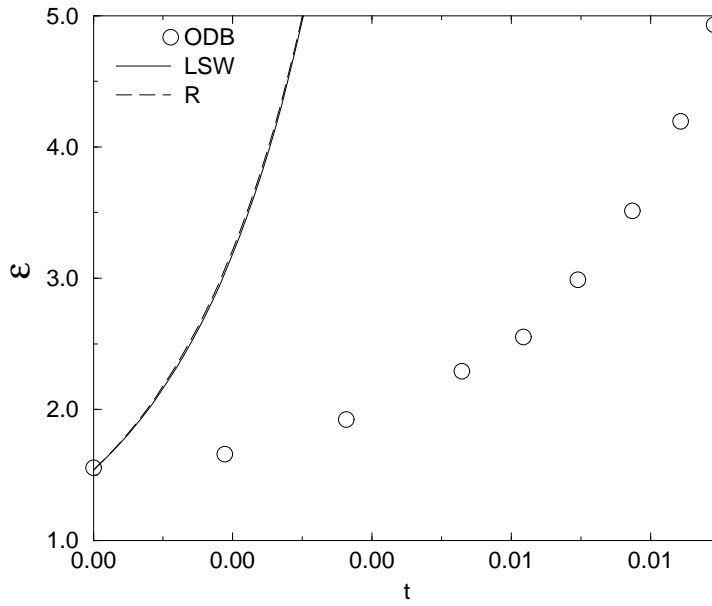


Figure 3.92: *Dissipation of the kinetic energy evolution for the ODB one-dimensional compression.*



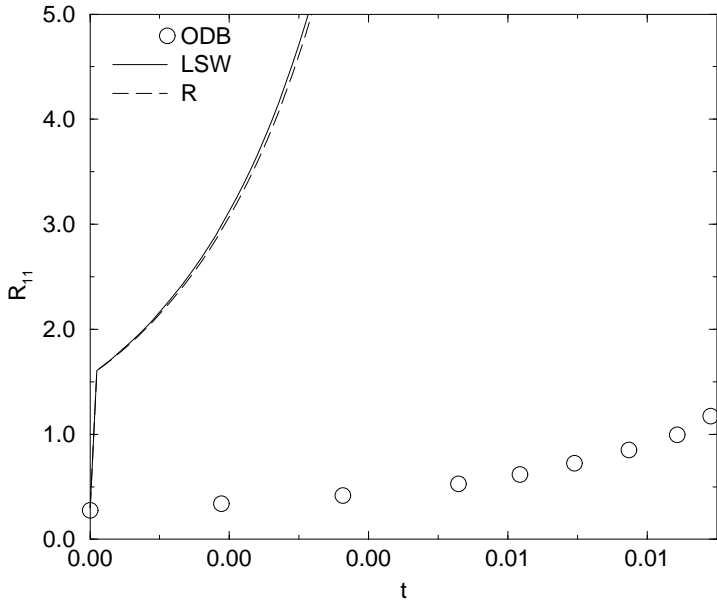


Figure 3.93: Prediction of R_{11} for the ODB one-dimensional compression.

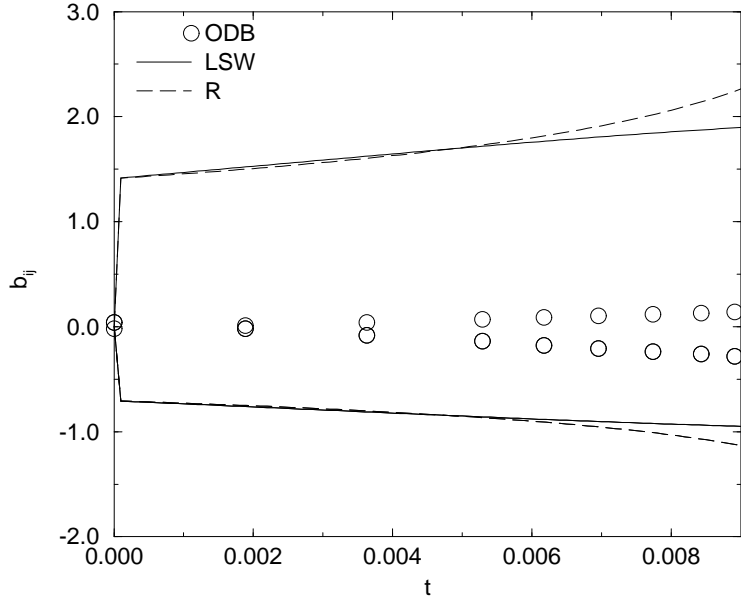


Figure 3.94: Anisotropy tensor for the ODB one-dimensional compression.



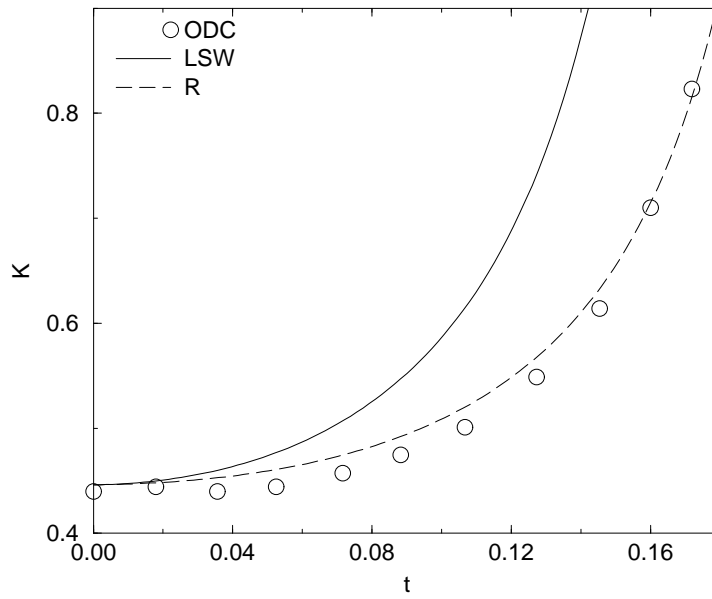


Figure 3.95: *Kinetic energy evolution for the ODC one-dimensional compression.*

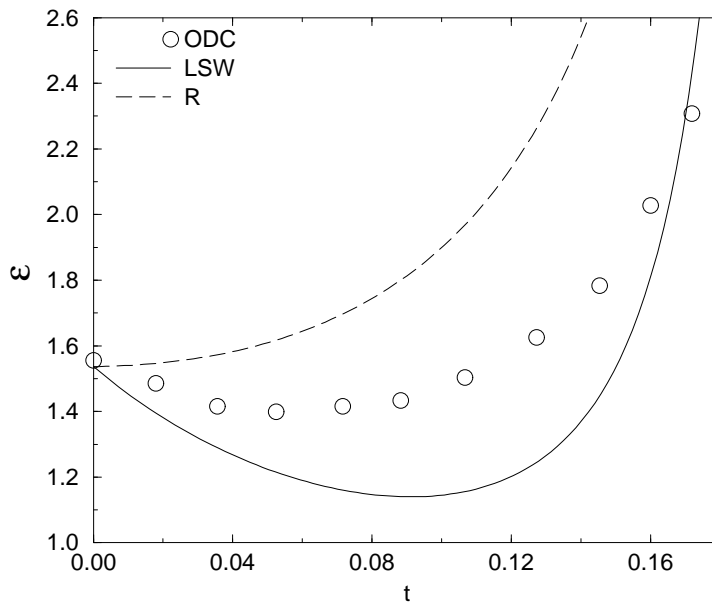


Figure 3.96: *Dissipation of the kinetic energy evolution for the ODC one-dimensional compression.*



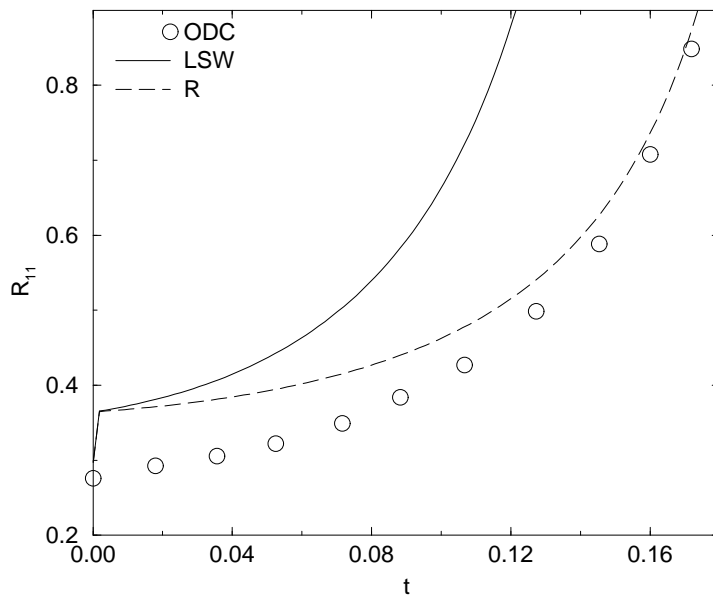


Figure 3.97: Prediction of R_{11} for the ODC one-dimensional compression.

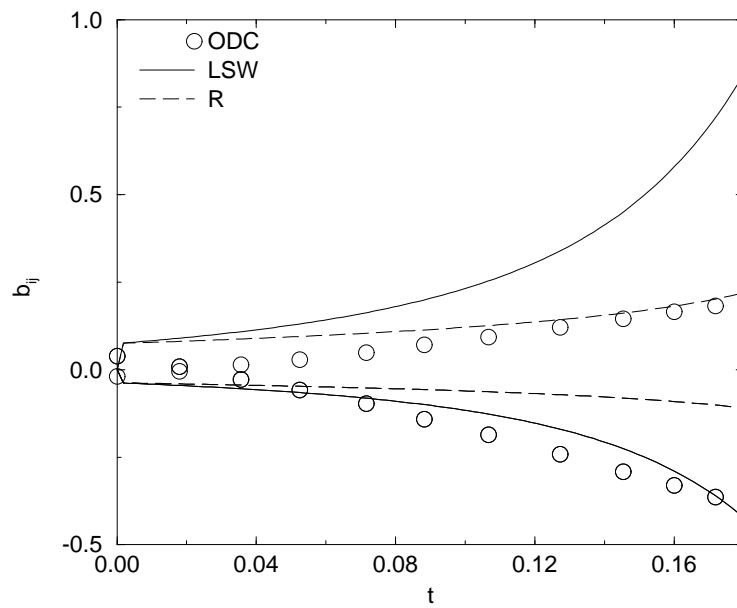


Figure 3.98: Anisotropy tensor for the ODC one-dimensional compression.



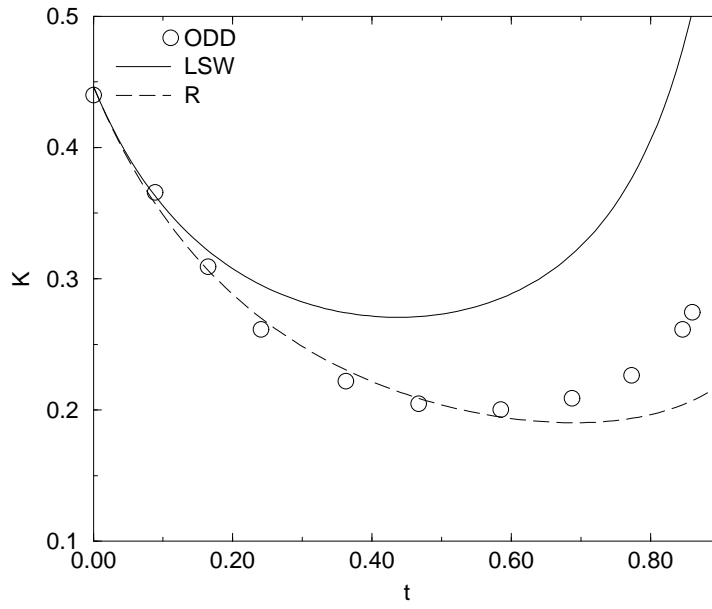


Figure 3.99: *Kinetic energy evolution for the ODD one-dimensional compression.*

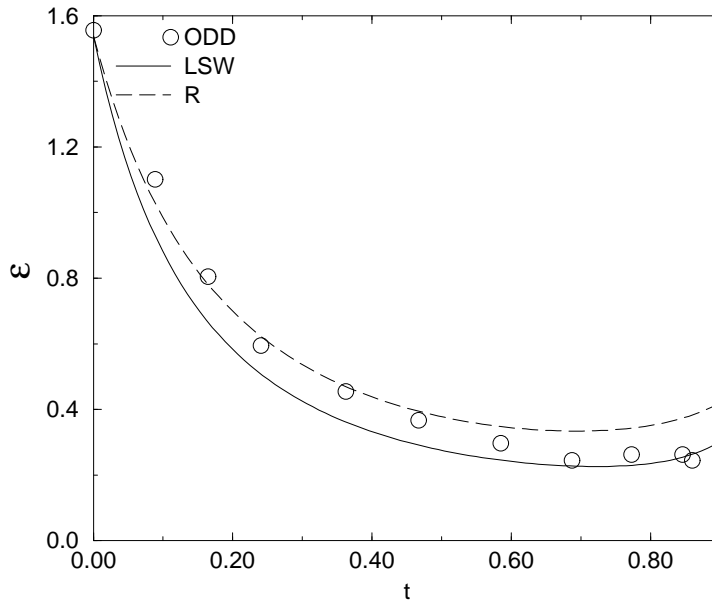


Figure 3.100: *Dissipation of the kinetic energy evolution for the ODD one-dimensional compression.*



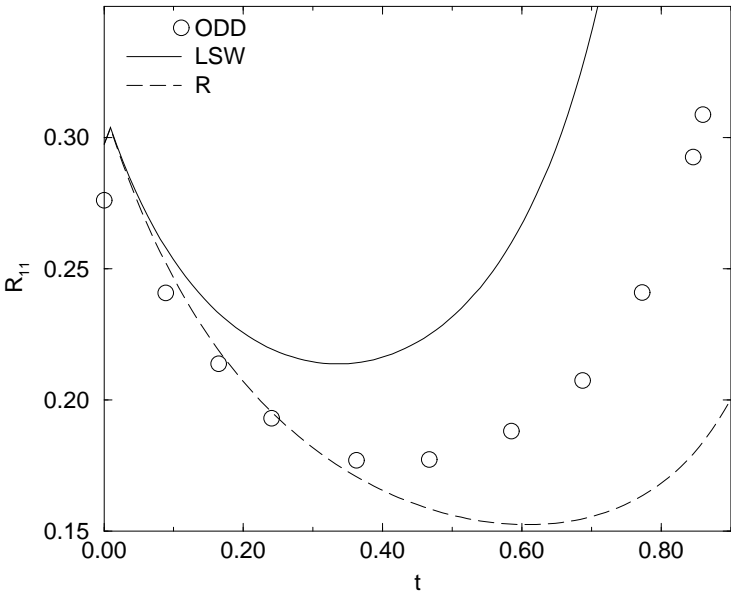


Figure 3.101: Prediction of R_{11} for the ODD one-dimensional compression.

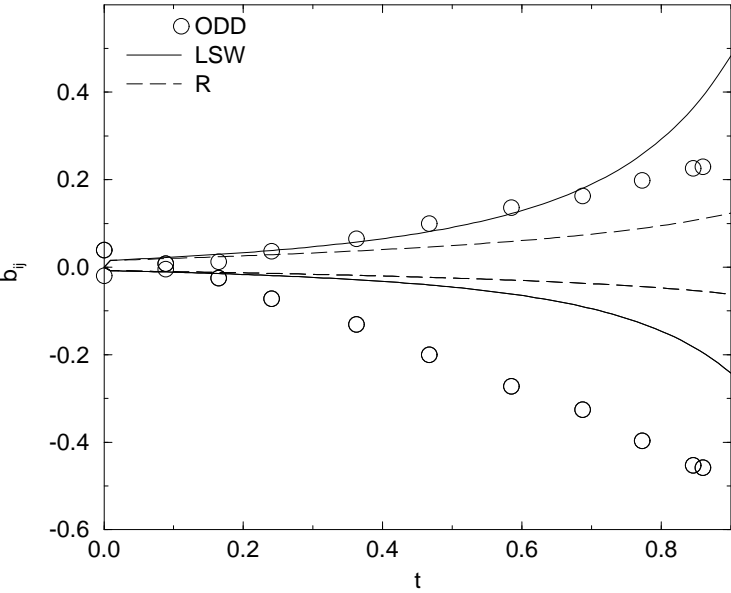


Figure 3.102: Anisotropy tensor for the ODD one-dimensional compression.



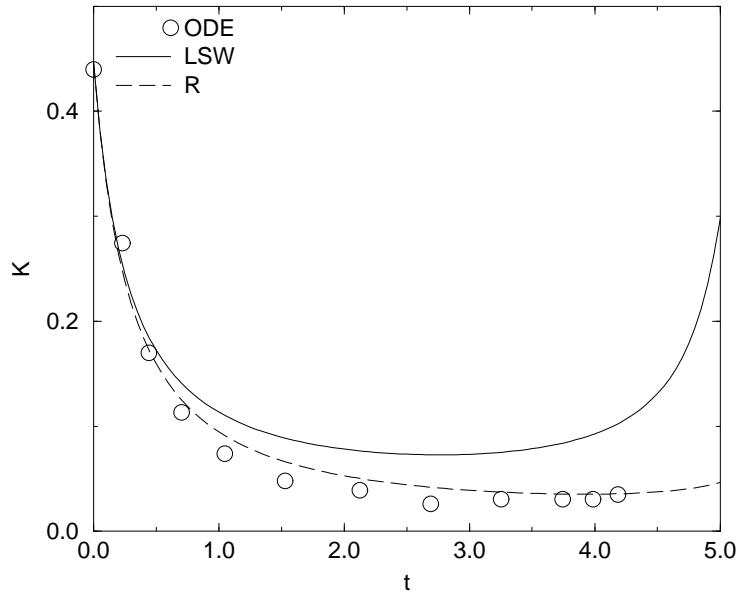


Figure 3.103: *Kinetic energy evolution for the ODE one-dimensional compression.*

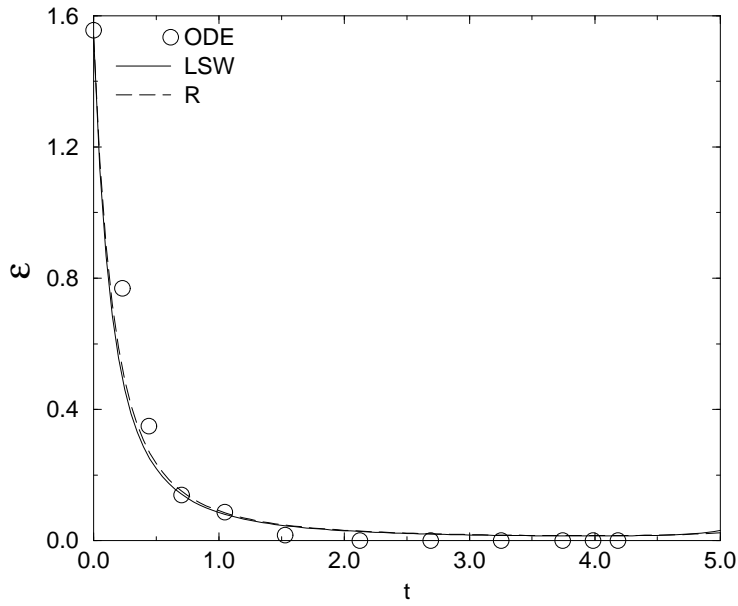


Figure 3.104: *Dissipation of the kinetic energy evolution for the ODE one-dimensional compression.*



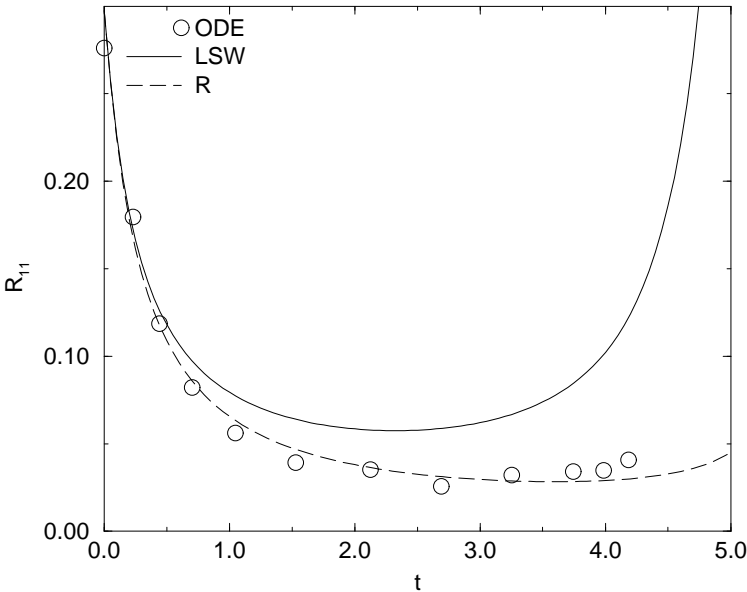


Figure 3.105: Prediction of R_{11} for the ODE one-dimensional compression.

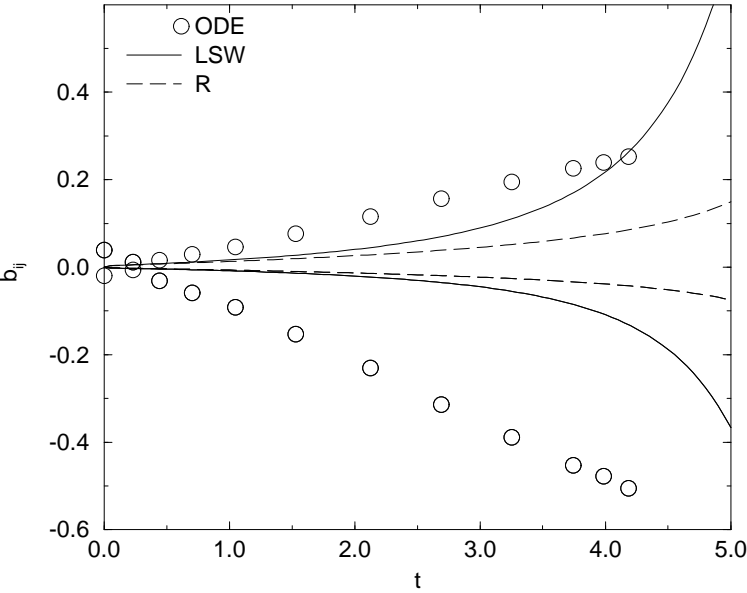


Figure 3.106: Anisotropy tensor for the ODE one-dimensional compression.



3.6 Comments

The study of the performances of various closure models for homogeneous flows in a range of classic test cases gave no conclusive evidence for a general ranking of the models. In fact, no model was found to perform superior in all cases considered. Depending on the importance of the slow term, the Reynolds number and the imposed distortions, the hierarchy of the performances of the complete models changes.

Based on the overall performances and taking into account all aspects, it can, however, be noted that the model of Shih and Lumley (1993) (SL) behaves generally better as compared to the other models, when the influence of the slow term is important. When the distortion is more rapid, the model of Speziale *et al.* (1991) (SSG) gives reasonable results in the whole. In view of its simplicity and reasonable performance in non-homogeneous, wall-attached flows, the SSG model seems at present to be the best compromise. The-Launder *et al.* (1975) model (LRR) also yields in most cases reasonable results and is the simplest formulation that is able to relatively correctly predict the pure deformation cases.

Bibliography

BARDINA, J., FERZIGER, J.H., AND REYNOLDS, W.C. (1983) Improved turbulence models based on large-eddy simulation of homogeneous, incompressible turbulent flows. Technical Report TF-19, Stanford University, Thermosciences Division.

BERTOGLIO, J.P. (1982) Homogeneous turbulent field within a rotating frame. *AIAA Journal*, **20**, pp. 1175–1181.

CADIOU, A., AND PIQUET, J. (1994) Distorsion rapide d'une turbulence en rotation pure. *C. R. Acad. Sc. Paris*, **318**, pp. 1301–1304.

COMTE-BELLOT, G., AND CORRSIN, S. (1966) The use of a contraction to improve the isotropy of grid-generated turbulence. *J. Fluid Mech.*, **25**, pp. 657–682.

FU, S., LAUNDER, B.E., AND TSELEPIDAKIS, D.P. (1987) Accomodating the effects of high strain rates in modelling the pressure-strain correlation. Technical Report TFD/87/5, UMIST Mechanical Engineering Dep.

GENCE, J.N., AND MATHIEU, J. (1980) The return to isotropy of an homogeneous turbulence having been submitted to two successive plane strains. *J. Fluid Mech.*, **101**(3), pp. 555–566.

KASSINOS, S.C., AND REYNOLDS, W.C. (1995) A structure-based model for the rapid distorsion of homogeneous turbulence. Technical Report TF-61, Stanford University, Thermosciences Division.

LAUNDER, B.E., REECE, G.J., AND RODI, W. (1975) Progress in the development of a Reynolds stress turbulent closure. *J. Fluid Mech.*, **183**, pp. 63–63.

LEE, M.J., AND REYNOLDS, W.C. (1985) Numerical experiments on the structure of homogeneous turbulence. Technical Report TF-24, Stanford University, Thermosciences Division.

LEE, M.J. (1990) A contribution toward rational modeling of the pressure-strain-rate correlation. *Phys. Fluids, Series A*, **2**(4), pp. 630–633.

LEITH, C.E. (1968) Diffusion approximation for two-dimensional turbulence. *Phys. Fluids*, **11**, pp. 671–673.

LUMLEY, J.L. (1970) Toward a turbulent constitutive relation. *J. Fluid Mech.*, **41**(2), pp. 413–434.

LUMLEY, J.L. (1978) *Computational Modeling of Turbulent Flows*. Advances in Applied Mechanics.

MILLS, R.R., AND CORRISIN, S. (1959) Effect of contraction on turbulence and temperature fluctuations generated by a warm grid. *J. Fluid Mech.*, **32**, pp. 657–674.

NAOT, D., SHAVIT, A., AND WOLFSTHEIN, M. (1973) Two-point correlation model and the redistribution of Reynolds stresses. *Phys. Fluids*, **16**, pp. 738–743.

REYNOLDS, W.C. (1980) Modeling of fluid motions in engines. an introductory overview. In *Symposium on combustion modeling in reciprocating engines, volume = 1*, pages = 41–66.

RISTORCELLI, J.R., LUMLEY, J.L., AND ABID, R. (1994) A rapid-pressure correlation representation consistent with the Taylor-Proudman theorem materially-frame-indifferent in the 2D limit. Technical Report 94-1, ICASE.

ROGERS, M.M., MOIN, P., AND REYNOLDS, W.C. (1986) The structure and modeling of the hydrodynamic and passive scalar fields in homogeneous turbulent shear flow. Technical Report TF-25, Stanford University, Thermosciences Division.

ROTTA, J.C. (1951) Statistische theorie nichthomogener turbulenz. *ZAMM*, **5**, pp. 136–139.

SARKAR, S., AND SPEZIALE, C.G. (1990) A simple nonlinear model for the return to isotropy in turbulence. *Phys. Fluids, Series A*, **2**, pp. 84–93.

SHIH, T.H., AND LUMLEY, J.L. (1985) Modeling the pressure correlation terms in Reynolds stress and scalar flux equations. Technical Report TR-FDA 85-03, Cornell University.

SHIH, T.H., AND LUMLEY, J.L. (1993) Critical comparison of second-order closures with direct numerical simulations of homogeneous turbulence. *AIAA Journal*, **31**(4), pp. 663–670.

SPEZIALE, C.G., AND MHUIRIS, N. MAC GIOLLA (1988) Scaling laws for homogeneous turbulent shear flows in a rotating frame. Technical Report 88-34, ICASE.

SPEZIALE, C.G., GATSKI, T.B., AND MHUIRIS, N. MAC GIOLLA (1990) A critical comparison of turbulence models for homogeneous shear flows in a rotating frame. *Phys. Fluids, Series A*, **9**, pp. 1678–1684.

SPEZIALE, C.G., SARKAR, S., AND GATSKI, T.B. (1991) Modelling the pressure-strain correlation of turbulence: an invariant dynamical systems approach. *J. Fluid Mech.*, **227**, pp. 245–272.

SPEZIALE, C.G., GATSKI, T.B., AND SARKAR, S. (1992) On testing models for the pressure-strain correlation of turbulence using direct simulations. *Phys. Fluids, Series A*, **4**(12), pp. 2887–2899.

TAVOULARIS, S., AND CORRISIN, S. (1981) Experiments in nearly homogeneous turbulent shear flow with a uniform mean temperature gradient. *J. Fluid Mech.*, **104**, pp. 311–347.

TAVOULARIS, S., AND KARNIK, U. (1989) Further experiments on the evolution of turbulent stresses and scales in uniformly sheared turbulence. *J. Fluid Mech.*, **204**, pp. 457–472.

TUCKER, H.J., AND REYNOLDS, A.J. (1968) The distortion of turbulence by irrotational plane strain. *J. Fluid Mech.*, **32**, pp. 657–674.

WATKINS, A.P. (1977) *Flow and Heat transfer in piston/cylinder assemblies*. PhD thesis, University of London.

WU, C.T., FERZIGER, J.H., AND CHAPMAN, D.R. (1985) Simulation and modelling of homogeneous compressed turbulence. Technical Report TF-21, Stanford University, Thermosciences Division.